

ARL 67-0056
MARCH 1967



Aerospace Research Laboratories

**THE FLOW FIELD AND HEAT TRANSFER
DOWNSTREAM OF A REARWARD FACING
STEP IN SUPERSONIC FLOW**

HOWARD E. SMITH
THE UNIVERSITY OF DAYTON
DAYTON, OHIO

Project No. 7063

Distribution of this document is unlimited

OFFICE OF AEROSPACE RESEARCH
United States Air Force



RECEIVED

AUG 3 1967

CFSTI

63

AD 655370

ARL 67-0056

**THE FLOW FIELD AND HEAT TRANSFER DOWNSTREAM
OF A REARWARD FACING STEP IN SUPERSONIC FLOW**

HOWARD E. SMITH
THE UNIVERSITY OF DAYTON
DAYTON, OHIO

MARCH 1967

Project 7063

Distribution of this document is unlimited.

AEROSPACE RESEARCH LABORATORIES
OFFICE OF AEROSPACE RESEARCH
UNITED STATES AIR FORCE
WRIGHT-PATTERSON AIR FORCE BASE, OHIO

FOREWORD

This technical report was prepared at the Thermo-Mechanics Research Laboratory of the Aerospace Research Laboratories, Office of Aerospace Research, USAF. The research was performed by Professor Howard E. Smith of the University of Dayton, who was in residence at W-PAFB as a Visiting Research Associate for the period 1963 through July, 1966 at the invitation by Dr. Max G. Scherberg, ARL.

The author wishes to acknowledge Dr. Max G. Scherberg for his guidance, contributions, and many fruitful discussions related to this work. Mr. Donald Clemm of the Applied Mathematics Research Laboratory, ARL, is acknowledged for programming the computer solutions of the corner expansion described in this report. The excellent cooperation and helpfulness of Mr. J. C. Donaldson, Project Engineer, together with the staff of the Von Karman Gas Dynamics Facility of the Arnold Engineering and Development Center, Arnold Air Force Station, Tennessee, who conducted the wind tunnel tests reported herein are also acknowledged.

ABSTRACT

An experimental investigation of the flow field, and the model pressure and steady-state heat transfer distributions for a rearward-facing step in supersonic flow is described. Tests were conducted using a water-cooled model with a step height adjustable to 0.443 and 0.750 inches at free stream Mach numbers of 2.5, 3.5, and 5.0, and at Reynolds numbers based on length of surface ahead of separation of approximately 2.5×10^5 to 1.8×10^6 . It was found that the Reynolds number based on step height (Re_h) is an important parameter and that both the base pressure and the maximum heat transfer at reattachment may be predicted as a function of this parameter.

Several representative flow fields are presented along with analyses of the various regions of these fields. It was found that the depressed base pressure is communicated upstream of the step through the subsonic portion of the attached boundary layer resulting in a pressure gradient immediately upstream of the step. It is shown that the rapid corner expansion is not the commonly used Prandtl-Meyer expansion, but rather is accurately described by the method of inviscid rotational characteristics which accounts for both the entropy gradient in the boundary layer and the pressure gradient upstream of the step. This description of the corner expansion also accurately predicts the position of the lip shock associated with the rapid expansion.

TABLE OF CONTENTS

Section		Page
I	Introduction	1
II	Test Model and Probes	3
III	Instrumentation and Techniques	5
IV	Experiments	7
V	Results	8
	(A) Step Model Data	8
	(B) Overhang Model Data	14
	(C) Surface Yarns	15
	(D) Probe Data	16
VI	Prediction of Base Pressure and Peak Heat Transfer	17
VII	Analysis	18
	(A) Corner Expansion and Lip Shock	18
	(B) Constant Base Pressure Region	27
	(C) Free Shear Layer	27
	(D) Recirculating Cavity Flow	28
	(E) Reattachment Region	29
	(F) Constant Pressure Reattached Flow Region	30
VIII	Conclusions	32
IX	Recommendations for Future Work	33
X	References	34

LIST OF SYMBOLS

$C = \frac{(P_t'/P_t)_{\alpha=0} - (P_t'/P_t)_{\alpha=\alpha}}{(P_t'/P_t)_{\alpha=0}}$	Pitot probe correction factor
C_p	Specific heat at constant pressure (BTU/lbm-°F)
g	Acceleration of gravity (32.17 ft/sec ²)
h	Step height (inches)
h	Film coefficient (BTU/in ² -sec-°F)
k	Thermal conductivity (BTU/sec-in-°F)
L	Length of surface ahead of separation (inches)
$Nu_x = \frac{hx}{k}$	Local Nusselt number
P	Local static pressure (psi)
P_0	Free stream total pressure (psi)
P_t	Local total pressure (psi)
P_t'	Pitot reading (psi)
$Pr = \frac{u_{\infty} C_p}{k}$	Prandtl number
q	Local heat flux (BTU/ft ² - sec)
R	Gas constant (ft/°R)
$Re_h = \frac{u_{\infty} h}{\nu_{\infty}}$	Reynolds number based on h
$Re_L = \frac{u_{\infty} L}{\nu_{\infty}}$	Reynolds number based on L
$Re_x = \frac{u_{\infty} x}{\nu_{\infty}}$	Reynolds number based on distance from leading edge
S	Entropy (ft/°R)
T	Local temperature (°R)
T°	Reference temperature (°R)

T_o	Free stream total temperature (°R)
u	Local velocity (ft/sec)
x	Distance downstream of separation (inches)
y	Distance above model surface (inches)
$\alpha = \arctan \left(\frac{h}{x} \right)$ PIT	(degrees) or local flow angle relative to pitot probe (degrees)
$\gamma = C_p/C_v$	Ratio of specific heats
θ	Local flow angle (degrees)
μ	Local Mach angle (degrees) or Local dynamic viscosity (lbm/ft.sec)
ν	Prandtl-Meyer angle (degrees) or Local kinematic viscosity (ft ² /sec)
$\xi = P_2/P_1$	Static pressure ratio across oblique shock
ϕ	Angle of downstream flow with oblique shock (degrees)

Subscripts:

a	Mesh point in flow field of method of characteristics solution
aw	Adiabatic wall conditions
b	Mesh point in flow field of method of characteristics solution or base conditions
c	Mesh point in flow field method of characteristics solution
DSL	Dividing stream line
e	Value at edge of shear layer
exp	Experimentally determined value
ext	Extrapolated value
fp	Flat plate conditions
i	Initial value
max	Maximum value

PHF	Peak heat transfer
r	Recovery conditions downstream of reattachment shock
reat	Reattachment conditions
sep	Separation conditions
w	Wall conditions
α	Angle of local flow with pitot probe
1	Conditions upstream of oblique shock
2	Conditions downstream of oblique shock
3	Conditions behind normal shock in front of pitot probe
-	Free stream conditions

I. INTRODUCTION

During the past fifteen years many experimental and theoretical investigations have been undertaken to determine the flow characteristics and heat transfer in the separated and reattaching flow region downstream of a rearward facing step and in the near wake of a body in flight at supersonic speeds in order to develop a realistic theory for the prediction of base pressure and heat transfer in this region. The most commonly referenced theories are those of Chapman (1) for a laminar boundary layer at separation and of Korst (2) for a turbulent boundary layer at separation. Both of these theories make use of the "dividing streamline" concept (Figure 1) in which all of the flow coming over the step remains above the dividing streamline and passes downstream, while all of the flow below it is reversed at reattachment and remains within the cavity beneath the dividing streamline. These theories assume that the total pressure of the dividing streamline at reattachment is equal to the static pressure downstream of reattachment. Both theories also assume a negligibly thin boundary layer thickness at separation, and are therefore Reynolds number independent and fail to accurately predict base pressure when this condition is violated. Crocco and Lees (3) have developed a general theory attempting to cover all types of separated flows, but the application of this theory in practice is very difficult and requires the evaluation of many empirical constants dependent upon model geometry. Chapman, Kuehn and Larson (4) conducted an extensive experimental investigation and examined separated flows created by ramps and forward and rearward facing steps. They found that the pressure in the separated region is strongly dependent upon the location of transition relative to the point of separation or reattachment. For the case of the rearward facing step, if transition occurs well downstream of reattachment (laminar flow throughout), the base pressure is relatively high and is a weak function of Reynolds number. If

Manuscript released September 1966 for publication as an ARL Technical Documentary Report.

transition is upstream of separation (turbulent flow throughout) the base pressure is much lower, but is again a weak function of Reynolds number. For the case where transition occurs near reattachment, or between separation and reattachment, the base pressure is strongly dependent upon Reynolds number and may in some cases be lower than the fully turbulent case.

Nash (5) observed that the dividing streamline stagnates within the region of pressure rise at reattachment rather than at the peak pressure as the Chapman-Korst theories assume. He proposed that the Chapman-Korst theories be modified to take this fact into account. Ginoux (6) found evidence of three-dimensional regular perturbations at the reattachment of two-dimensional laminar boundary layers. These perturbations appear to be similar to Goertler type streamwise vortices. Hoshko and Thomke (7) found similar patterns in the reattachment downstream of an axi-symmetric rearward facing step.

In spite of the numerous investigations of separated flows which have been conducted, many details of the flow field still remain obscure and only a limited amount of information has been obtained on the local heat transfer distribution downstream of separation. For the past several years Dr. Rom (8)(9) of the Technion in Haifa, Israel has been conducting an experimental and theoretical research program in this area for ARL. He used small two-dimensional rearward facing step models in a blow-down wind tunnel and in a shock tube. He has measured base pressures and heat transfers at Mach numbers of 2.25 and 3.50 and Reynolds numbers, based on length of flat plate upstream of separation, of 1 to 2×10^5 (laminar separation) and 0.6 to 5×10^6 (turbulent separation). He found a plausible base pressure correlation using a modified Crocco-Lees theory and also found high rates of heat transfer in the reattachment region under certain flow conditions.

An ARL in-house program was undertaken to compliment the work of Dr. Rom. This program was devised to use larger models in a continuous run wind tunnel facility.

Test variables were specified so as to cover the Reynolds number range between Rom's laminar and turbulent studies at free stream Mach numbers of 2.5, 3.5 and 5.0 to check the validity of his shock tube heat transfer measurements and to study the flow details. Tests were conducted at the von Karman Gas Dynamics Facility at Arnold Engineering and Development Center, Tennessee in tunnel A, a 40 inch x 40 inch continuous run wind tunnel with a Mach number range of 1.5 to 6.0. A more complete description of this facility is contained in Reference 10. This report summarizes the results of the ARL in-house program. Preliminary reports of some of these results have been presented previously (11)(12).

II. TEST MODEL AND PROCES

A two-dimensional, water-cooled, rearward facing step model 9 inches wide with variable step heights of 0, 0.443, and 0.75 inches was used in this investigation. This model, shown in Figure 2, was equipped with side plates containing optical quality windows to obtain approximately two-dimensional flow and was instrumented with 46 pressure orifices and 40 heat transfer gauges. The 4 inch long section upstream of the step consisted of a 1/8 inch thick sheet of type 416 stainless steel backed by a 1/8 inch thick sheet of phenolic nylon to maintain an adiabatic surface upstream of separation. The vertical riser surface and the horizontal reattachment surface downstream of the step were made of type 304 stainless steel and were cooled by circulating water through channels within the model. Early in the test program, the vertical riser section developed water leaks which could not be repaired so that no data were obtained from heat transfer gauges numbers 1 through 4. To make a step height change in the model, the side plates were removed and spacers inserted or removed beneath the downstream reattachment plate. Each time this was done all joints were carefully sealed with sealastic to insure that air did not leak into or out of the separated region.

The steady state heat transfer gauges, shown in Figure 3, consisted of type 304 stainless steel plugs 0.156 inches in diameter containing a copper-constantan thermocouple junction at each flow exposed surface. These plugs were mounted so that they were surrounded by a 0.0025 inch air gap over most of their length to reduce lateral conduction and thus approximate one dimensional heat flow across the gauge. Each end of these gauges was flush with the model surface, so that one end was in contact with the air flow and the other with the water flow. The water side of these gauges was sealed with epoxy and the air side of the plate was ground flat and polished after the final assembly of all the gauges.

A flattened combination thermocouple-pitot probe shown in Figure 4, designed at ARL and built by Rosemount Engineering Company of Minneapolis, Minnesota, was used to obtain total temperature and pitot pressure surveys in the expansion region, in the free shear layer and in the attached boundary layers upstream of separation and downstream of reattachment. Figure 5 shows two views of the model and the combination probe mounted in the tunnel.

Figure 6 shows the two wire hot-wire probe which was designed at ARL and built by Flow Corporation of Cambridge, Massachusetts to obtain velocity profiles in the low energy cavity flow beneath the free shear layer. This probe was designed so that the measuring wires were offset from the supporting stem which was made long and thin to cause a minimum of disturbance in the vortex type flow at the point of measurement. When this probe was used it was mounted on the tunnel probe drive head and replaced the combination probe shown in Figure 5. The sensing wires were made of 0.00035 inch diameter tungsten wire which was copper plated and tinned at each end and soldered to the support needles.

The probe shown in Figure 7, which was observed visually, was designed and built at ARL to determine the local flow direction in the cavity region. It consisted of two direction indicating flags, each cemented to a 0.025 inch o.d. stainless

steel sleeve. These sleeves were in turn mounted on stainless steel spindles, one oriented vertically and the other horizontally. The flag on the vertical spindle was made of foil while the one on the horizontal spindle was made of yarn to reduce gravity effects. This probe was offset in the same manner as the hot wire probe to cause minimum flow disturbance.

III. INSTRUMENTATION AND TECHNIQUES

The test data for Mach numbers 2.5, 3.5 and 5.0 were obtained in succeeding entries into the tunnel, and test techniques varied slightly for each entry as optimum conditions and improved measurements were sought each time. For all tests the model cooling water was chilled to below 40° F by pumping it through a copper coil immersed in an ice and brine solution. Cooling water entered the model re-attachment plate at the forward edge beneath the separation cavity and flowed parallel to the free stream air flow.

The combination thermocouple-pitot probe was connected to a three-way valve inside the probe head so that the probe could be connected to a pressure transducer for pressure measurement or to a vacuum system to allow air to be pulled over the thermocouple for temperature measurement. When used in this way, the probe measures a recovery temperature which is a function of probe design and free stream conditions and must be calibrated before the local total temperature may be determined. Calibration in various free stream conditions showed that the probe recovery factor was always between 91 and 93% so that a constant value of 92% was used for all data reduction. It was further assumed that the recovery factor in a shear flow was the same as in a free stream flow. The combination probe was not pitched to align with the local flow angle but was always pointed upstream into the free stream direction. A calibration of the probe for variation from true pitot pressure reading vs. angle at two different Reynolds numbers and various Mach numbers showed that the Reynolds

number effect was negligible and the reading variation was only a function of Mach number and angle. For subsequent data reduction it was found convenient to display this information as a family of constant correction curves on a Mach number vs. flow angle plot as shown in Figure 8. The transducers used to read out the pitot pressure for various test conditions are summarized in Table I.

When using the hot wire probe the four leads associated with each wire were fed from the tunnel to a Flow Corporation Hot Wire Probe Selector Model 4681 switching device. This permitted energizing and reading each of the probe wires separately. The switching device was connected to a Flow Corporation Hot Wire Anemometer Model HMB 2 which contained the wire current controls, the resistance bridge and the current and voltage meters. This unit was operated in the constant resistance ratio mode. Prior to mounting the probes in the tunnel, each wire was calibrated in a small calibration tunnel to obtain its current-velocity relation. In addition, a calibration of the variation of the zero velocity current vs. pressure was required since the pressure behind the step in the wind tunnel was very much below atmospheric pressure. This variation was determined by calibration in a vacuum chamber at various pressure levels.

The instrumentation used for measuring model temperatures and pressures at the various Mach numbers together with the estimated measurement error is described briefly in Table I.

A point light source single pass shadowgraph system was used to photograph flow details. In this system the light source was located in line with the separation point of the model 105.3 inches from the tunnel centerline while the film was located on the opposite side of the tunnel 32.0 inches from the tunnel centerline.

IV. EXPERIMENTS

During the initial tunnel entry, it was determined that the pressure distribution on the model remained unchanged regardless of whether or not the model was cooled. After this determination, the following test sequence was adopted for each model configuration ($h=0.00, 0.443$ and 0.750) and each Mach number:

(a) With the cooling water shut off, the model pressure and adiabatic wall temperature distributions were determined at various free stream Reynolds numbers. A shadowgraph photograph of each condition was also obtained.

(b) With the cooling water circulating, the model surface temperature and heat transfer distributions were obtained for some of the above Reynolds numbers. A summary of the tunnel conditions of the test is given in Table II.

In addition to the model information obtained above, detailed probings of the flow field using the combination thermocouple-pitot probe were obtained under the tunnel conditions and model configurations listed in Table III.

During the first tunnel entry, oil was sprayed on the model reattachment surface to determine the reattachment line and the local surface flow direction so as to check the two-dimensionality of the flow. These oil flow studies were abandoned as not being feasible in the continuous run tunnel being used. During the extended time required to bring the tunnel to flow conditions, most of the oil was blown downstream, and it could not be positively determined whether the observed flow pattern accurately depicted the run condition flow lines or whether some traces of flow lines left during the transient running period were being observed. During a later entry, yarn tufts were attached to the surface to determine the reattachment line and the two-dimensionality of the flow. The tufts gave a good indication of the location of the reattachment line within the accuracy of their $1/4$ inch spacing. They also showed the flow downstream of reattachment to be two-dimensional, but gave no indication of flow conditions within the extremely low energy separated region.

Attempts to measure the flow direction and velocity of the vortex type flow in the separated region using the hot-wire probe and the direction sensing probe net with only limited success and will be discussed below.

During the final tunnel entry a thin overhang equal in length to one step height was added to the basic model to determine the effect of a different flow entrainment condition at separation and the effect of a change in cavity shape upon the development of the flow in the cavity and downstream of separation.

V. RESULTS

(A) Step Model Data:

Figures 9a through 9i show shadograph photographs of the flow field for the 0.443 inch step at the high, intermediate, and low Reynolds number for each Mach number. The bright line parallel to the reattachment surface which is visible in some of these photographs is a light reflection off the reattachment surface. Of particular interest in these photographs is the white line denoting the upper edge of the free shear layer downstream of separation, the lip shock which emanates from the shear layer downstream of the corner, and the reattachment shock resulting from the coalescing of compression waves in the reattachment region. Detailed probing with the combination thermocouple-pitot probe verify this interpretation of these shadographs. Note that with increasing free stream Reynolds number the lip shock rotates downward relative to a horizontal reference line. Examination of the probe data shows that the losses across the lip shock increase with increasing free stream Reynolds number. Also of special interest is the fact that for the $M_\infty = 2.5$ high Reynolds number case (Figure 9a) a second shock appears at the beginning of the expansion fan. Lip shocks at the end of the expansion fan have been noted by several previous investigators, but only Roshko and Thorke (7) have reported a shock at the beginning of the expansion. The lip shock has been considered negligibly weak by

most investigators. Little attention has been given to this shock and all of the theories to date ignore it completely. Recently Hama (13) has made some estimate of the strength of the lip shock and concludes that it is not as weak as previously supposed. A further discussion of the lip shock will be given below.

Also shown in Figures 9a through 9i is the model pressure and heat transfer distribution obtained under the test conditions of the photographs. The model pressure has been non-dimensionalized by the pressure measured at the number one orifice located 1-1/2 inches upstream of the step, while the heat transfer data are non-dimensionalized by using the local flat plate heat transfer obtained under the same flow conditions. The non-dimensionalized heat transfer curve was obtained by fairing curves through the experimentally determined data for both the step and the flat plate and taking the ratio of points along these faired curves. This procedure will be discussed below in more detail. The increasing heat flux downstream of re-attachment observed in Figure 9c is undoubtedly brought about because the flow was turbulent there in the case of the step and laminar in the case of the flat plate reference condition.

Examination of the pressure distributions of Figures 9a through 9i shows a region of essentially constant pressure along the surface immediately downstream of the step. The pressure orifices in the vertical riser surface (numbers 39 through 42) showed the pressure on this face to be essentially constant at the same value as those along the floor. This pressure, the base pressure, normalized by the upstream pressure $P_1 = P_\infty$ is plotted vs. Reynolds number based on length of surface ahead of separation for all test points obtained in Figures 10a through 10c. Also shown in these figures are the base pressures predicted by the laminar theory of Chapman (1) and the turbulent theory of Korst (2). At the low values of Re_L the curves appear to be approaching a constant pressure plateau. This behavior is especially prominent in the case of the 0.750 inch step at $M_\infty = 5.0$ (Figure 10c) and

confirms similar findings by Chapman, Kuehn and Larson (4) for separated flows which are laminar throughout in that the base pressure is nearly independent of Reynolds number. Figures 10a through 10c show however, that this constant pressure plateau (if it is in fact reached for all separated flows) is considerably above the pressure predicted by the Chapman theory for laminar flows. It is also seen that the low Reynolds number base pressure appears to be a rather strong function of step height as evidenced by the results of the two step heights at each Mach number of this investigation.

For a given model configuration, it is seen that as the free stream Reynolds number is increased from the completely laminar condition the base pressure decreases. As evidenced for the case of the 0.750 step at $M_\infty = 2.5$ (Figure 10a), the base pressure reaches a minimum value and then begins to increase with increasing free stream Reynolds number. For reasons to be given later, it is believed that the base pressure for fully turbulent separated flow approaches that given by the Korst turbulent theory. The fully turbulent base pressure is lower than the fully laminar value, but higher than the minimum value obtained for transitional type flows. In general, for a given model configuration and free stream Mach number, the base pressure is dependent upon the location of transition relative to separation and reattachment as indicated schematically in Figure 11.

Because of the strong dependence of base pressure upon step height and free stream conditions indicated in Figures 10a through 10c, all of the available two-dimensional base pressure data (both from the present experiments and from the literature) were plotted vs. Reynolds number based on step height and free stream conditions. The data were obtained at various Mach numbers ranging from $M_\infty = 1.56$ to 5.0 and are displayed in Figure 12. Also shown in this figure are the base pressures predicted by the Korst turbulent theory at various Mach numbers. It is seen that except for a few turbulent flow points which are close to values predicted by

Korst's turbulent theory, all of the data fall within a relatively narrow envelope and may be approximately predicted by the empirical equation

$$P_b/P_\infty = \frac{0.393}{(Re_h)^{.2}} \quad Re_h < 0.52 \times 10^5 \quad (1)$$

$$P_b/P_\infty = \frac{0.31}{(Re_h)^{.58}} \quad Re_h > 0.52 \times 10^5$$

As transition moves upstream into the reattachment region the base pressure begins to fall from its relatively high laminar value as given by equation 1 and shown in Figure 12. When transition occurs upstream of separation, the base pressure prediction of Korst as shown in Figure 13 appears to be adequate and should be used. The exact method of moving from the curve of Figure 12 to that of Figure 13 is not known at present, and should be the object of a future investigation.

Because of limitations on the tunnel operating temperature and the model cooling water temperature only a small temperature differential was obtained across the heat transfer measurements. Figure 14 shows typical heat transfer distributions obtained for both a step and a flat plate configuration at the same flow conditions. The large heat transfer in the vicinity of the step location for the flat plate configuration occurs because of the surface temperature discontinuity existing at this location (insulated surface to cooled surface). It is seen that for the step configuration the maximum heat transfer occurs in the reattachment region and may be several times the local flat plate value, while in the separated region beneath the free shear layer the heat transfer is less than at the corresponding flat plate position.

Also shown in Figure 14 is the flat plate heat transfer which would have been obtained if the plate had been cooled to the uniform wall temperature of the test from the leading edge. This curve will hereafter be referred to as the extrapolated

flat plate curve, and was obtained by computing both the laminar and turbulent heat transfer distribution and fairing a curve between and parallel to them to coincide with the experimental heat transfer distribution downstream of the effect of the temperature discontinuity. The heat transfer as given by this extrapolated curve at $X = 0$ would be the heat transfer at separation (\dot{q}_{sep}) and may be used as a reference quantity. These heat transfers were computed by using the following flat plate empirical relations of Eckert (17):

$$\begin{aligned} Nu_x &= 0.332 (Re_x)^{1/2} (Pr)^{1/3} && \text{Laminar flow} \\ Nu_x &= \frac{0.195 (Pr)^{1/3} (Re_x)}{[\log_{10} Re_x]^{2.584}} && \text{Turbulent flow} \end{aligned} \quad (2)$$

Properties of the gas used in equation (2) were evaluated at a reference temperature given by

$$T^* = T_\infty + 0.5 (T_w - T_\infty) + 0.22 (T_{aw} - T_\infty). \quad (3)$$

To relate the maximum heat transfer at reattachment to conditions at the step, the following procedure was used to calculate the ratio ($\dot{q}_{max} / \dot{q}_{sep}$). At various positions along the reattachment surface the local ratio of measured step heat transfer to measured flat plate heat transfer $\left[(\dot{q} / \dot{q}_{fp})_{exp} \right]$ was determined from a plot such as Figure 14. Typical distributions of this ratio over the reattachment surface are shown in Figures 9a through 9i. At the location of maximum $(\dot{q} / \dot{q}_{fp})_{exp}$ determined from Figures 9a through 9i, the value of the local flat plate heat transfer $(\dot{q}_{fp})_{ext}$ was determined from plots similar to Figure 14. (This quantity is denoted as $(\dot{q}_{fp})_{ext}$ because it was usually necessary to use the extrapolated portion of the experimental curve. However, if the point of maximum heat transfer was far enough downstream, the actual experimental curve was used). The ratio of maximum reattachment heat transfer to heat transfer at the step was

determined by

$$\left(\frac{q_{max}}{q_{sep}} \right) = \left(\frac{q_{max}}{q_{fp}} \right)_{exp} \left(\frac{q_{fp, ext}}{q_{sep}} \right) \quad (4)$$

Figure 15 shows a plot of this ratio vs. Re_{θ} . The flagged points in this figure represent run conditions in which transition on the flat plate occurred between the separation and reattachment positions. For these conditions, the extrapolated flat plate curve was extended forward from the experimental curve as if transition had occurred upstream of the separation position. The values of heat flux at low Reynolds numbers reported by Rom (8) are considerably higher than the results of the present investigation and other reported results. The reason for this discrepancy is not known at present, but it should be pointed out that Rom's results were obtained in a shock tube, while the other measurements shown in Figure 15 were obtained in wind tunnels.

The high values of heat transfer at reattachment are believed to be due to transition to turbulence. From this curve it is concluded that:

- (a) If transition occurs far downstream of reattachment the peak heat transfer at reattachment is less than the value at separation.
- (b) If transition occurs in the reattachment region, the reattachment peak heat transfer is greater than the heat transfer at separation.
- (c) If transition occurs upstream of separation, the peak reattachment heat transfer is approximately equal to the separation value.

Examination of Figures 9a through 9i shows that the peak heat transfer always occurs at the neck of the recompressing shear layer downstream of the stagnation line. In order to correlate the distance from the separation point to the point of peak heat transfer (x_{PHT}) an angle $\alpha = \arctan (h/x_{PHT})$ is defined. Figure 16 shows

a plot of α/μ vs. Re_h which includes all of the experimental points of this investigation. The parameter α/μ is similar to the parameter β/μ used by Donaldson and Myers (21) to correlate the location of reattachment. Although there is considerable scatter in the data, it is seen that the variation of α/μ with Re_h may be approximated by:

$$\alpha/\mu = 1.07 (Re_h)^{0.3-0.5} \quad (5)$$

(B) Overhang Model Data:

A thin (1/64 inch) overhang of length equal to one step height (0.750 inch) was added to the basic model to determine the effect of a different entrainment condition at separation. It was found that both the pressure and heat transfer distributions downstream of the separation point were the same as for the step without the overhang if flow conditions were adjusted to the same Reynolds number based on step height (Re_h) for the two cases. However, if the flow was adjusted so that the same Reynolds number based on length ahead of separation (Re_L) was obtained for both cases, the heat transfer and pressure distribution for the step differed from those for the overhang. Thus this investigation also pointed to the fact that Re_h is an important parameter for the base type flow under investigation. It is believed that a system of two vortices develops beneath the step and shear layer, as shown in the accompanying sketch, to allow the flow to adjust to the same downstream conditions for both the step and the overhang.

(C) Surface Yarns:

In order to determine the local flow direction on the model surface and to define the location of the stagnation line, strands of yarn were attached to the model surface downstream of the step. Experimentation with various types of yarns showed that a 50% wool-50% nylon yarn was the most responsive to air flow direction and had the necessary resistance to fiber breakage due to buffeting in the wind tunnel air flow.

These strands were threaded through a ruled sheet of heavy paper in a regular pattern and attached to the underside of the paper by double-sided pressure sensitive tape. The free yarn ends were then cut to a length of $3/4$ inches and the paper was attached to the model by using another layer of double-sided pressure sensitive tape. This arrangement provided a smoother reattachment surface and a better response of the yarns than would have been obtained if the yarns had been cemented directly to the model surface. Photographs of the orientation of the yarn strands for the 0.75 step at the highest Reynolds number for each test Mach number are shown in Figure 17. The rulings are $1/4$ inch apart with heavy accented lines every inch. It is seen that the reattachment line is well defined within the accuracy of the rulings, that it is essentially straight and that the surface flow downstream of reattachment is two-dimensional. The yarns upstream of reattachment in the separated region showed no motion at all, as if the air in this region were truly dead air. This vividly demonstrated the extremely low energy level of the low density, low velocity flow in the cavity beneath the free shear layer.

When the reattachment position determined by the yarn strands is indicated on the pressure plots of Figures 9a through 9i, the total pressure of the dividing stream line (stagnating streamline) at reattachment is determined, since this total pressure is equal to the local static pressure. If the flow to reattachment is assumed to be isentropic, the Mach number of the dividing stream line at the beginning

of recompression may be determined as follows:

The ratio of static to total pressure on the dividing stream line at reattachment is computed from:

$$(P/P_t)_{DSL} = \left(\frac{P_D}{P_\infty} \right) \left(\frac{P_\infty}{P} \right)_{reat} \quad (6)$$

From this pressure ratio, the Mach number of the dividing stream line at the beginning of reattachment is given by the isentropic relation:

$$M = \left[\frac{(P/P_t) \frac{1-\gamma}{\gamma-1}}{\frac{\gamma-1}{2}} \right]^{1/2} \quad (7)$$

Results of this determination are shown in Table IV for the 0.75 inch step at the various test conditions.

It is seen that in all cases the Mach number of the dividing stream line is subsonic, and is usually of the order $M = 0.6$ to 0.8 . This is lower than the Mach number of the dividing stream line given by the theories of Chapman and Korst. For the higher supersonic free stream Mach numbers these theories result in a supersonic dividing stream line.

(D) Probe Data:

To obtain information about the flow downstream of the step, vertical traverses at various distances downstream of the step were made with the combination thermocouple-pitot probe. Since the pitot probe was maintained in a fixed direction parallel to the free stream, the readings had to be corrected for flow angle by using the calibration curves of Figure 8. Figure 18 shows selected uncorrected pitot traverse data. Each curve corresponds to a fixed x position and represents the pitot reading distribution with y , the distance above the reattachment surface. These curves have been selected to show a typical traverse in each of the various regions

of the flow field. The curves $x = 0.06$, $x = 0.2$, and $x = 1.0$ are traverses through the separated region and the expansion fan. The local wave in these curves at $y = 0.3$ to 0.4 inches corresponds to the position of the lip shock visible in the shadographs of Figures 9a through 9i. Notice that there is no evidence of the lip shock in the probing just downstream of the step ($x = 0.06$), indicating that the shock does not extend to the step. The curves $x = 2.0$ and $x = 4.0$ are traverses downstream of reattachment. The sudden change in pitot reading at $y = 0.73$ inches indicates the position of the reattachment shock.

Probing of the cavity flow beneath the free shear layer with the crossed hot-wire probe and the direction sensing probe yielded little information about the flow. In many positions the direction sensing probe oscillated or rotated rapidly so that the local flow direction could not be determined. The flow angles computed from the hot-wire probe were not consistent with those which could be determined by the direction sensing probe and the computed velocities were much too high to be consistent with other observations of this low energy flow. For one flow condition which was examined, the direction sensing probe indicated a large recirculating vortex beneath the free shear layer with a small second vortex in the corner of the vertical riser and the cavity floor.

VI. PREDICTION OF BASE PRESSURE AND PEAK HEAT TRANSFER

From the experimental information described above the base pressure, the peak heat transfer and the location of the peak heat transfer may be empirically determined as follows:

- (a) Compute the step height Reynolds number $Re_h = \frac{u_\infty h}{\nu_\infty}$.
- (b) Determine whether the attached boundary layer at the separation point is laminar ($Re_L < 5 \times 10^5$), transitional ($5 \times 10^5 < Re_L < 10^6$), or turbulent ($Re_L > 10^6$).

(c) If the separating boundary layer is turbulent use Korst's theory (Figure 13) to determine the base pressure. If the separating boundary layer is laminar or transitional determine the base pressure from equation 1.

(d) Compute the value of the heat flux at separation (q_{sep}^*) by using standard attached boundary layer techniques. (For example Eckert's reference temperature method.)

(e) From Figure 15 determine the ratio $\left(q_{max}^* / q_{sep}^* \right)$ and from this compute the maximum heat flux at reattachment.

(f) Determine α/μ from equation 5 and from this calculate the distance to the position of peak heat transfer (x_{PHT}).

VII. ANALYSIS

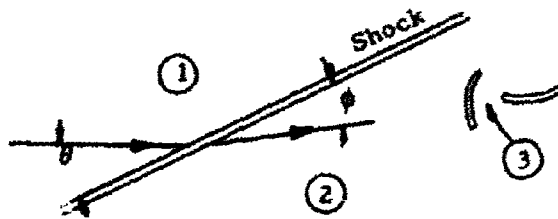
A detailed examination of the results reported above discloses the typical flow field shown in Figure 19 to exist downstream of the step. This figure shows that the complicated flow field is divided into regions which may be studied separately, then properly matched and fitted together. Each of these regions will be discussed separately below. Figures 20 through 22 show specific examples of this flow field constructed from experimental information and will be referred to in the discussion to follow. Figures 20 and 21 show static pressure changes and total head losses across the lip shock and the region of constant pitot reading beneath it. Figure 22 shows the complete flow field along with model pressures measured at each orifice. Also shown in Figure 22 are static pressure changes, Mach number changes, and total head losses across the reattachment shock.

(A) Corner Expansion and Lip Shock:

The flow approaches the separation point with a conventional boundary layer attached to the body, some portion of which is subsonic. This subsonic portion allows

pressure signals to be fed upstream of the step. Model pressure orifices placed upstream of, but very close to the separation point show that reduced pressure is felt upstream of the step. This effect is indicated in the pressure distributions of Figures 9a through 9i. Once this reduced pressure is communicated upstream, it is propagated into the supersonic flow along the local Mach waves resulting in a pressure gradient in both the horizontal and vertical direction in the vicinity of the separation point. Figures 23 and 24 show constant pressure lines in the expansion region as determined experimentally from corrected pitot readings and the assumption that the total pressure throughout this region is equal to the tunnel total pressure. The constant pressure lines are extended into the shear layer to points on the model of corresponding measured pressures. The exact location of these lines can not be determined because of the unknown pressure gradient within the shear layer. Notice the strong warping of the constant pressure lines in the case of Figure 23 and the lesser warping in Figure 24. Notice also the low pressures measured just above the 1° shock indicating a strong overexpansion. It is seen that these constant pressure lines are definitely not the straight constant pressure lines of the commonly used Prandtl-Meyer expansion. Comparison of the experimental fan with the theoretical Prandtl-Meyer fan further shows that the total included angle of the experimental fan is less than that of the Prandtl-Meyer fan required to expand to the same pressure. This same effect was reported in Reference 22. Figures 20 through 22 show a region of constant pitot reading immediately below the lip shock. It was at first assumed that this implied constant pressure in this region. Preliminary attempts to treat the lip shock as an oblique shock parallel to a constant pressure line with uniform conditions on each side and base pressure on the downstream side did not permit a consistent interpretation of the data. Closer examination showed that the lip shock varies in strength along its length, with the point of greatest strength being in the vicinity of the shock-shear layer intersection. Computations of the

flow conditions on two sides of an oblique shock were made using the measured constant total pressure upstream of the shock and the measured constant pitot reading downstream. Using the nomenclature of the accompanying sketch and equations for an oblique shock and for isentropic flow where appropriate, the procedure was as follows:



(a) Given P_{t1} and P_{t3}

(b) Assume various values of $\xi = P_2/P_1$

(c) Compute $P_{t2}/P_{t1} = \left[\frac{(\gamma+1)\xi + (\gamma-1)}{(\gamma-1)\xi + (\gamma+1)} \right] \frac{\gamma}{\gamma-1} \left[\xi - \frac{1}{\gamma-1} \right]$ (8)

(d) Compute $T_2/T_1 = \left[\frac{(\gamma-1)\xi + (\gamma+1)}{(\gamma+1)\xi + (\gamma-1)} \right]$ (9)

(e) Compute $P_{t3}/P_{t2} = \frac{(P_{t3}/P_{t1})}{(P_{t2}/P_{t1})}$ (10)

(f) Solve $P_{t3}/P_{t2} = \left[\frac{(\gamma+1) M_2^2}{(\gamma-1) M_2^2 + 2} \right]^{\frac{\gamma}{\gamma-1}} \left[\frac{\gamma+1}{2\gamma M_2^2 (\gamma-1)} \right]^{\frac{1}{\gamma-1}}$ (11)

explicitly for M_2

(g) Compute $T_2/T_{o2} = \left[1 + \frac{(\gamma-1)}{2} M_2^2 \right]^{-1} \frac{T_2/T_1}{T_2/T_{o2}}$ (12)

(h) Compute $T_1/T_{o1} = T_2/T_{o2} = \frac{T_2/T_1}{T_2/T_1}$ (13)

(i) Compute $M_1 = \left[\frac{1 - (T_1/T_{o2})}{(T_1/T_{o1}) \left(\frac{\gamma-1}{2} \right)} \right]^{1/2}$ (14)

$$(j) \text{ Compute } P_1 = P_{t_1} \left[1 + \left(\frac{\gamma-1}{2} \right) M_1^2 \right]^{\frac{\gamma}{\gamma-1}} \quad (15)$$

$$(k) \text{ Compute } P_2 = (P_2/P_1) P_1 \quad (16)$$

$$(l) \text{ Compute } \theta = \arcsin \frac{1}{M_1} \left[\frac{(\gamma+1)\xi + (\gamma-1)}{2\gamma} \right]^{1/2} \quad (17)$$

$$(m) \text{ Compute } \phi = \arctan \left[\frac{(\gamma-1)\xi + (\gamma+1)}{(\gamma+1)\xi + (\gamma-1)} \tan \theta \right] \quad (18)$$

Multiplying and dividing the right hand side of this equation by ξ gives:

$$\phi = \arctan \left\{ \frac{\xi \left(\frac{(\gamma-1)\xi + (\gamma+1)}{(\gamma+1)\xi + (\gamma-1)} \right)}{\xi} \tan \theta \right\} \quad (19)$$

$$\phi = \arctan \left\{ \left[\frac{T_2/T_1}{P_2/P_1} \right] \tan \theta \right\} \quad (20)$$

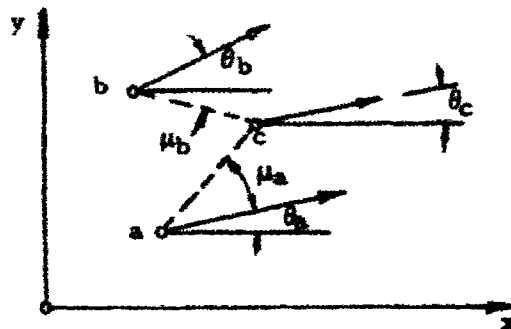
Most of the labor of the computation of these equations was eliminated by using the appropriate tables of Reference 23. A representative result is shown in Figure 25 where all variables are shown as a function of the pressure upstream of the shock. This figure shows that the total head losses decrease with increasing upstream pressure while the downstream pressure decreases to an essentially constant value reached when the pressure ratio P_1/P_2 is about 0.5. The flow angles and the total head losses continue to change with increasing P_1 ; the flow angles approach the Mach angle while the total head losses decrease to zero. It is thus clear that even though the total pressure is constant upstream of the shock and the pitot reading is constant downstream of the shock, the shock strength and flow conditions on both sides of the shock are not necessarily uniform.

For the $M_\infty = 2.5$ data it was found that at the high Reynolds number of this test the downstream pressure P_2 was somewhat below the measured base pressure. For this case curve (a) in Figure 25 represents base pressure. The intersection of the P_2 and (a) curve is the point where the pressure downstream of the shock is equal to base pressure and it is seen that the total head losses are greatest at this point with the losses decreasing as P_2 becomes less than base pressure. An example of this case is shown in Figure 20 where several streamlines are shown crossing the lip shock. At these crossings the pressure change and loss of total pressure are shown. Notice the decrease in total head loss with increasing distance from the shear layer. At intermediate Reynolds numbers P_2 was approximately equal to base pressure while at the low Reynolds numbers of the test P_2 was slightly above base pressure. The same trends were seen in the $M_\infty = 3.5$ data, but in much milder form. The $M_\infty = 5.0$ data were not investigated in this regard.

To further investigate the appearance of the lip shock and the deviation of the actual expansion from a Prandtl-Meyer expansion an inviscid rotational characteristics solution was obtained for the case shown in Figure 24 assuming isoenergetic flow. This solution should be a valid approximation in this region because:

- (a) In the rapid corner expansion, viscous forces are small compared to pressure forces and may be neglected.
- (b) The entropy gradients in the approaching rotational boundary layer flow are taken into account.
- (c) The flow to separation is over an adiabatic surface, so that the flow is essentially isoenergetic.
- (d) The warping of the expansion fan and the presence of the lip shock, which the experimental data show to exist over a great distance, must be due to inviscid effects rather than to viscous effects.

The properties of the point c (see accompanying sketch), any interior point of the flow, which lies at the intersection of the characteristic (Mach) lines through points a and b are determined from the following known quantities of points a and b: x, y, M, T_0, S , and the related quantities T, v, θ, μ and u .



If this expansive flow field is assumed to be isenergetic ($T_0 = \text{Constant}$), the equations relating these quantities are the following (24):

$$v_c - \theta_c = v_a - \theta_a - \frac{\cot \mu_a}{u_a^2} \left[g T_a (S_c - S_a) \right] \quad (21)$$

$$v_c + \theta_c = v_b + \theta_b - \frac{\cot \mu_b}{u_b^2} \left[g T_b (S_c - S_b) \right].$$

An initial guess of $S_{c1} = \frac{S_a + S_b}{2}$ allows the calculation of a trial v_c and θ_c and the determination of a trial M_c from the isentropic relation

$$v_c = \sqrt{\frac{\gamma+1}{\gamma-1}} \arctan \sqrt{\left| \frac{\gamma-1}{\gamma+1} \right|} (M_c^2 - 1) - \arccos \left(\frac{1}{M_c} \right). \quad (22)$$

Also a trial μ_c may be calculated: $\mu_c = \arcsin \left(\frac{1}{M_c} \right)$ (23)

From the geometry of the sketch it may be seen that if average angles are used the following equations relate the position of point c to those of a and b:

$$y_c - y_a = \left[\tan \left(\frac{\theta_a + \theta_c}{2} + \frac{\mu_a + \mu_c}{2} \right) \right] (x_c - x_a)$$

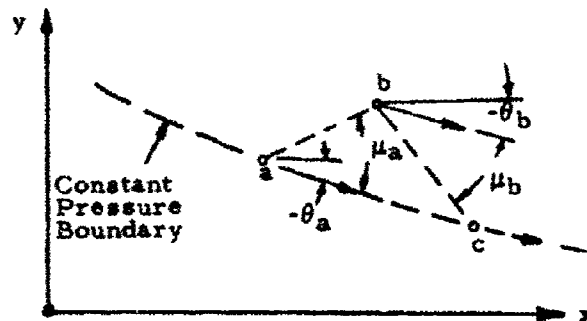
$$y_c - y_b = \left[\tan \left(\frac{\theta_b + \theta_c}{2} - \frac{\mu_b + \mu_c}{2} \right) \right] (x_c - x_b) \quad (24)$$

The entropy at point c may then be determined from (25):

$$S_c = S_a + \frac{(S_b - S_a) (X_c - X_a) \left[\frac{\sin \nu_a}{\cos (\theta_a + \nu_a)} \right]}{(X_c - X_a) \left[\frac{\sin \nu_a}{\cos (\theta_a + \nu_a)} \right]} + (X_c - X_b) \left[\frac{\sin \nu_b}{\cos (\theta_b + \nu_b)} \right] \quad (25)$$

The value of S_c computed from equation (25) is compared to the initial guess S_{c_1} . If they do not agree replace S_{c_1} with the value S_c computed from (25) and repeat the computation. Satisfactory agreement was usually obtained in three or less iterations.

For a point on the inner constant pressure boundary of the expanding shear layer the calculation is simpler than the procedure above. For this case



$S_c = S_a$ and $M_c = M_a$. Therefore S_c , M_c , v_c , u_c , T_c , and ρ_c are known and all that remains to be calculated are the flow angle and position of point c. These may be obtained from the following equations:

$$\theta_c = \nu_b - \nu_c + \theta_b - \frac{\cot \mu_b}{u_b} \left[g T_b (S_c - S_b) \right] \quad (26)$$

$$y_c - y_a = \left[\tan \theta_a \right] (x_c - x_a)$$

$$y_c - y_b = \left[\tan \left(\frac{\theta_b + \theta_c}{2} - \frac{\mu_b + \mu_c}{2} \right) \right] (x_c - x_b) \quad (27)$$

In the inviscid flow considered here a line of constant entropy is a streamline and also a line of constant total pressure. If the entropy of the free stream is assigned the value of zero ahead of the expansion where the total pressure is P_{∞} ,

then at any point c in the flow the total pressure is

$$P_{0c} = \frac{P_{0\infty}}{(S_c/R)^e} \quad (28)$$

The local static pressure may then be computed from

$$P_c = P_{0c} \left[1 + \left(\frac{\gamma - 1}{2} \right) M_c^2 \right]^{-\frac{\gamma}{\gamma - 1}} \quad (29)$$

The initial conditions required to start the solution were obtained from experimentally measured pitot readings and an assumed pressure distribution at the separation station. Solutions obtained for several different static pressure distributions showed widely varying results, indicating the importance of the pressure variation at separation. The pressure distribution which gave results very close to those actually measured was obtained as follows:

(a) The surface pressure at separation (the $x = 0$ station) was obtained from a linear extrapolation of nearby measured surface pressures. (This value was approximately 87% of free stream pressure).

(b) The pressure at the $x = 0$ station was assumed to vary linearly from the above surface pressure to free stream pressure at the point where the pitot probe read essentially its free stream value. Above this point the pressure was of course assumed constant at the free stream value. The Mach number distribution at $x = 0$, as determined from the experimental pitot readings and the above pressure distribution, is seen in Figure 26 to be a simple linear function of y . Since the method of characteristics may not be applied to steady subsonic flow the mass of fluid below the $M_1 = 1$ streamline was neglected in this computation and the expanded $M_1 = 1$ streamline was considered to be the edge of the free shear layer at the constant base pressure. Furthermore, since the exact shape of the $M_1 = 1$ streamline through the expansion is unknown it was assumed that this streamline instantaneously passed

from its upstream zero deflection angle at $x = 0$ to the deflection angle given by a Prandtl-Meyer expansion to base pressure. The computation of this expansion was carried out on an IBM 709⁴ computer and the results are presented in Figures 27, 28 and 29.*

Figure 27 shows the characteristics networks resulting from this computation. The coalescing of the compression waves, which are reflections of expansion waves off the constant pressure shear layer boundary, into the lip shock is clearly evident. Experimentally, no evidence of the lip shock was found at $x = 0.2$. The experimentally measured positions of the lip shock at $x = 0.4$ and $x = 0.6$ are shown in this figure. It is seen that the calculated position matches the measured positions very well. An examination of the pressures printed out by the computer shows a very slight increase in pressure at the leading edge of the expansion. Apparently this increase in pressure becomes more pronounced with increasing Reynolds number (reflected in these computations as a change in the initial Mach number and pressure distributions) resulting in the secondary lip shock at the beginning of the expansion which was mentioned above.

Figure 28 shows computed lines of constant pressure. Comparison of this figure with Figure 24, the experimentally determined lines of constant pressure, shows good agreement for all values except the $P = 0.391$ line. However, the computed constant pressure lines do not show the tendency toward warping which the experimentally determined constant pressure lines show. An explanation for this warping is not available at the present time. Notice that the low pressure region, as evidenced by the

* While performing this analysis the author became aware of a similar treatment of the corner expansion by Weiss and Weinbaum (26).

$P = 0.064$ line (and consequently the overexpansion and the recompression lip shock) does not originate at a solid boundary, but rather originates within the flow in order to satisfy the imposed boundary conditions. The lower $P = 0.092$ line is the lower edge of the shear layer at the constant base pressure.

Figure 29 shows some typical streamlines as they pass through the expansion and recompression region into the constant base pressure region. The location of the lip shock in this figure was determined from Figure 27. Notice that all streamlines which pass beneath the lip shock (not through it) are first convex upward, then concave upward (in the case of the edge streamline, the convex position has been contracted to a single point) while those which pass through the lip shock are convex upward above it and approximately straight below it.*

(B) Constant Base Pressure Region:

A region of essentially constant base pressure exists immediately behind the step riser. Although a pressure gradient has been seen to exist in the region of constant pitot reading downstream of the lip shock, in most instances this gradient is small. This essentially constant base pressure region is bounded by the model surfaces, the lip shock and the beginning of the pressure rise associated with the turning of the flow parallel to the downstream surface (the origin of the reattachment shock). As seen in Figure 19, the free shear layer and the recirculating cavity flow beneath it are both included in this region.

(C) Free Shear Layer:

The free shear layer lies within the region of constant base pressure and consists of two parts, the outer driving portion and the inner driven portion which are separated by the "dividing stream line". All of the fluid which comes over the step

* A slight error is involved in these calculations in the vicinity of the lip shock. No provision has been made for an increase in entropy with the result that the calculations show recompression beginning ahead of the shock and continuing beyond the shock.

remains above the dividing stream line and continues downstream while the fluid which makes up the driven portion is a part of the low velocity recirculating vortex flow in the cavity. This interpretation of the shear layer requires that the velocity profiles contain a point of inflection on the dividing stream line, with the driving profiles concave upward and the driven profiles convex upward. Probing of the free shear layer with the pitot probe shows the upper portion of the velocity profiles to be concave upward, but the velocity on the lower side of the shear layer falls off so rapidly that it is not possible to determine the location of the point of inflection. As mentioned above, experimental evidence obtained at reattachment shows the velocity of the dividing stream line to be subsonic at a Mach number of 0.6 to 0.8. Any successful theoretical analysis of the free shear layer must treat it as a constant pressure viscous free shear layer with starting profiles obtained from a consideration of the flow emerging from the corner expansion and lip shock region.

(D) Recirculating Cavity Flow:

As seen in Figure 19, the recirculating cavity flow is at essentially constant base pressure, except for a small portion at reattachment. Attempts to experimentally measure the flow characteristics in this region met with little success. Probing with the pitot probe, the direction sensing probe and the crossed hot-wire probe yielded no conclusive information. Surface oil flow studies and yarn tufts attached to the model surface gave no indication of surface flow conditions in this region. All indications are that the flow in the cavity is a very low energy flow. It is a separate flow from the external flow, coupled to it and driven by shear forces acting along the dividing stream line. Since the flow velocity is so low, the total pressure of this flow is essentially equal to base pressure. The measured total temperature was essentially constant throughout the region at a value approximately half way between free stream total temperature and the cooled model surface

temperature. In some cases indications were that this recirculating flow is made up of two vortices as shown in Figure 19.

(E) Reattachment Region:

In the reattachment region the pressure on the model surface rises from the constant base pressure (P_b) to the constant reattachment pressure (P_r). In this process compression waves travel from the surface through the reattaching shear layer into the "inviscid" flow above. Most of the reattaching shear layer is supersonic and these waves emerge from the top of the shear layer at the local Mach angle relative to the flow. As the flow streamlines cross these compression waves, they are deflected and slowed down so that succeeding compression waves coalesce and form the beginning of the reattachment shock as shown in Figure 19. Close examination of Figures 9a through 9i shows that for the high Reynolds numbers runs of this investigation the pressure rise is steep and the reattachment shock appears to be a continuation of the top of the shear layer. For the low Reynolds number cases the pressure rise is more gradual with a slower coalescing of the pressure waves into the reattachment shock. In this case the reattachment shock becomes visible in the shadowgraph only at a considerable distance above the top of the shear layer. Pitot pressure probings of this region also indicate this type of flow structure. As compression continues, the reattachment shock becomes stronger, swings around and extends into the inviscid flow intersecting the lip shock and the corner expansion fan. In passing through the reattachment shock, the expanded flow is turned parallel to the reattachment surface. The reattachment shock continually varies in strength along its length since each streamline approaching it in the expansion is at a different flow angle and Mach number.

Examination of the heat transfer distributions of Figures 9a through 9i shows that the heat transfer increases from the low cavity value at the stagnation line to a maximum value in the neighborhood of the neck of the reattaching shear layer where

the pressure is essentially constant. This is in opposition to the usual condition at a stagnation point where the heat transfer is a maximum at stagnation and decreases from the value. An explanation for this heat transfer distribution is not available at the present time.

The compression and turning of the reattaching shear layer is believed to be nearly isentropic (small heat transfer and no shocks) with the reattachment shock being formed above it by the coalescing of compression waves originating in the reattaching shear layer. It is believed that this region may be handled as an inviscid rotational compressor in a manner similar to that used in the corner expansion, since in this region also the viscous forces will be of much smaller magnitude than the pressure forces.

(F) Constant Pressure Reattached Flow Region:

Downstream of the reattachment region and the reattachment shock the flow is parallel to the model surface and the pressure is essentially constant at some value less than free stream pressure. Other investigators have found similar results for two-dimensional models, however, investigators using axi-symmetric models have found reattachment pressures to be higher than free stream pressure.

Figure 30 shows a typical pressure distribution downstream of separation and the averaging process used to determine a mean constant reattachment pressure (P_r) from the experimental data. Figure 31 shows a plot of the recompression ratio (P_r/P_∞) vs. Re_h for $M_\infty = 2.5$ while Figure 32 shows the same plot for $M_\infty = 3.5$ and 5.0. The recompression pressure for the low Reynolds number $M_\infty = 5.0$ tests could not be determined because the pressure did not reach a constant value within the length of the instrumented reattachment surface of the model. For the $M_\infty = 3.5$ and 5.0 data a good linear correlation is evident, while for the $M_\infty = 2.5$ data the ratio appears to approach a constant value at the higher Reynolds numbers. Examination of Figures 31 and 32 shows that for each Mach number a critical Reynolds number exists where the

recompression ratio is a maximum value. The significance of this critical Reynolds number is not yet clear, however, it appears that its value increases with increasing Mach number.

The flow downstream of the reattachment shock is a parallel rotational type flow because each streamline of the expansion fan approaches the shock at a different flow angle and a different Mach number and each is turned through a different angle. There is thus a variation in total pressure across the constant pressure flow. This is evident in Figure 33 where the total pressure distribution between the model surface and the reattachment shock is shown for three probe positions of the flow shown in Figure 22. These total pressure distributions were obtained from pitot probe readings and the assumption of constant pressure at each station. These probings also show the presence of the slip line which originates at the intersection of the lip shock and the reattachment shock. A slip line of this type is most clearly visible in the shadowgraph photograph of Figure 9b.

VIII. CONCLUSIONS

Examination of the results of this investigation along with the results of other investigators leads to the following conclusions:

(1) For the case where a laminar approach boundary layer is present and the flow is laminar throughout, the base pressure is a rather strong function of step height and is considerably higher than the value predicted by the Chapman theory.

(2) When the approach boundary layer is turbulent and the flow is turbulent throughout Korst's theory may be used to predict base pressure.

(3) The flow in the cavity beneath the free shear layer is an extremely low energy flow with small heat transfers. The maximum heat transfer occurs somewhat downstream of the stagnation line at the neck of the reattaching shear layer. When large values of heat transfer are obtained there they appear to be due to transition to turbulence in the reattaching shear layer.

(4) For the transitional type of flows of this investigation the Reynolds number based on step height (Re_h) is an important parameter. Both the base pressure and the maximum heat transfer may be predicted as a function of this parameter.

(5) For the body shapes of this investigation (rearward facing step and overhang) and those investigated by Hastings (14) (undercut rearward facing step) the development of the flow downstream of separation is independent of the shape of the vertical riser.

(6) The Mach number of the dividing streamline at reattachment is subsonic and of the order of $M = 0.6$ to 0.8 .

(7) The rapid corner expansion and the appearance of the lip shock may be accurately described by the method of inviscid rotational characteristics if the correct starting conditions are used.

(8) The reattachment pressure ratio is always less than unity for the two-dimensional case and has a maximum value at some critical Reynolds number which is a

function of Mach number.

- (9) The flow downstream of reattachment is a parallel rotational type flow.

IX. RECOMMENDATIONS FOR FUTURE WORK

A continuation of the experimentation and analysis described in this report is required before a complete understanding of the complicated flow field under investigation is obtained. Research which would seem to be fruitful at the present time is the following:

- (1) Extension of the present investigation to both higher and lower Reynolds numbers. Extension to lower Reynolds numbers should be done to verify that the base pressure becomes constant and independent of Reynolds number and that the maximum heat transfer falls off as predicted. The experiments should be extended to higher Reynolds numbers to determine how the base pressure varies with Reynolds number and to verify that the base pressure again becomes constant and independent of Reynolds number at the higher Reynolds numbers as predicted by Korst.

- (2) The shock equations should be incorporated into the procedure used to calculate the rapid corner expansion so that property changes across the lip shock may be accounted for.

- (3) Further experimental and analytical investigation of the free shear layer, the low energy cavity flow, the reattachment region and the flow downstream of reattachment is necessary.

- (4) Additional checks of heat transfer measured in a shock tube vs. that measured in a wind tunnel are necessary to determine the validity of the shock tube heat transfer measurements.

X. REFERENCES

1. Chapman, D. R., "An Analysis of Base Pressure at Supersonic Velocities and Comparison With Experiments." NACA TR 1051, 1951.
2. Korst, H. H., Page, R. H., and Childs, M. E., "A Theory for Base Pressure in Transonic and Supersonic Flow." University of Illinois, ME TN 392-2, March 1955.
3. Crocco, L. and Lees, L., "A Mixing Theory for the Interaction Between Dissipative Flows and Nearly Isentropic Streams." Journal of Aeronautical Sciences, Volume 19, No. 10, October 1952, Pp 649-676.
4. Chapman, D. R., Kuehn, D. M., and Larson, H. K., "Investigation of Separated Flows in Supersonic and Subsonic Streams with Emphasis on the Effect of Transition." NACA Report 1356, 1958.
5. Nash, J. F., "An Analysis of Two-Dimensional Turbulent Base Flow Including the Effect of the Approaching Boundary Layer." ARC R&M 3344, 1963.
6. Ginox, J., "Experimental Evidence of Three-Dimensional Perturbations in the Reattachment of a Two-Dimensional Laminar Boundary Layer at $M = 2.05$." Brussels University Training Center for Experimental Aerodynamics TN-1, 1958.
7. Roshko, A. and Thomke, G. J., "Flow Separation and Reattachment Behind a Downstream Facing Step." Douglas Report S4-43056-1, January 1964.
8. Rom, J. and Segner, A., "Laminar Heat Transfer to a Two-Dimensional Backward Facing Step From the High Enthalpy Supersonic Flow in the Shock Tube." AIAA Journal, Volume 2, No. 2, Pp. 251-255, February 1964.
9. Rom, J. "Near Wake Flow Studies in Supersonic Flow". Technion-Israel Institute of Technology, Haifa, Israel, TAE Report No. 38, March 1965.
10. Test Facilities Handbook, (5th Edition). "von Karman Gas Dynamics Facility, Volume 4." Arnold Engineering Development Center, July 1963.
11. Scherberg, M. G. and Smith, H. E., "Experimental Study of the Flow Structure and Heat Transfer for a Rearward Facing Step in Supersonic Flow" Paper presented at the VIII Israel Annual Conference For Aviation and Astronautics, February 1966. Published in Israel Journal of Technology Volume 4, No. 1, Pp. 55-62, 1966.
12. Scherberg, M. G. and Smith, H. E., "On the Supersonic Flow Structure for a Rearward Facing Step" Paper presented at the 5th U. S. National Congress of Applied Mechanics. Minneapolis, Minnesota. June 1966. Submitted to AIAA Journal for publication.
13. Hama, F. R., "Estimation of the Strength of Lip Shock." AIAA Journal, Volume 4, No. 1, Pp. 166-167, April 1966.
14. Hastings, R. C., "Turbulent Flow Past Two-Dimensional Bases in Supersonic Streams." RAE TN No. Aero. 2931, December 1963.

15. Thomann, H., "Measurements of Heat Transfer and Recovery Temperature in Regions of Separated Flow at a Mach Number of 1.8." The Aeronautical Research Institute of Sweden (FFA) Report 82, 1959.
16. Rom, J., "Supersonic Flow Over Two-Dimensional and Axially Symmetric Backward Facing Steps." Technion-Israel Institute of Technology, Haifa, Israel, TAE Report No. 33, March 1964.
17. Eckert, E. R. G., "Survey of Boundary Layer Heat Transfer at High Velocities and High Temperatures." WADC TR 59-624, April 1960.
18. Holloway, P. F., Sterrett, J. R., and Creekmore, H. S., "An Investigation of Heat Transfer within Regions of Separated Flow at a Mach Number of 6.0." NASA TN D-3074, November 1965.
19. Strack, S. L., "Heat Transfer at Reattachment of a Turbulent Boundary Layer." Boeing Document No. D2-22430, April 1963.
20. Strack, S. L. and Lorenz, G. C., "Heat Transfer at Reattachment of a Turbulent Boundary Layer at $M = 6.0$." Boeing Document No. D2-23058, March 1964.
21. Donaldson, J. C., and Myers, A. W., "Investigation of the Separation and Reattachment of Flow Downstream of Two-Dimensional, Rearward-Facing Steps at Mach Numbers 2.5, 3.5, 5." AEDC-TR-66-106, May 1966.
22. Murthy, K. R. A. and Hammit, A. G., "Investigation of the Interaction of a Turbulent Boundary Layer with Prandtl-Meyer Expansion Fans at $M = 1.83$." Princeton University, AROSR TM 58-839, August 1958.
23. Ames Research Staff, "Equations, Tables and Charts for Compressible Flow." NACA Report 1135, 1953.
24. Liepmann, H. W. and Roshko, A. Elements of Gasdynamics John Wiley and Sons, Inc. New York, Pp. 295, 1960.
25. Sears, W. R. Edition, General Theory of High Speed Aerodynamics, Princeton University Press, Princeton, New Jersey, Pp. 636, 1954.
26. Weiss, R. F. and Weinbaum, S., "Hypersonic Boundary Layer Separation and the Base Flow Problem." AVCO Everett Research Laboratory Research Report 221, July 1965.

Table I - Instrumentation

Free Stream Mach Number	Pitot Pressure Transducer	Model Pressure Transducer	Model Temperature
2.5	50 psid Calibrated for ranges of 20, 10, 5 psi \pm 1.0%	15 psid Calibrated for ranges 15, 5, 1 \pm 0.2%	Tunnel A Temperature Scanner \pm 0.75 °F
3.5	15 psid Calibrated for ranges of 15, 5, 1 psi \pm 1.0%	15 psid Calibrated for ranges 15, 5, 1 \pm 0.2%	Tunnel A Temperature Scanner \pm 0.75 °F
5.0	15 psid Calibrated for ranges of 15, 5, 1 psi \pm 1.0%	1 psid Calibrated for ranges of 1.0 psi \pm 0.3% 0.3 psi \pm 0.5% 0.06 psi \pm 2.0%	Berkman 210 Digital Con- verter \pm 0.5 °F

Table II - Tunnel Conditions

Nominal Free Stream Mach Number & Total Temperature	Nominal Tunnel Stagnation Pressure psia	Nominal Free Stream Reynolds Number Per Inch $\times 10^{-6}$	Data Obtained
$M_{\infty} = 2.5$ $T_0 = 620 \text{ }^{\circ}\text{R}$	4.5	.06	Pres. & Heat Transfer
	5.5	.08	Pressure Only
	7.5	.11	Pressure Only
	11.0	.16	Pres. & Heat Transfer
	14.5	.20	Pressure Only
	18.5	.26	Pres. & Heat Transfer
	23.0	.32	Pressure Only
	27.0	.37	Pres. & Heat Transfer
33.0	.46	Pres. & Heat Transfer	
$M_{\infty} = 3.5$ $T_0 = 630 \text{ }^{\circ}\text{R}$	7.5	.06	Pres. & Heat Transfer
	13.0	.11	Pressure Only
	19.0	.15	Pres. & Heat Transfer
	25.5	.20	Pressure Only
	31.5	.25	Pres. & Heat Transfer
	38.0	.30	Pressure Only
	44.5	.35	Pres. & Heat Transfer
	50.5	.40	Pressure Only
54.5	.43	Pres. & Heat Transfer	
$M_{\infty} = 5.0$ $T_0 = 680 \text{ }^{\circ}\text{R}$	28.0	.10	Pres. & Heat Transfer
	42.0	.14	Pres. & Heat Transfer
	71.0	.24	Pres. & Heat Transfer
	84.0	.28	Pres. & Heat Transfer
	126.0	.42	Pres. & Heat Transfer
	140.0	.47	Pressure Only
	150.0	.50	Pres. & Heat Transfer

Table III - Pitot Probe Survey Conditions

Nominal Free Stream Mach Number & Total Temperature	Nominal Tunnel Stagnation Pressure psia	Nominal Step Height Inches
2.5 $T_0 = 620 \text{ }^\circ\text{R}$	18.5	0.443
3.5 $T_0 = 630 \text{ }^\circ\text{R}$	31.5 54.5	0.443 & 0.750 0.443 & 0.750
5.0 $T_0 = 680 \text{ }^\circ\text{R}$	84.0 150.0	0.443 & 0.750 0.443 & 0.750

Table IV - Dividing Stream Line Mach Number For 0.75 Inch Step

M_∞	P_o psia	M_{DSL}
2.5	4.5	0.21
	18.5	0.75
	27.0	0.81
	33.0	0.37
3.5	7.5	0.78
	19.0	0.86
	31.5	0.63
	44.5	0.54
	54.5	0.84
5.0	42.0	0.69
	84.0	0.86
	126.0	0.98
	140.0	0.72
	150.0	0.82

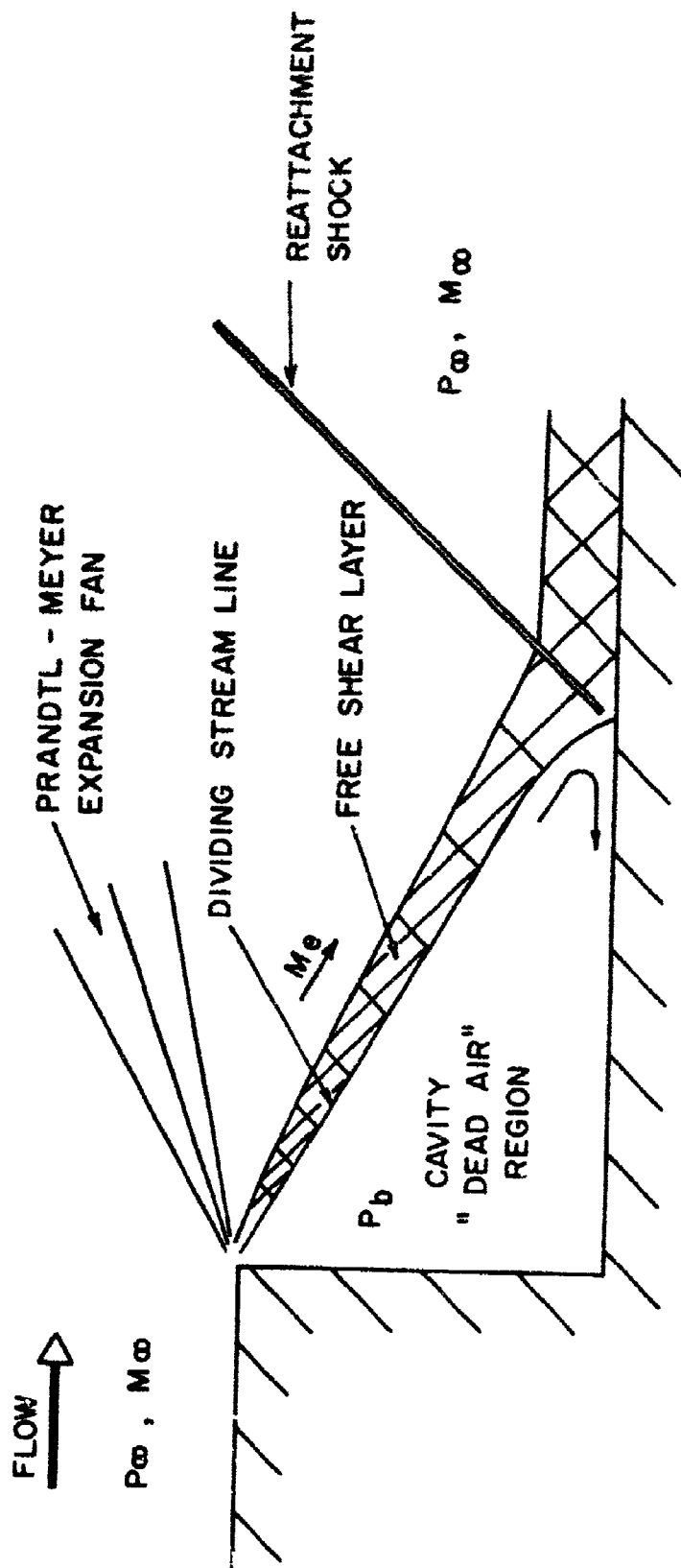
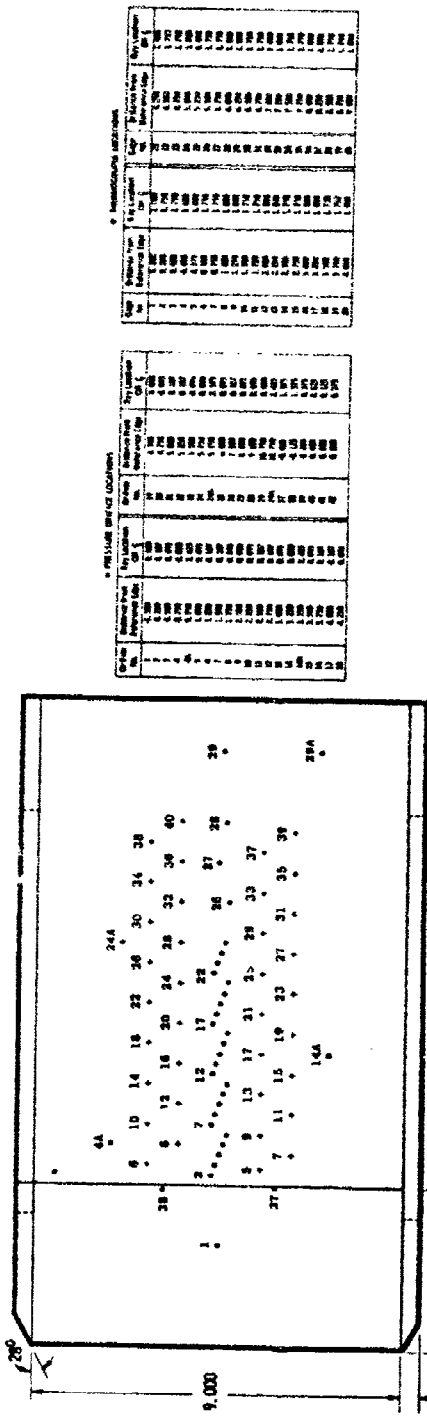


Fig. 1 CHAPMAN - KORST MODEL FOR SUPERSONIC FLOW OVER REARWARD FACING STEP.

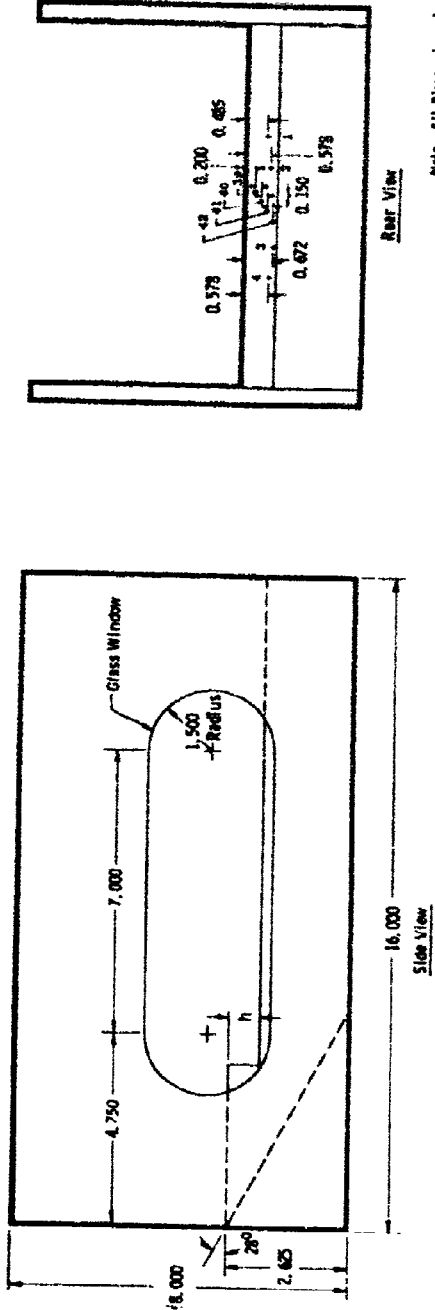


PRE-LAMB BENCH LOCATIONS

Point	Reference File	Part						
1
2
3
4
5
6
7
8
9
10
11
12
13
14
15
16
17
18
19
20
21
22
23
24
25
26
27
28
29
30
31
32
33
34
35
36
37
38
39
40
41
42
43
44

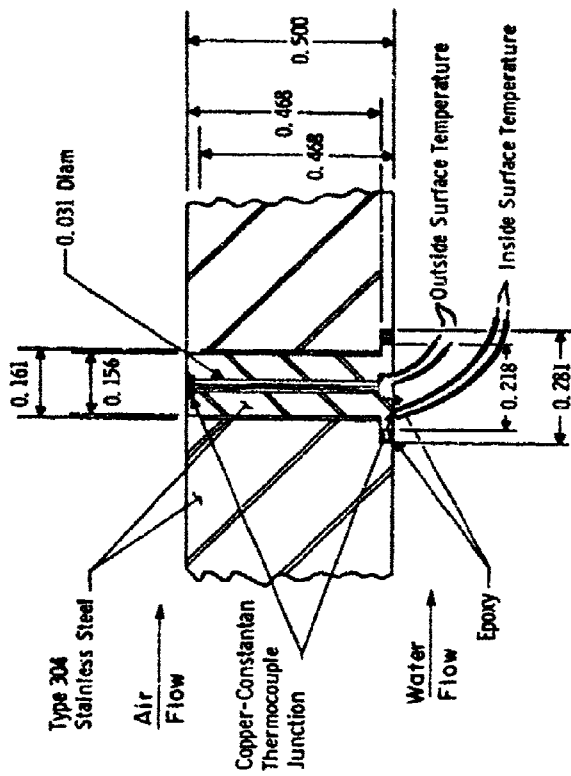
POST-LAMB BENCH LOCATIONS

Point	Reference File	Part						
45
46
47
48
49
50
51
52
53
54
55
56
57
58
59
60
61
62
63
64
65
66
67
68
69
70
71
72
73
74
75
76
77
78
79
80
81
82
83
84
85
86
87
88
89
90
91
92
93
94
95
96
97
98
99
100



Note: All Dimensions in Inches

Fig. 2 Model Details



Note: All Dimensions in Inches

Fig. 3 HEAT TRANSFER GAUGE DETAILS

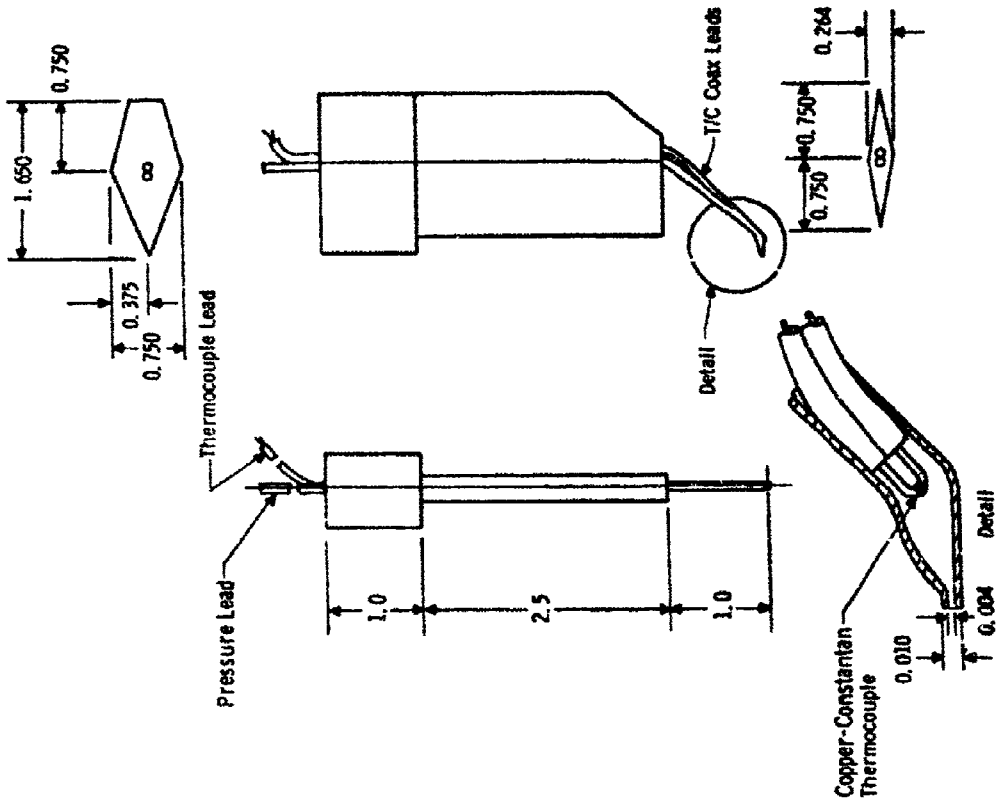
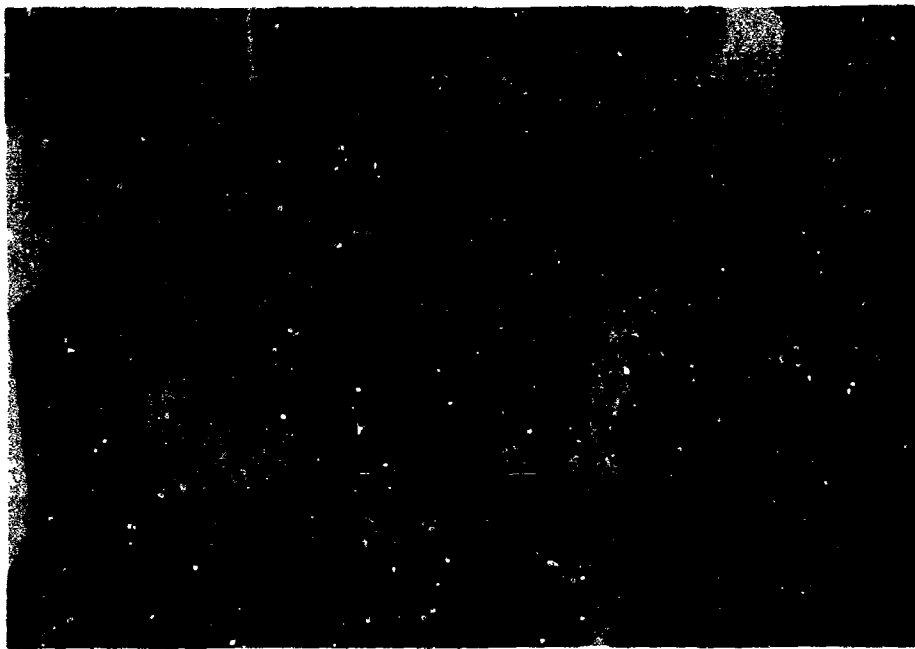


Fig. 4 COMBINATION THERMOCOUPLE PITOT PROBE DETAILS

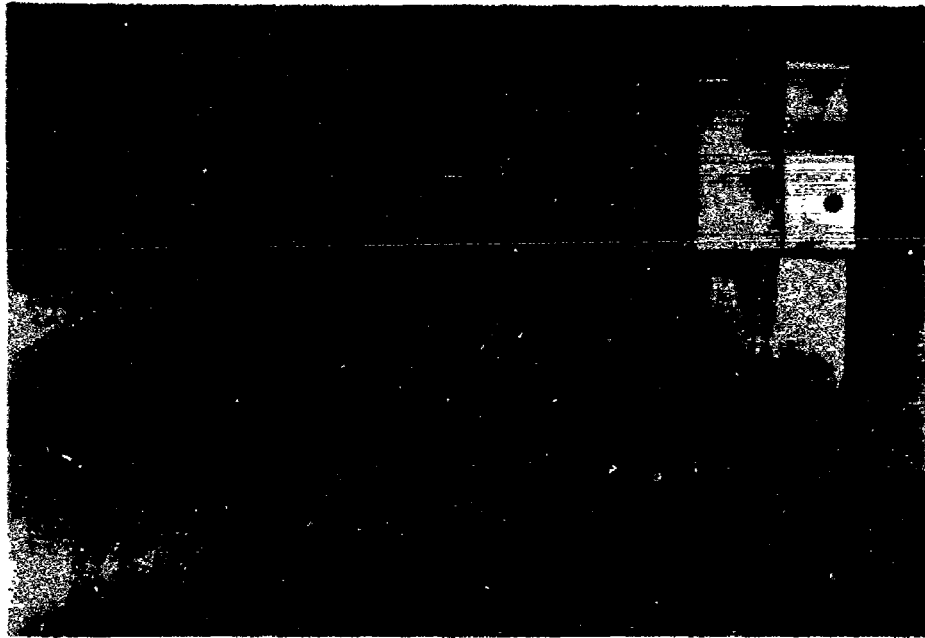


a. Side View



b. Front View Showing Survey Probe

Fig. 5 MODEL PHOTOGRAPHS

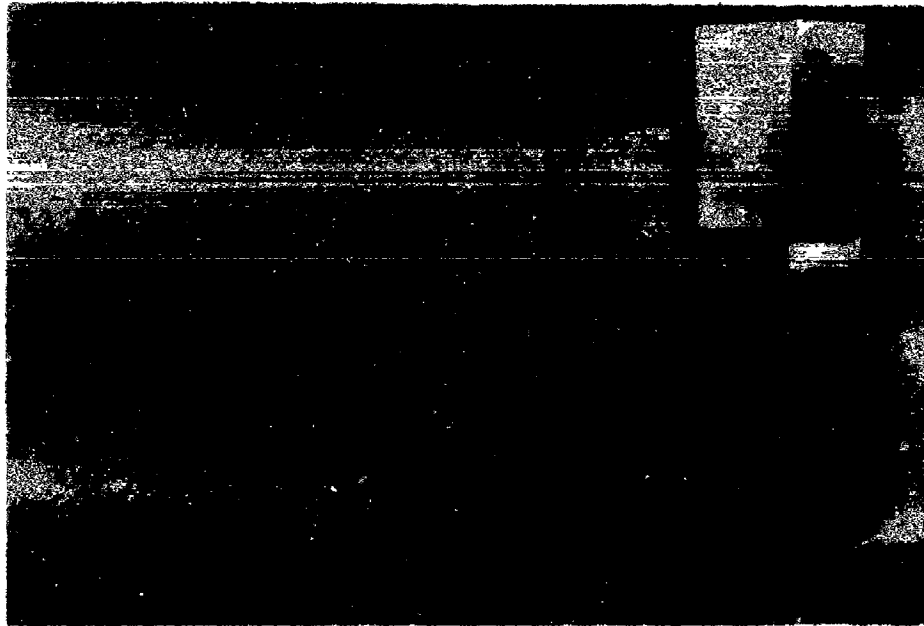


a. Side View



b. Detail of Hot Wire Support Needles

Fig. 6 CROSSED HOT WIRE PROBE



a. Side View



b. Detail of Direction Sensing Flags

Fig. 7 DIRECTION SENSING PROBE

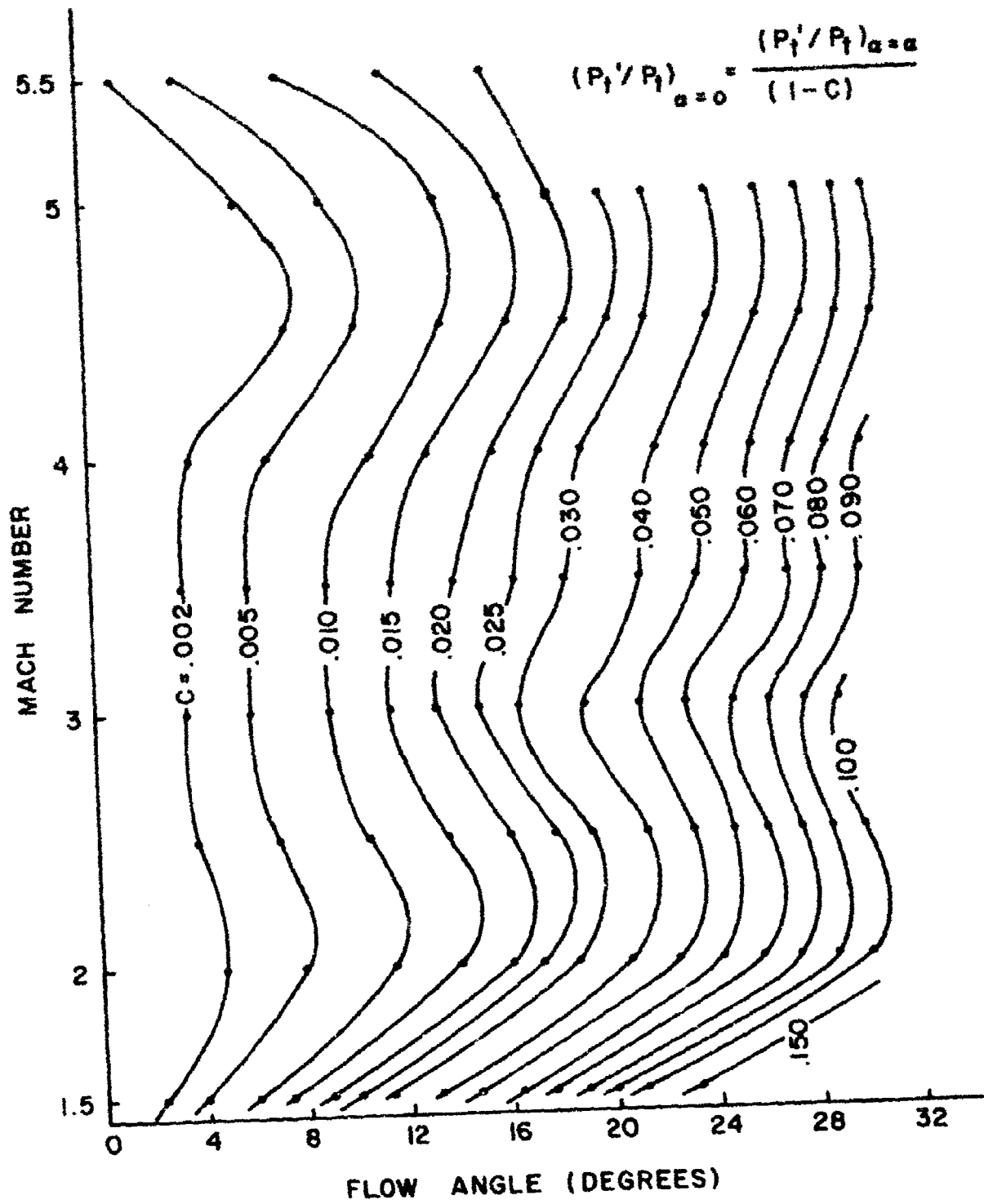


Fig. 8 PITOT PROBE CALIBRATION FOR LOCAL FLOW ANGLE CORRECTION.

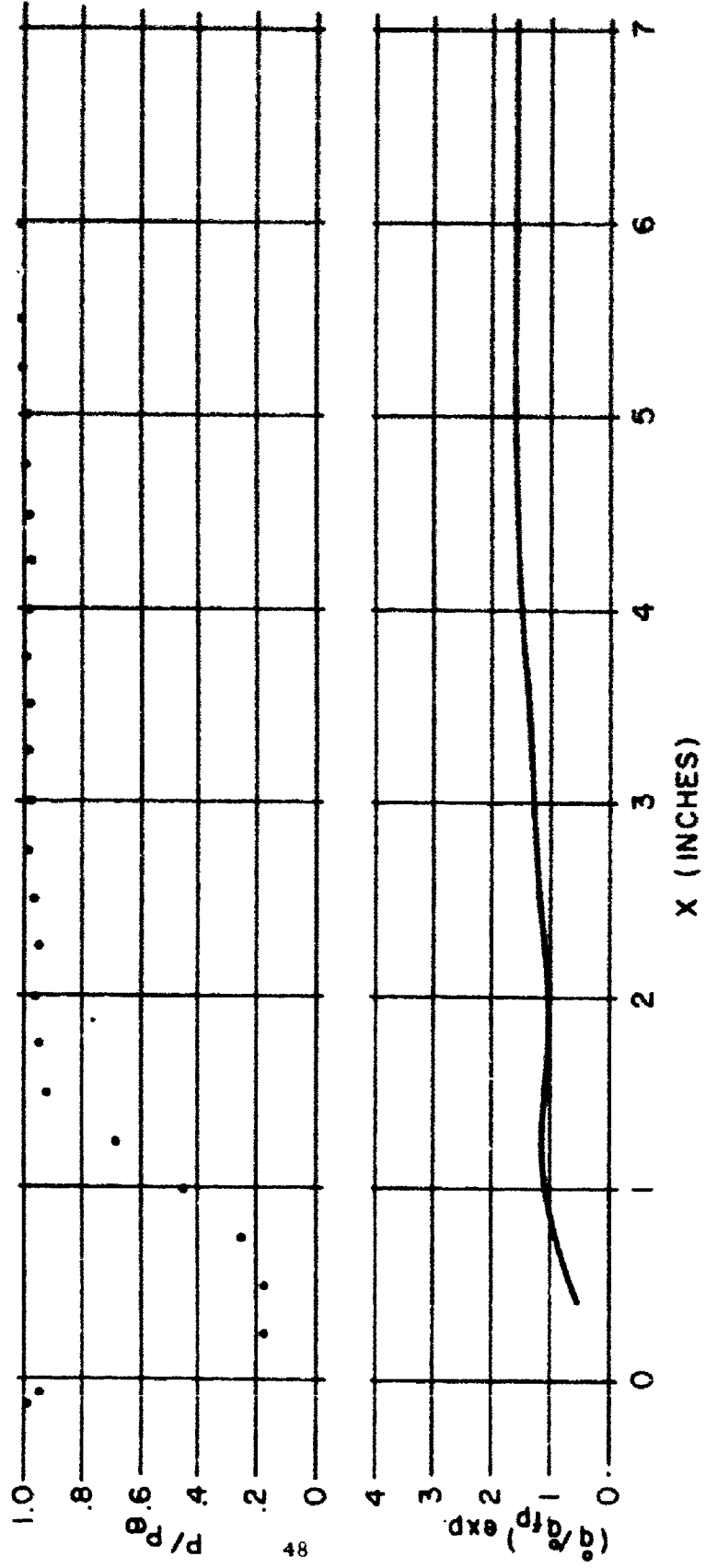


Fig. 9a SHADOGRAPH, PRESSURE AND HEAT FLUX DISTRIBUTION FOR
 $h = 0.443$ $M_\infty = 2.5$ $P_0 = 33$ PSIA.

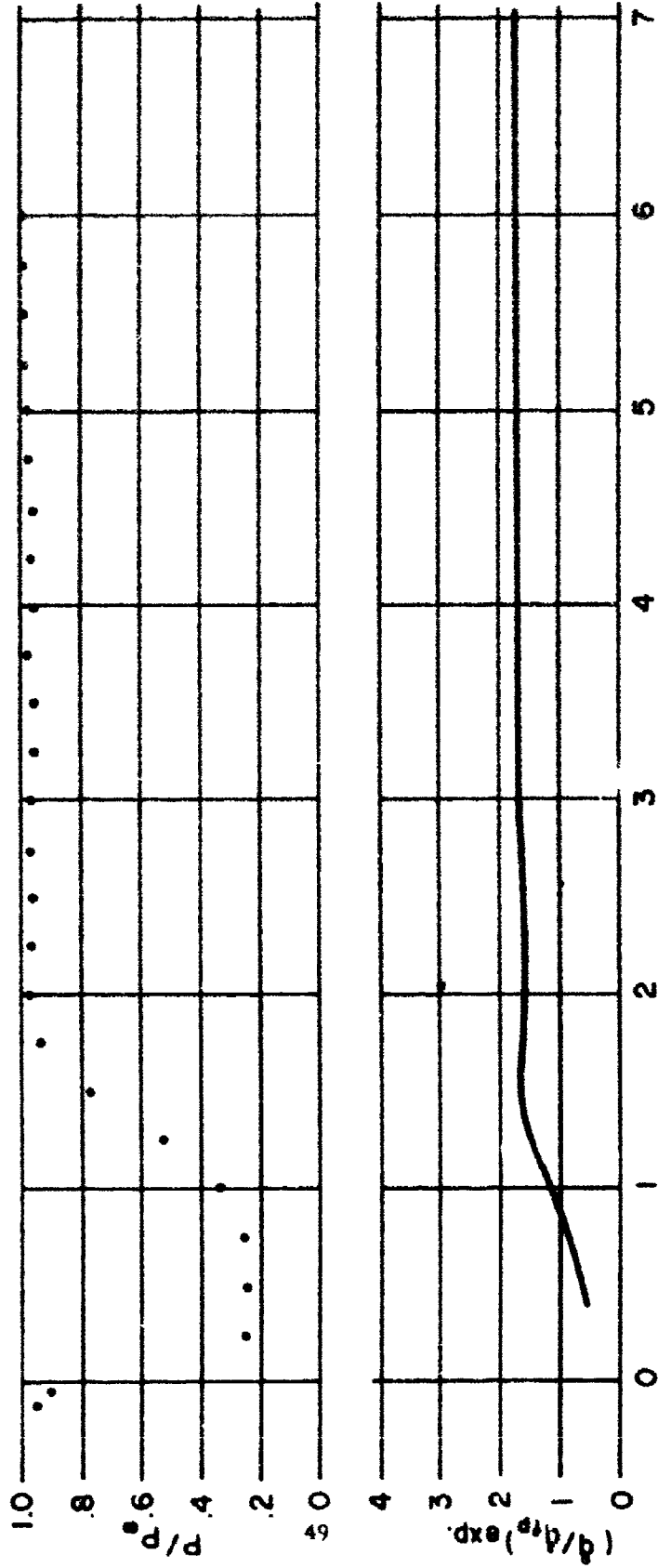


Fig. 9 b SHADOGRAPH, PRESSURE AND HEAT FLUX DISTRIBUTION FOR
 $h = 0.443$ $M_0 = 2.5$ $P_0 = 18.5$ PSIA.

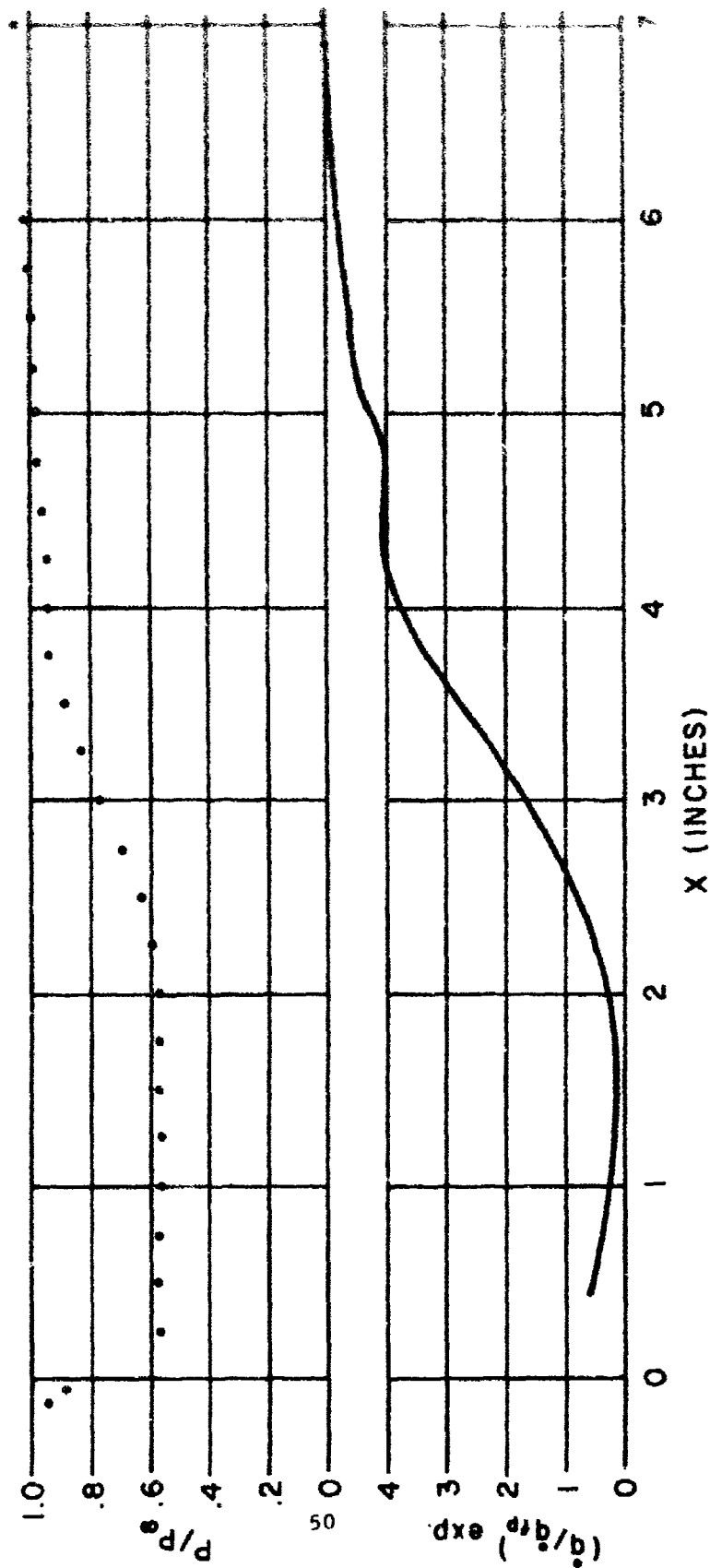


Fig. 9c SHADOGRAPH, PRESSURE AND HEAT FLUX DISTRIBUTION FOR
 $h = 0.443$ $M_\infty = 2.5$ $P_0 = 4.5$ PSIA.

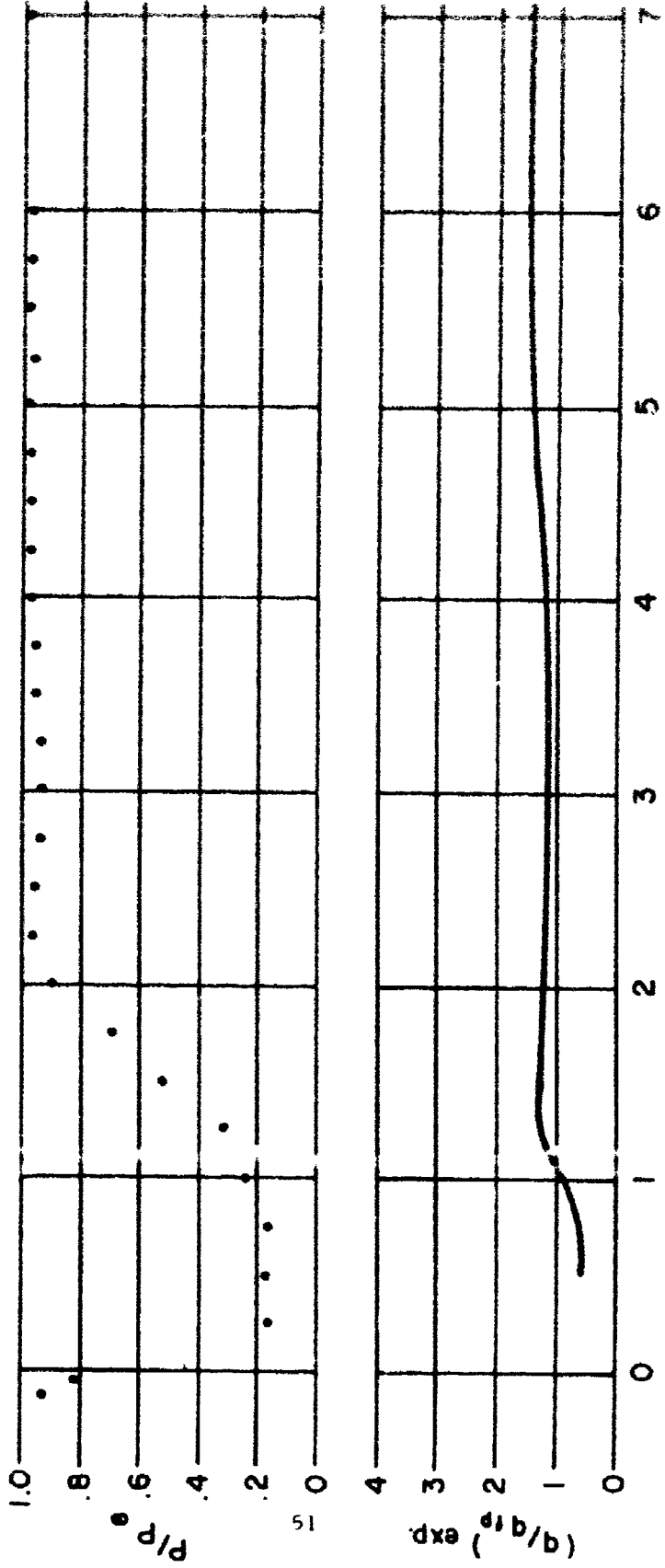
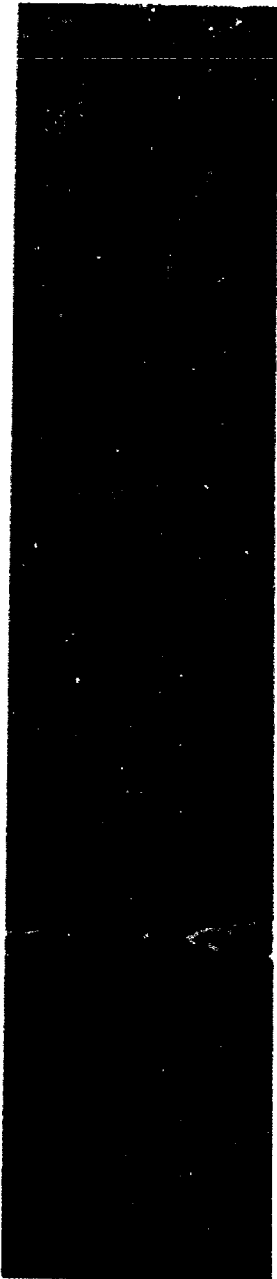


Fig. 9d SHADOGRAPH, PRESSURE AND HEAT FLUX DISTRIBUTION FOR
 $h = 0.443$ $M_0 = 3.5$ $P_0 = 54.5$ PSIA.

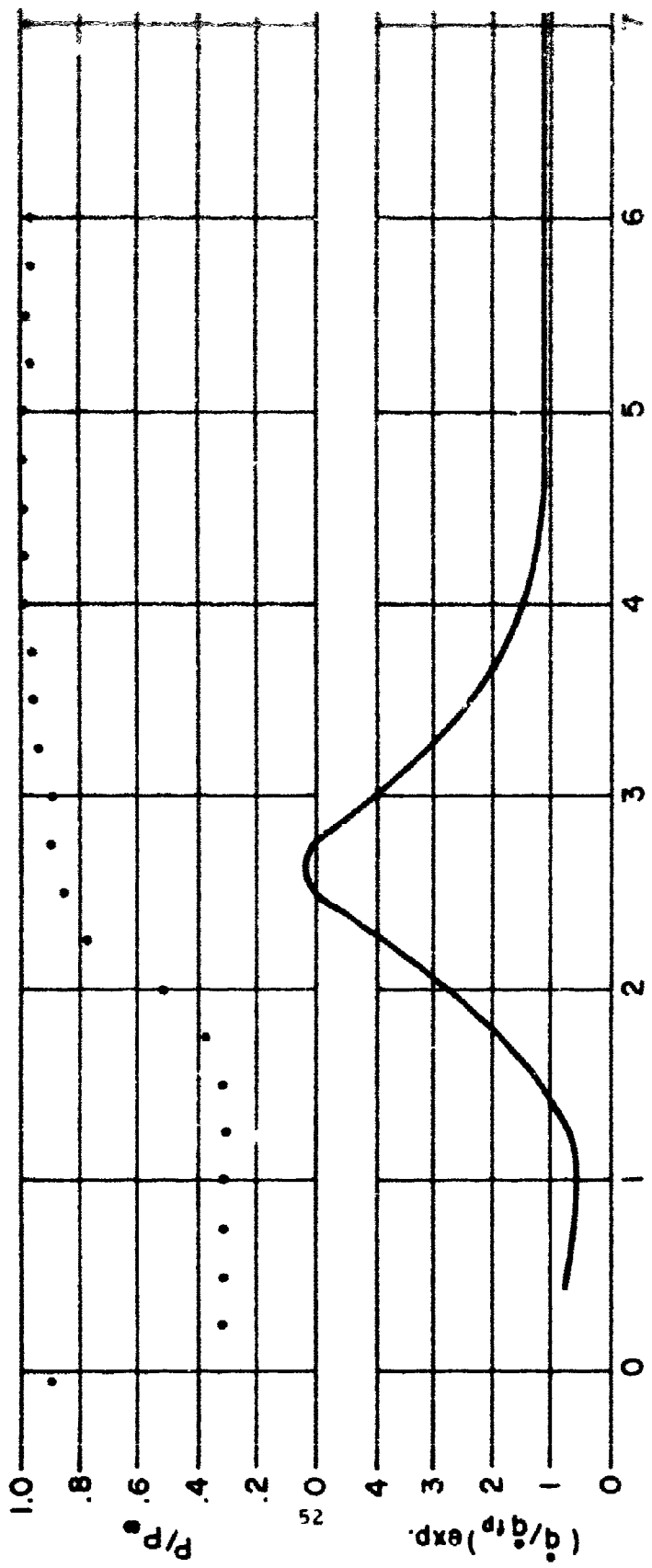
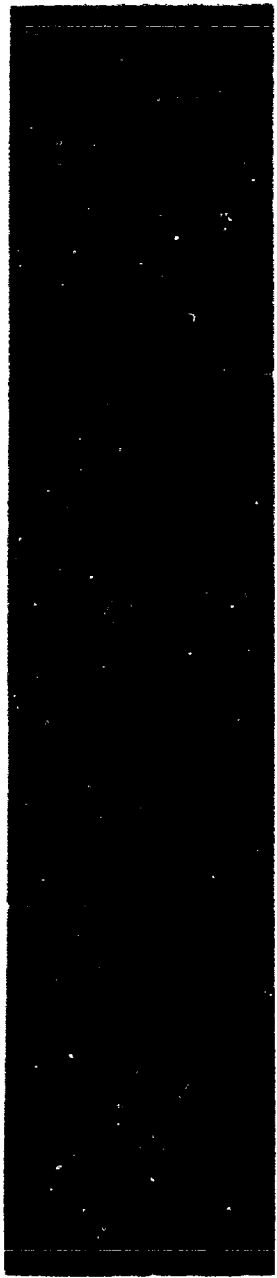


Fig. 9e SHADOGRAPH, PRESSURE AND HEAT FLUX DISTRIBUTION FOR
 $h = 0.443$ $M_\infty = 3.5$ $P_0 = 31.5$ PSIA.

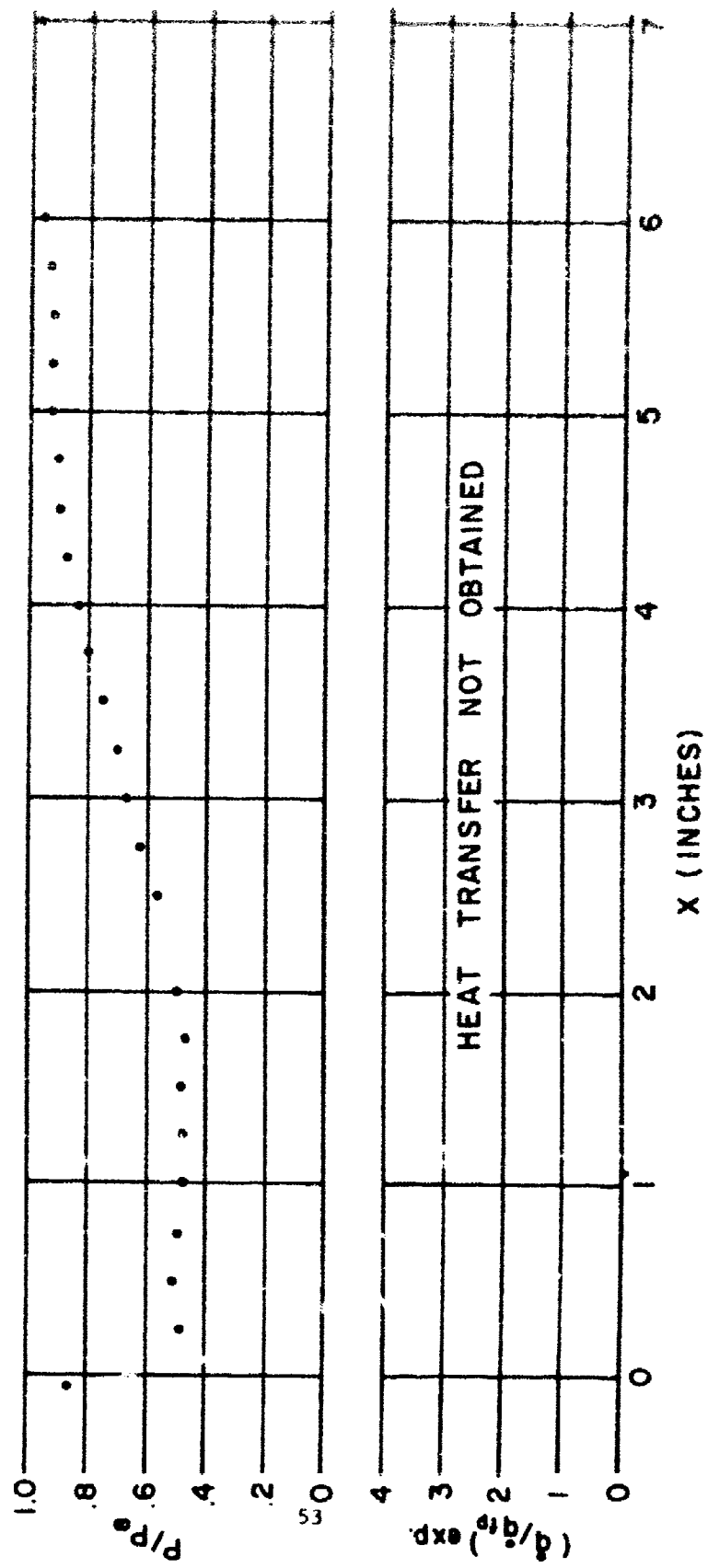


Fig. 9f SHADOGRAPH, PRESSURE AND HEAT FLUX DISTRIBUTION FOR
 $h = 0.443$ $M_0 = 3.5$ $P_0 = 7.5$ PSIA.

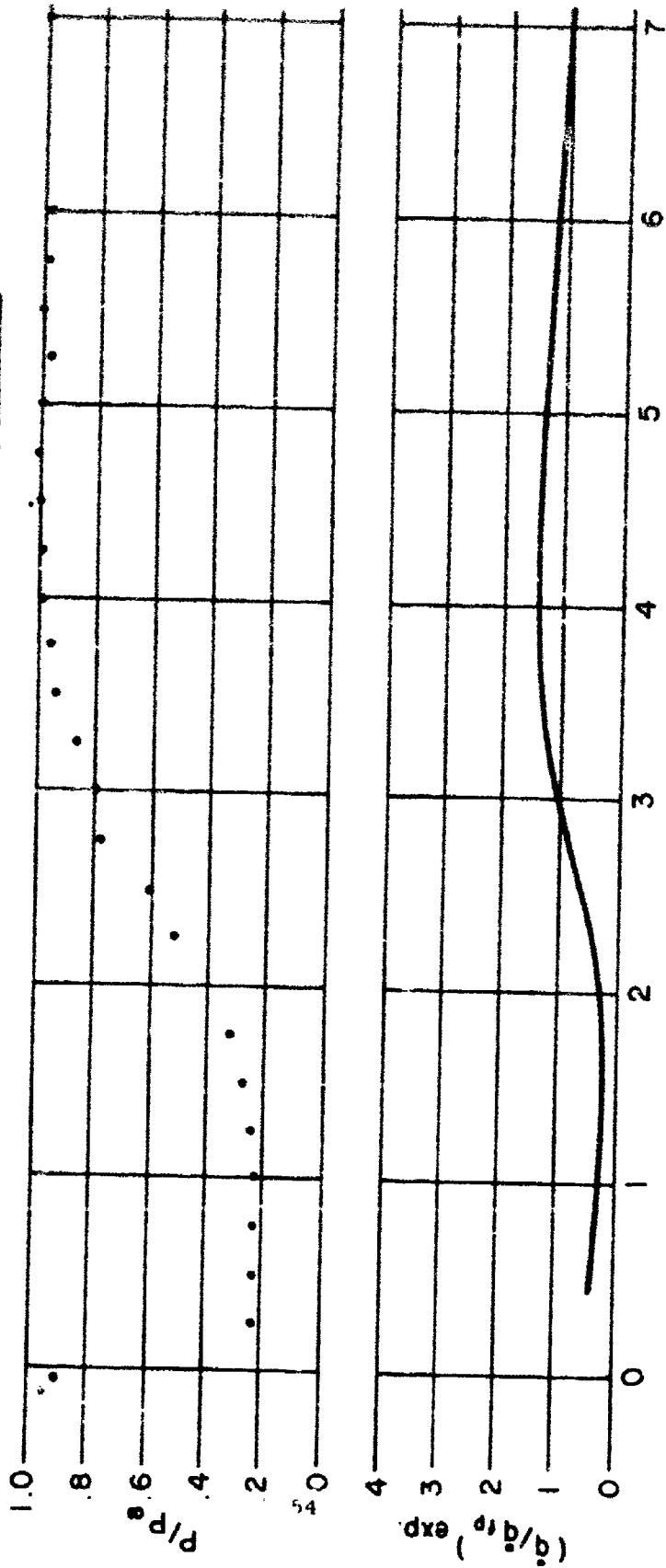
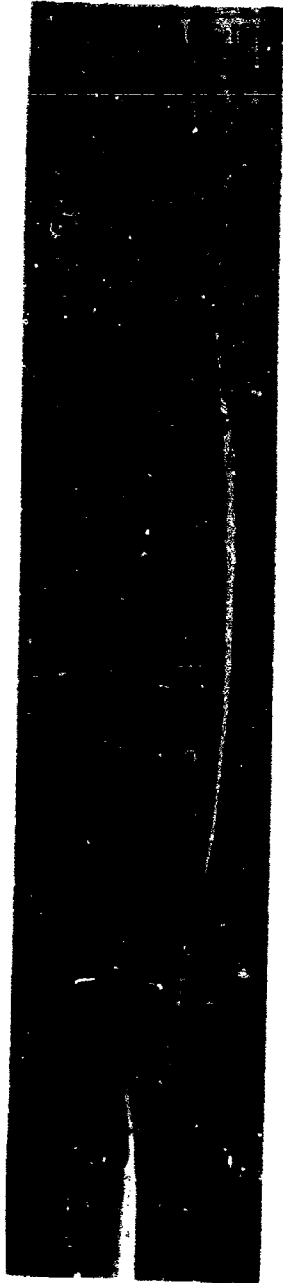


Fig. 9g SHADOGRAPH, PRESSURE AND HEAT FLUX DISTRIBUTION FOR
 $h = 0.443$ $M_0 = 5.0$ $P_0 = 150$ PSIA.

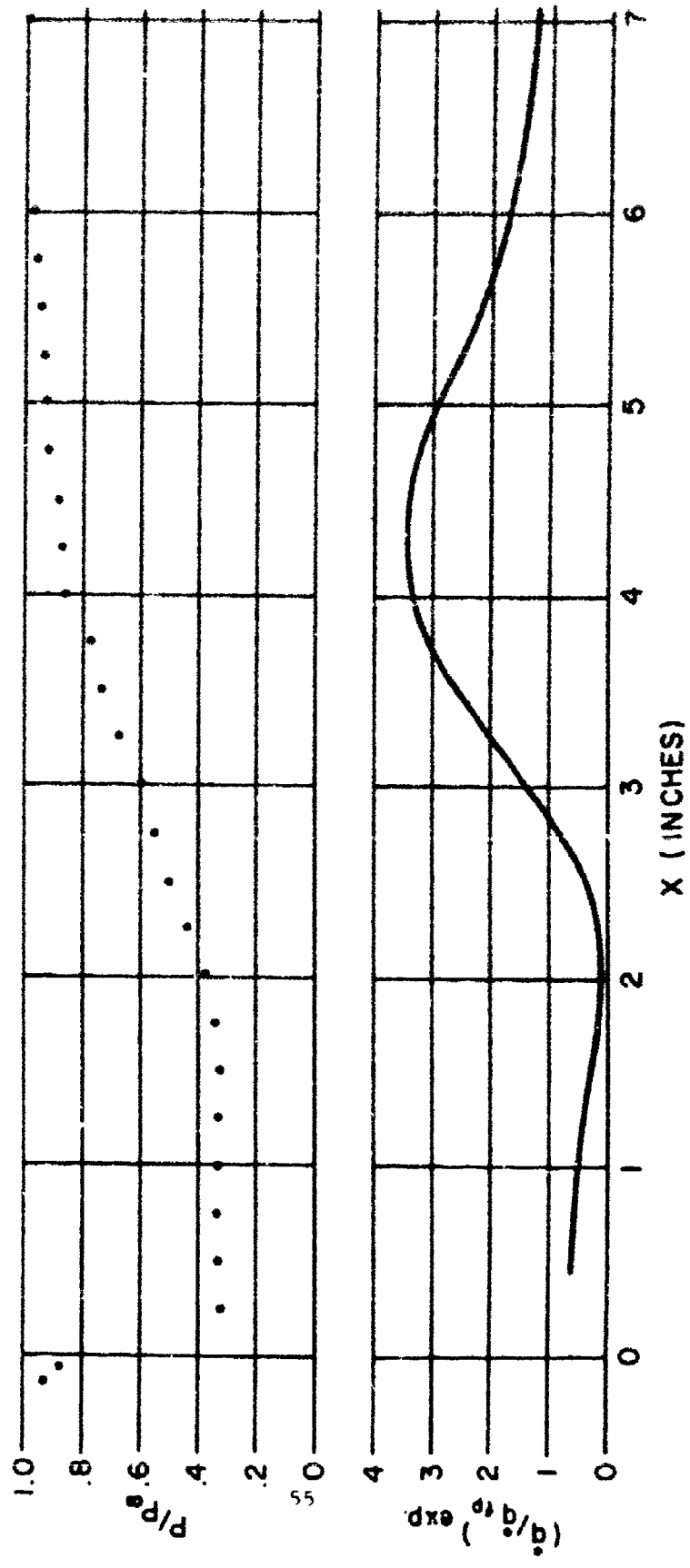
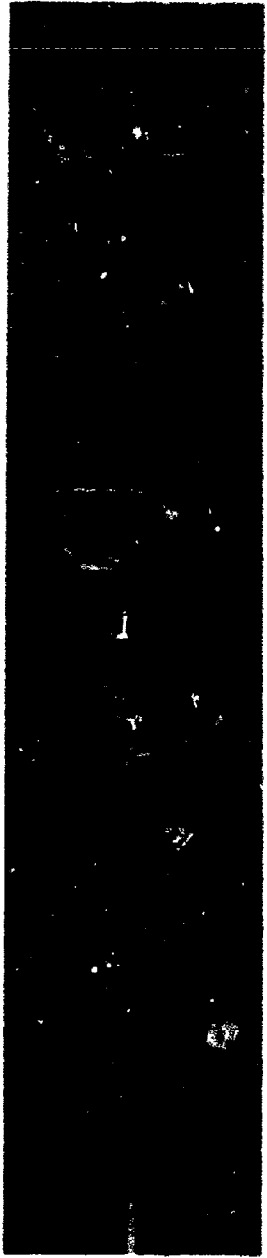


Fig. 9h SHADOGRAPH, PRESSURE AND HEAT FLUX DISTRIBUTION FOR
 $h = 0.443$ $M_0 = 5.0$ $P_0 = 84$ PSIA.

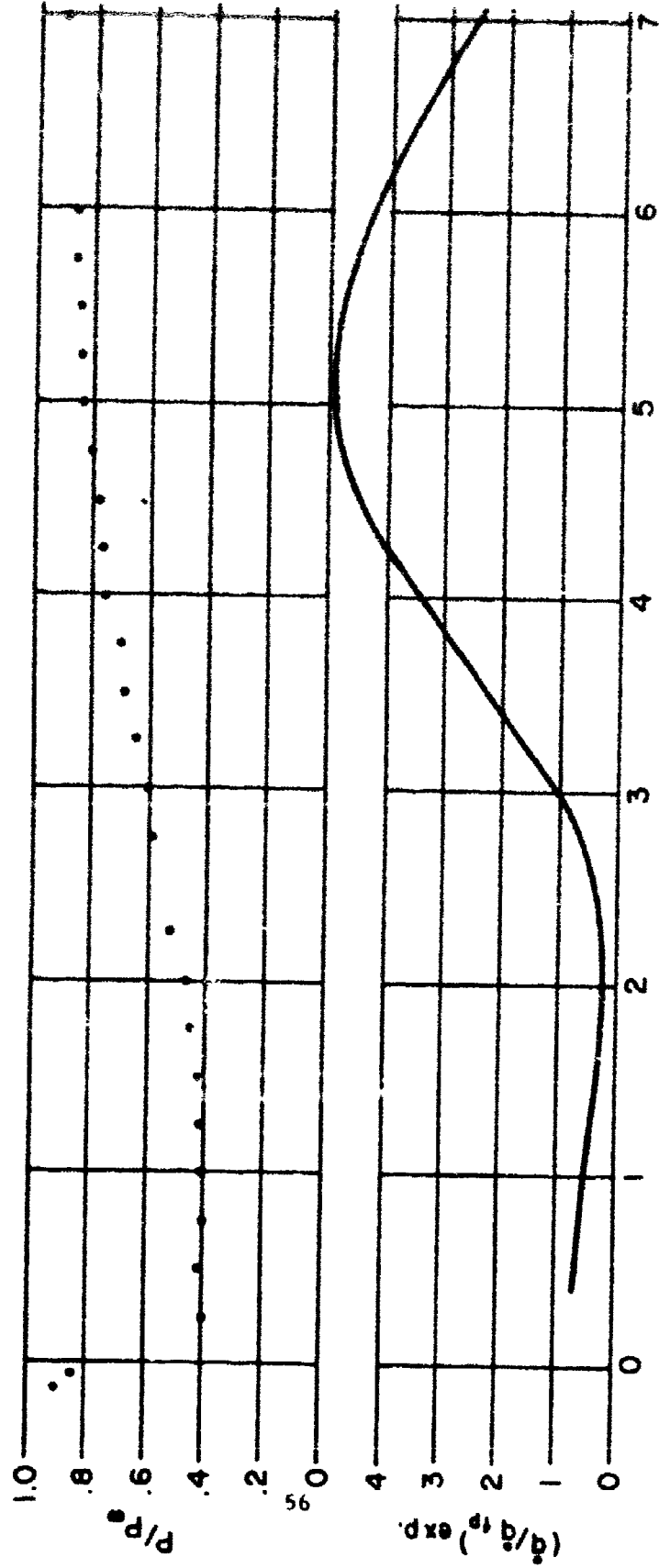
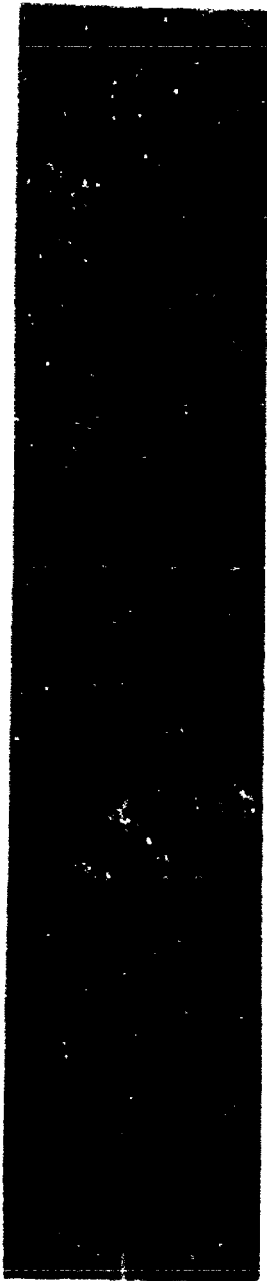


Fig. 91 SHADOGRAPH, PRESSURE AND HEAT FLUX DISTRIBUTION FOR
 $h = 0.443$ $M_0 = 5.0$ $P_0 = 28$ PSIA.

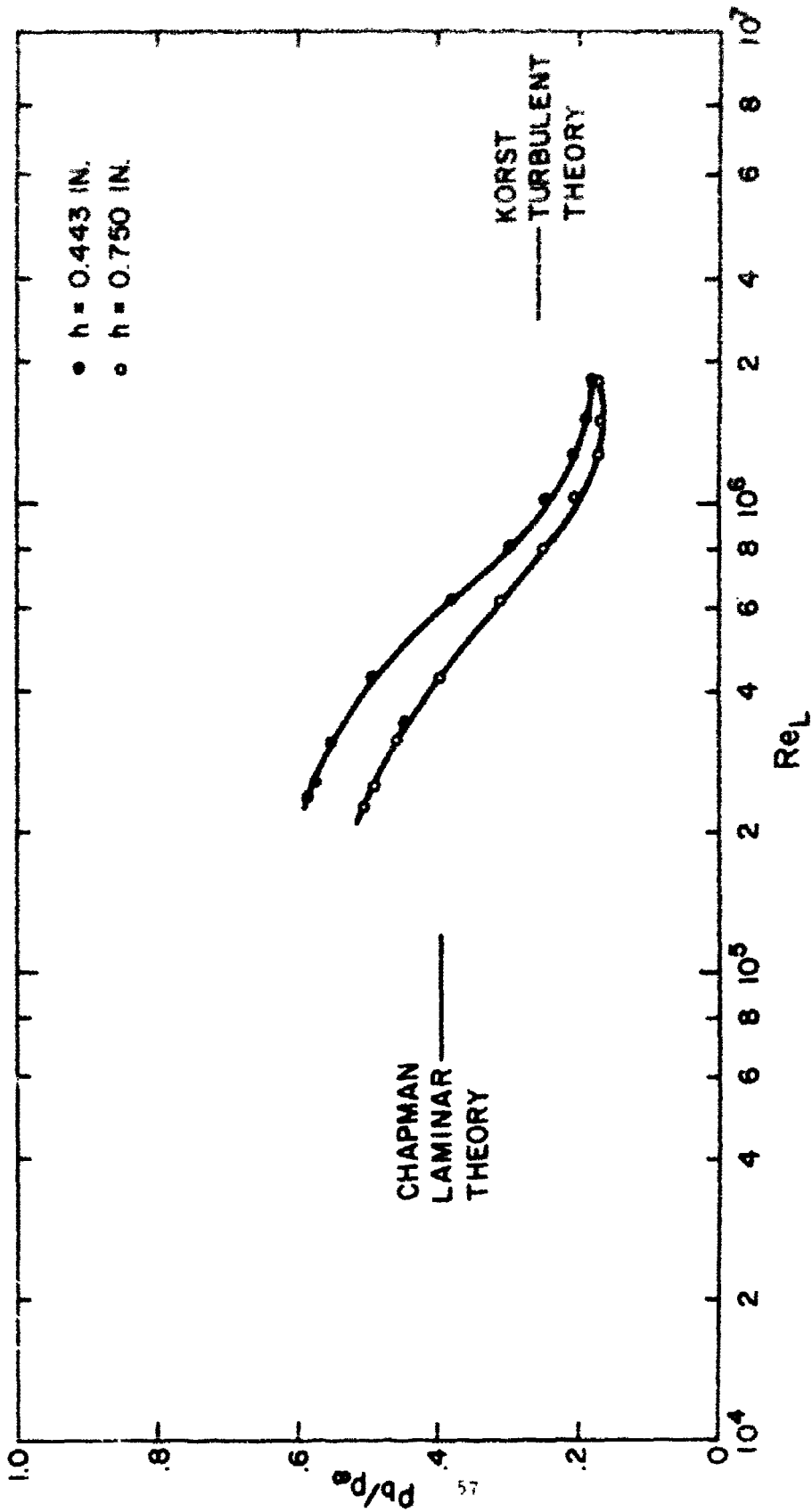


Fig. 10a BASE PRESSURE RATIO Vs. Re_L FOR $M_\infty = 2.5$

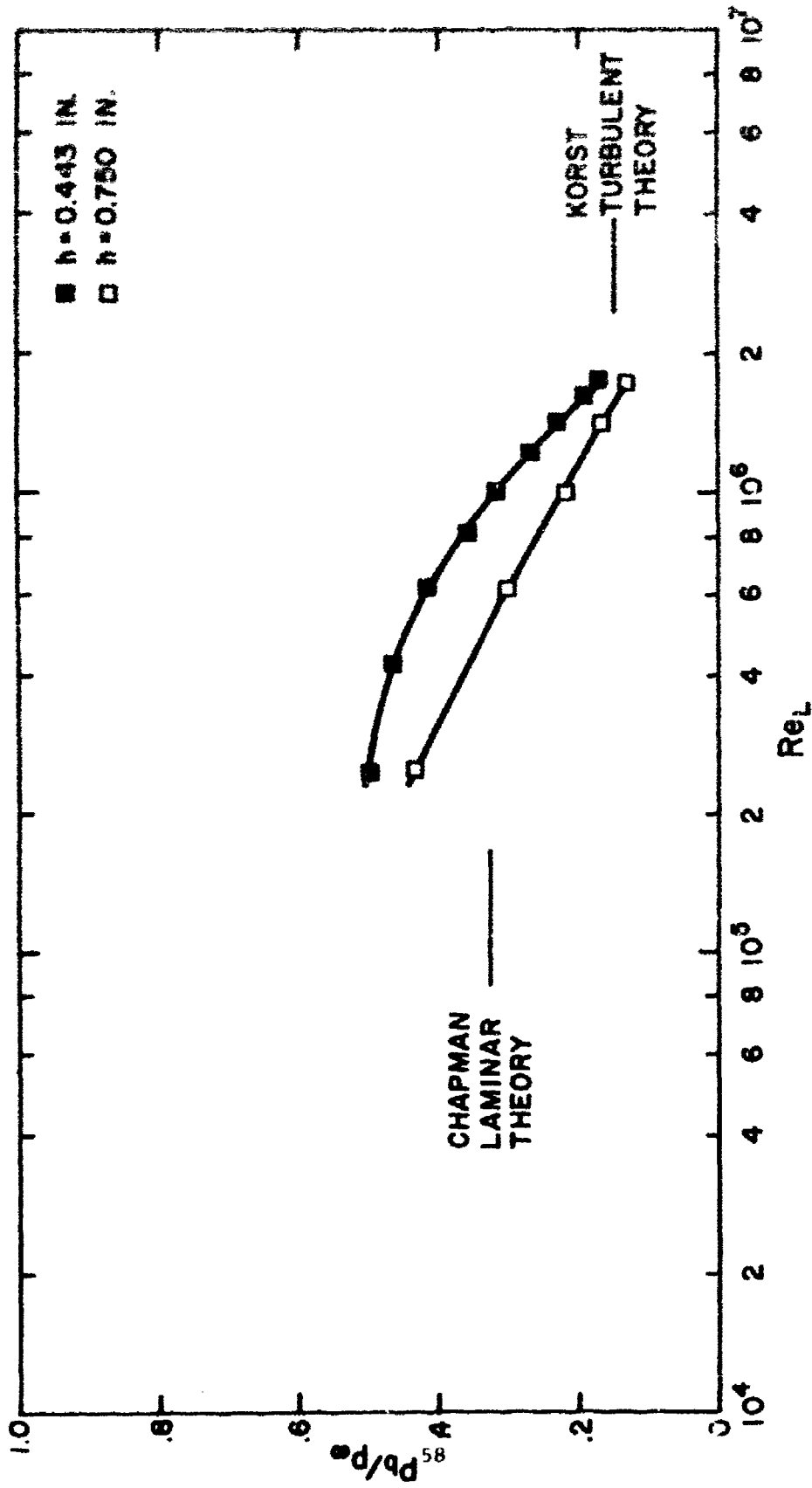


Fig. 10b BASE PRESSURE RATIO Vs. Re_L FOR $M_\infty = 3.5$

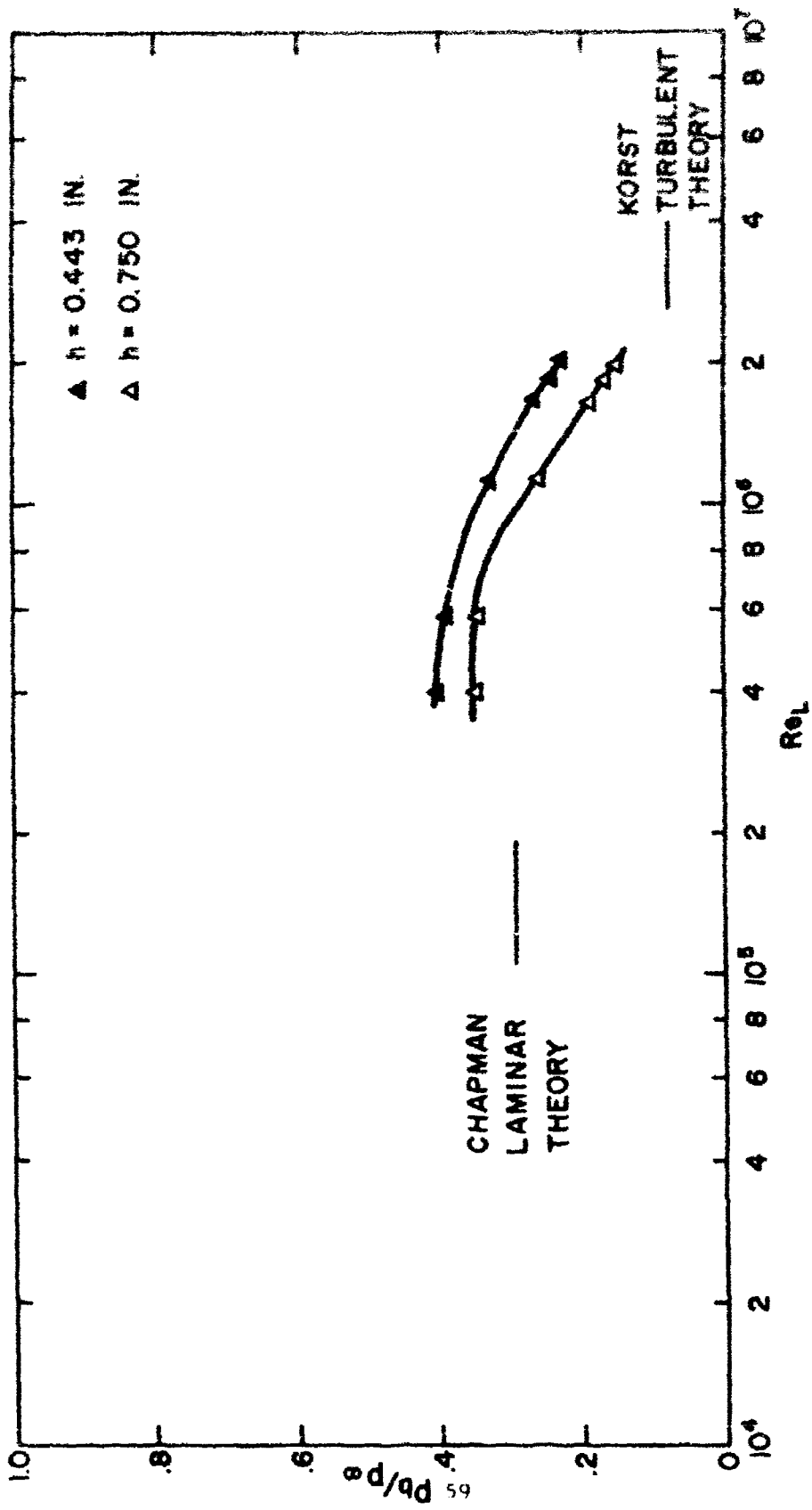


Fig. 10c BASE PRESSURE RATIO Vs. Re_L FOR $Mo = 5.0$

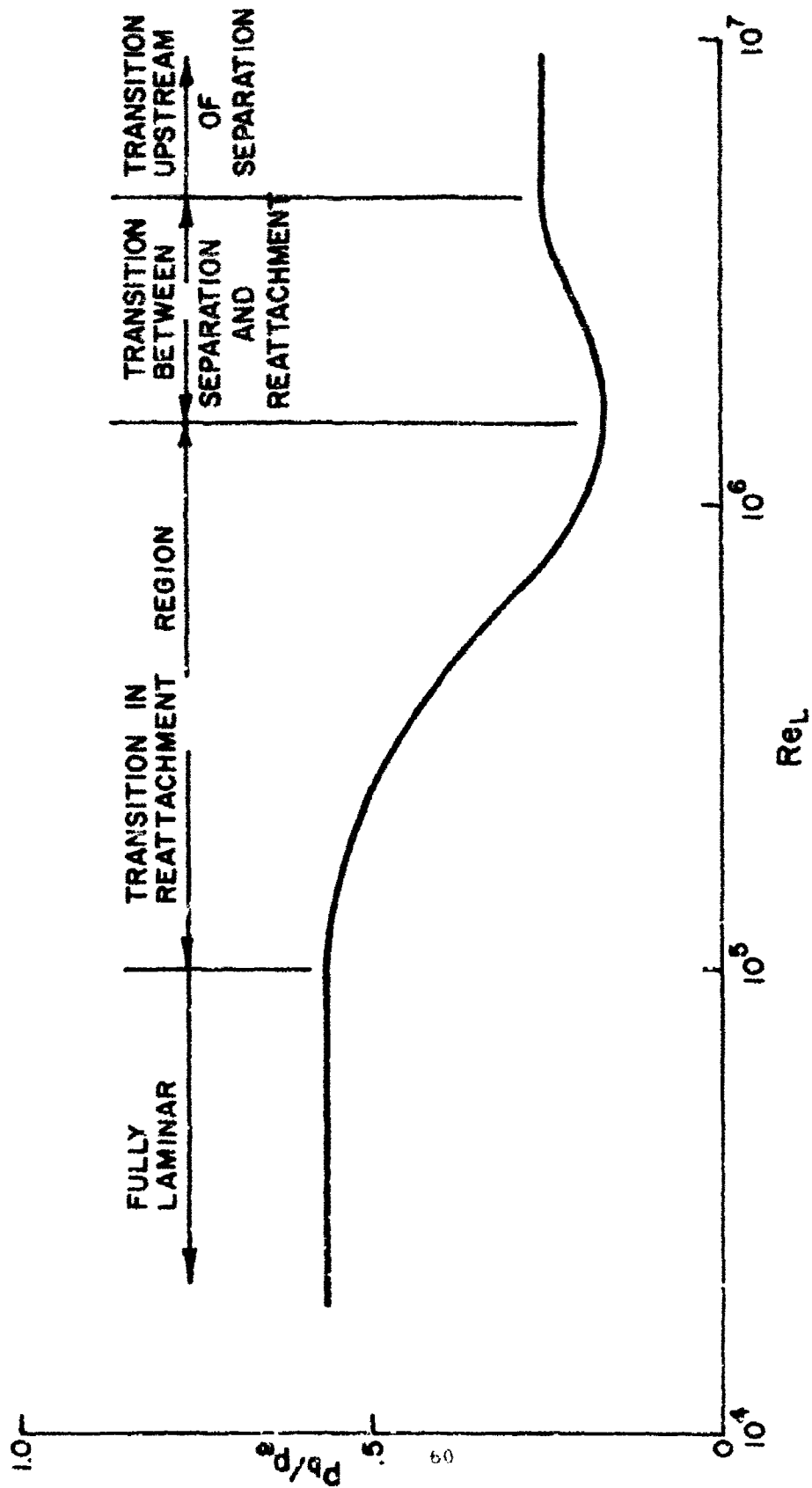


Fig. II BASE PRESSURE RATIO Vs. Re_L (SCHEMATIC) $M_0 \approx 2.5$

KORST THEORY (TURBULENT)

A	$M_{op} = 2.5$	$h = .443"$
B	$M_{op} = 2.5$	$h = .750"$
C	$M_{op} = 3.5$	$h = .443"$
D	$M_{op} = 3.5$	$h = .750"$
E	$M_{op} = 5.0$	$h = .443"$
F	$M_{op} = 5.0$	$h = .750"$
G	$M_{op} = 1.56$	REFERENCE (14)
H	$M_{op} = 2.41$	$h = .010"$ TO $.8"$
I	$M_{op} = 3.1$	TURBULENT SEPARATION
J	$M_{op} = 1.8$	REF. (15) $h = 20$ mm
K	$M_{op} = 2.25$	$h = 8$ mm
L	$M_{op} = 3.55$	$h = 18$ mm
N	$M_{op} = 2.25$	$h = 0.42$ mm
O	$M_{op} = 3.55$	$h = 0.42$ mm
P	$M_{op} = 2.25$	$h = 0.65$ mm
Q	$M_{op} = 3.55$	$h = 0.65$ mm
R	$M_{op} = 2.25$	$h = 0.85$ mm
S	$M_{op} = 2.25$	$h = 2.00$ mm
T	$M_{op} = 3.5$	$h = 6.00$ mm
U	$M_{op} = 3.5$	$h = 2.00$ mm

LAMINAR
TURB. REFERENCE (16)

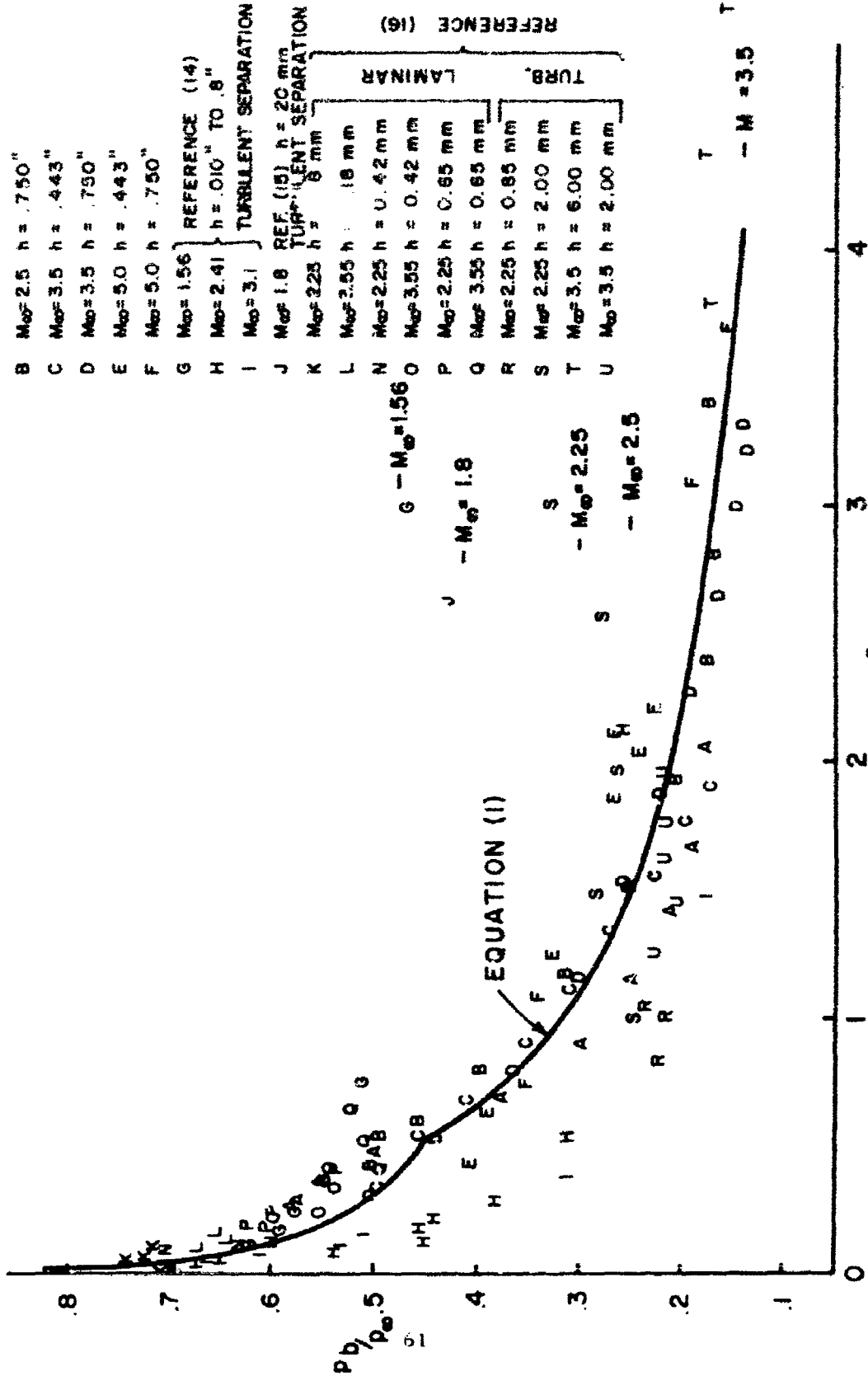


Fig. 12 BASE PRESSURE RATIO VS. Re_h

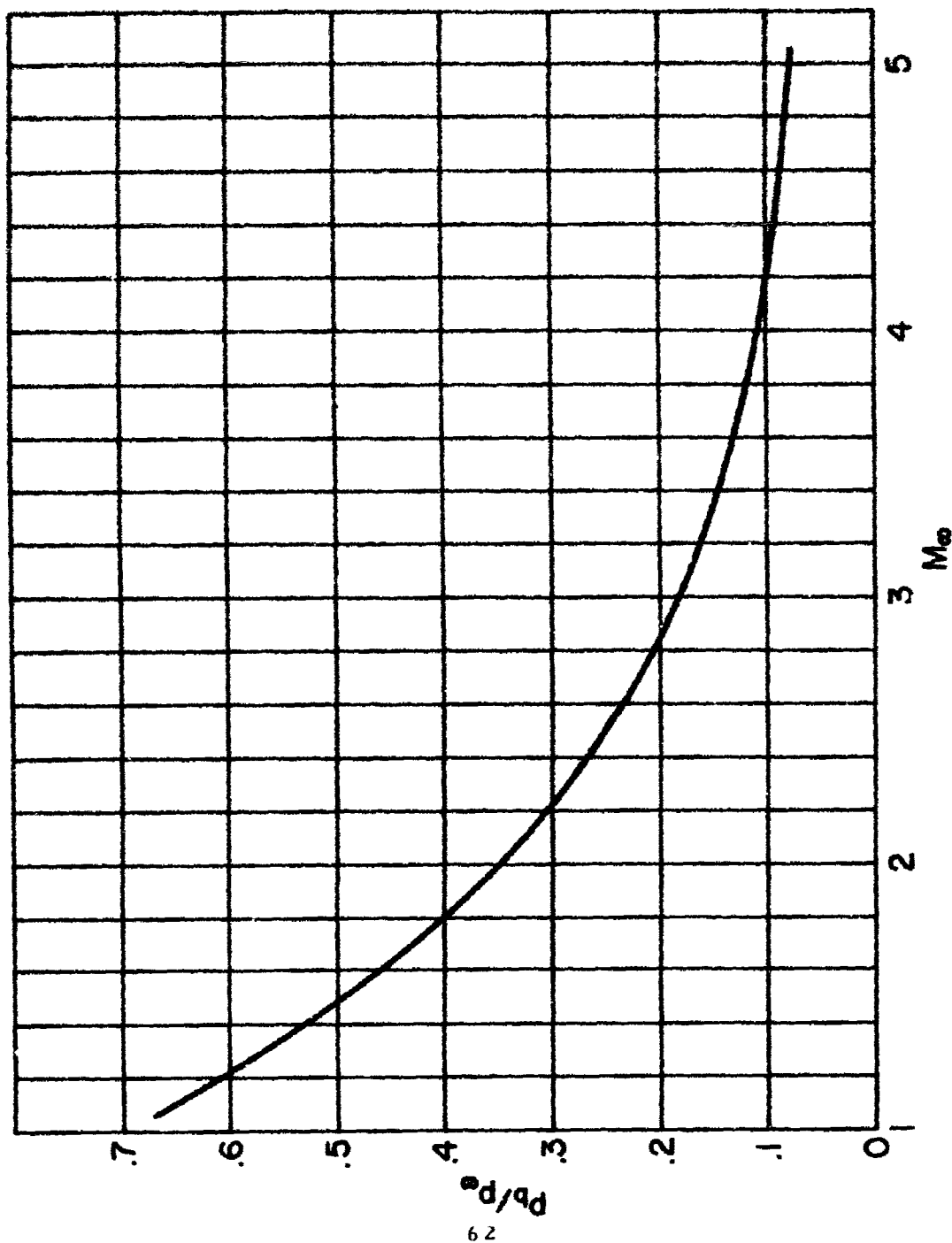


Fig. 13 TURBULENT BASE PRESSURE RATIO FROM KORST THEORY

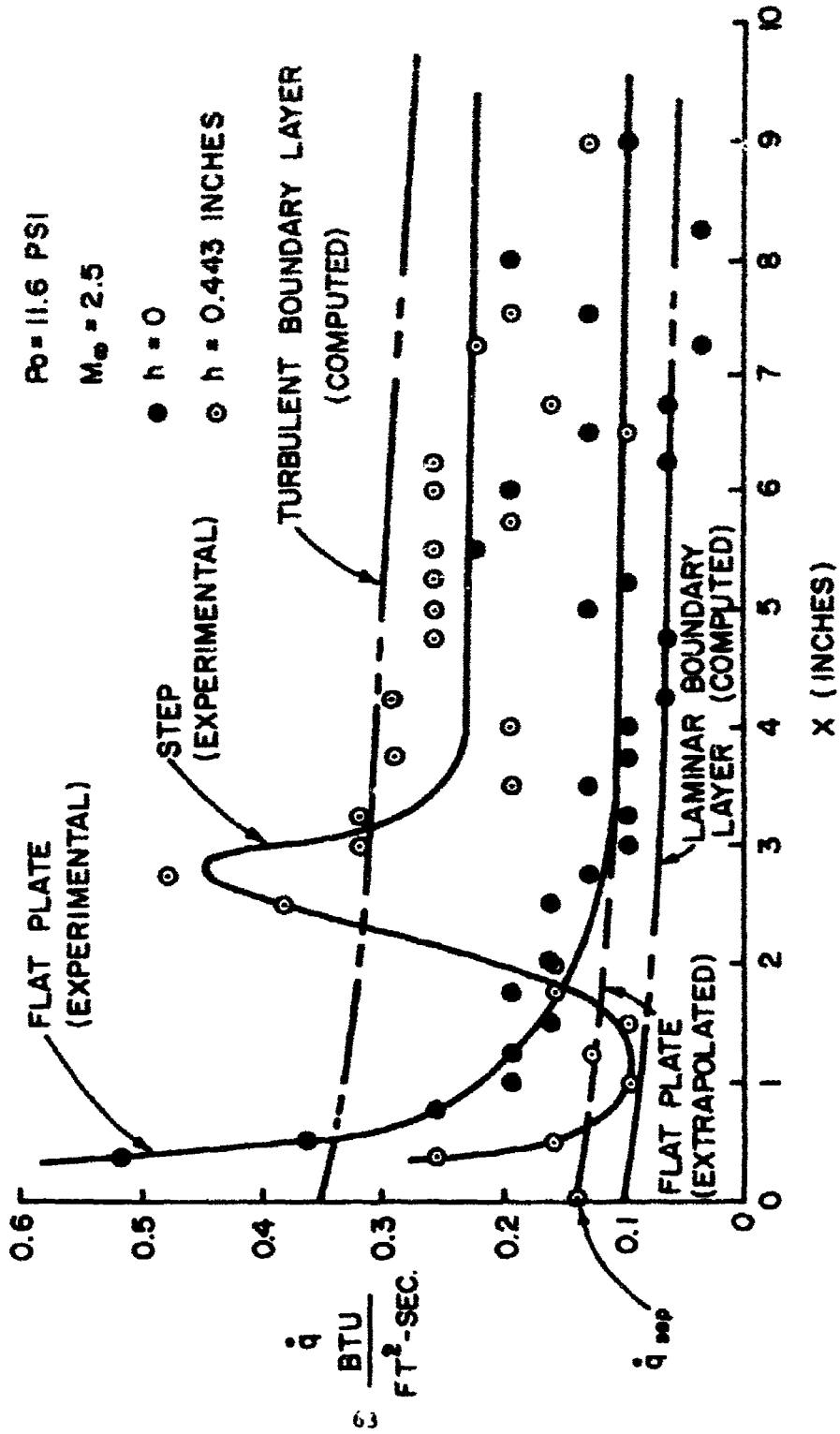


Fig. 14 HEAT FLUX VS. X FOR FLAT PLATE
 AND 0.443 STEP $M_0 = 2.5$ $P_0 = 11.6 \text{ PSIA.}$

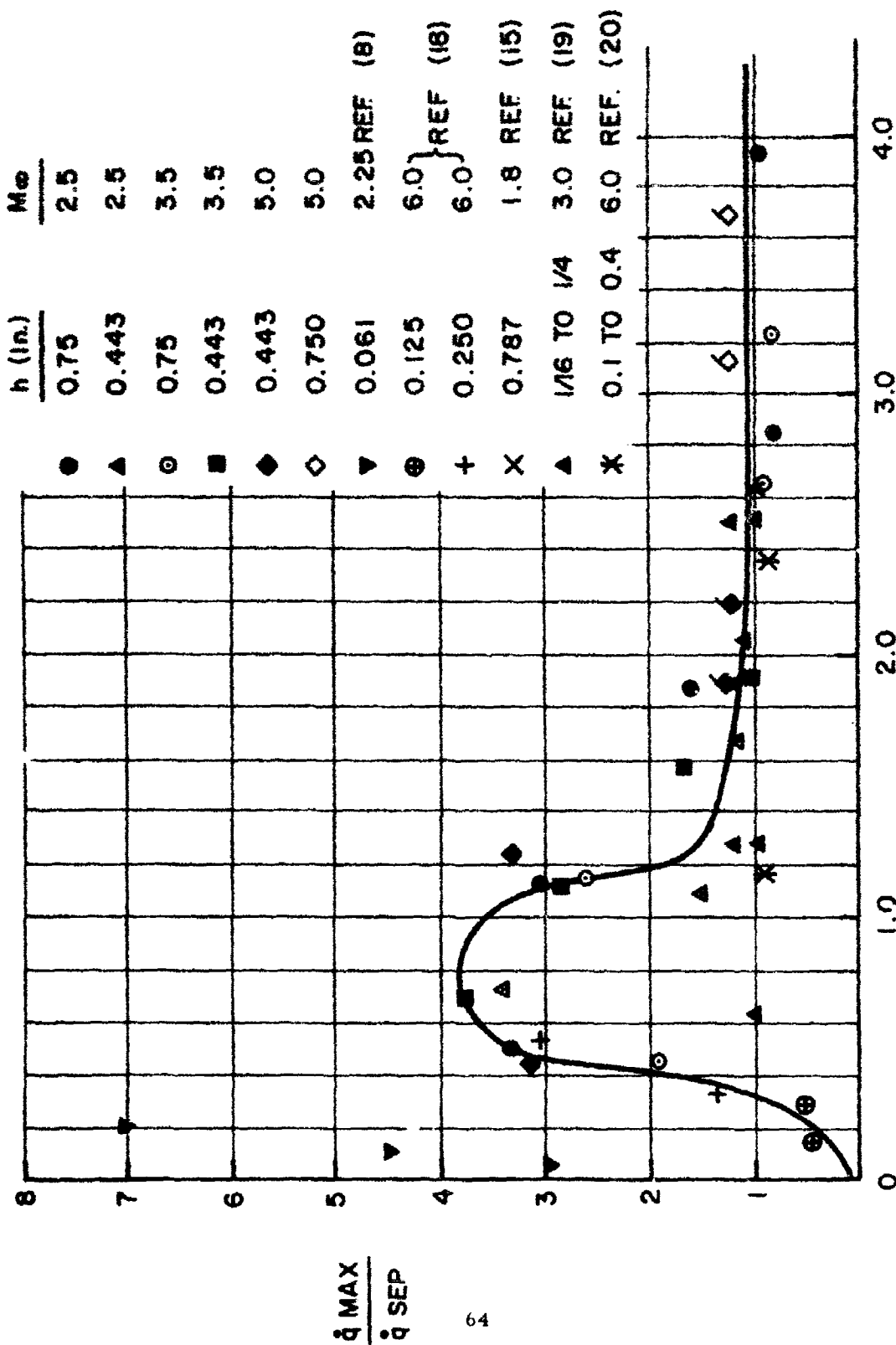


Fig. 15 RATIO OF MAXIMUM HEAT FLUX AT REATTACHMENT TO HEAT FLUX AT SEPARATION VS. Re_h .

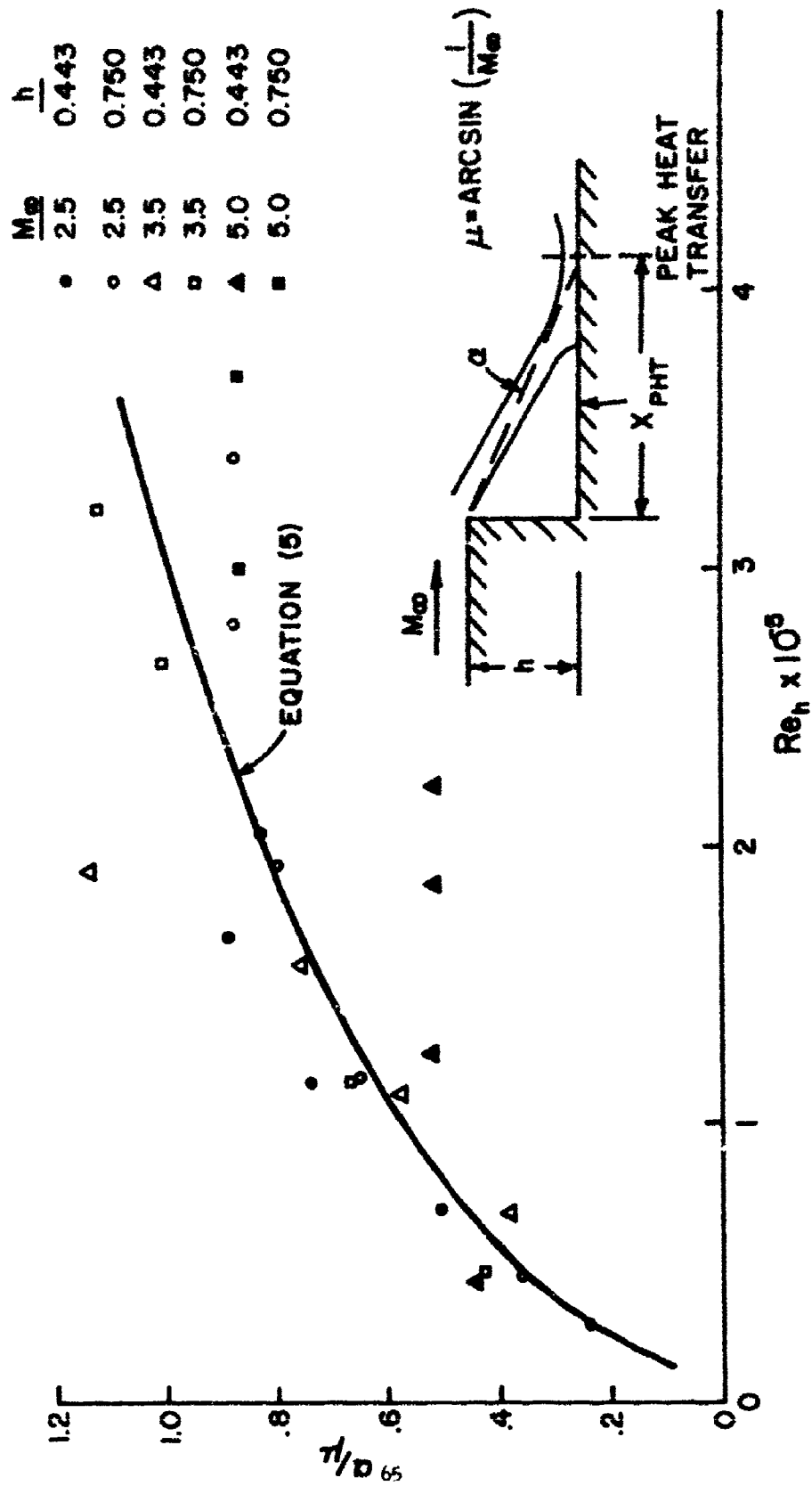


Fig. 16 α/μ Vs. Re_h



$M_{\infty} = 2.5$ $P_0 = 33$ PSIA



$M_{\infty} = 3.5$ $P_0 = 54.5$ PSIA



$M_{\infty} = 5.0$ $P_0 = 150$ PSIA

Fig. 17 PHOTOGRAPHS OF YARN STRAND ORIENTATION
AT MAXIMUM REYNOLDS₆ NUMBER $h = 0.75$ IN.

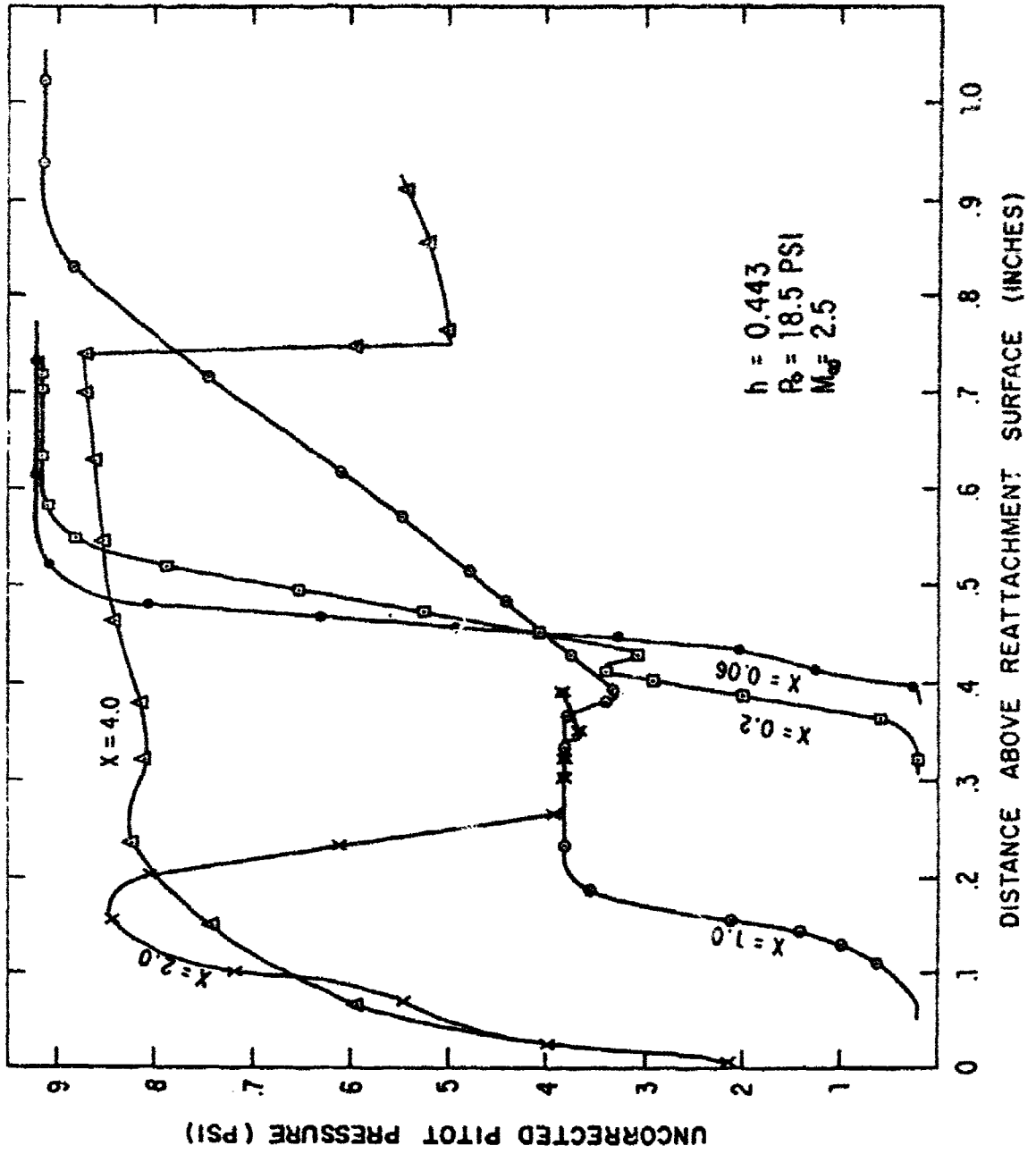


Fig. 18 SELECTED TYPICAL UNCORRECTED PITOT PROBE DATA

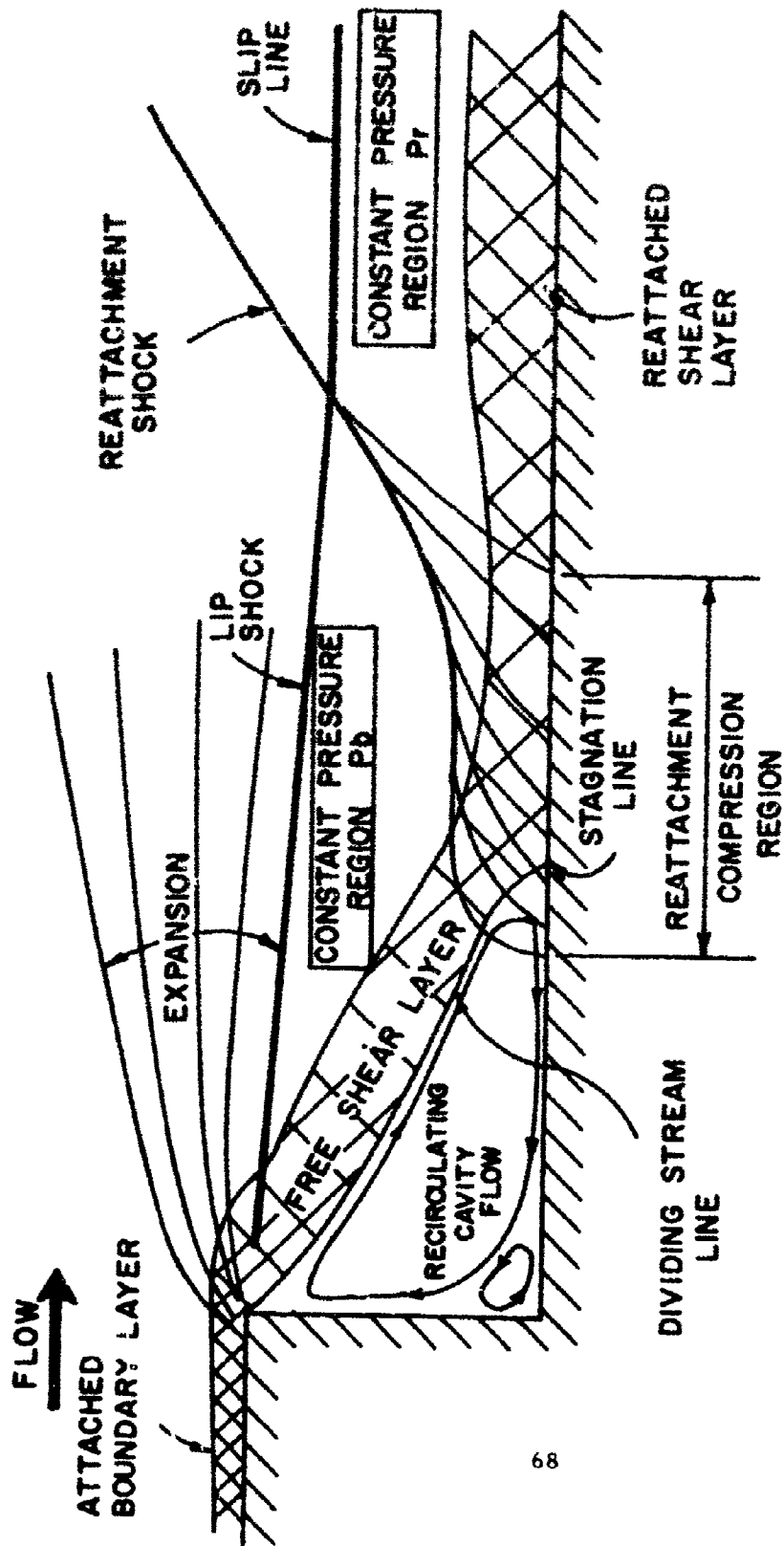


Fig. 19 FLOW FIELD DOWNSTREAM OF A REARWARD FACING STEP

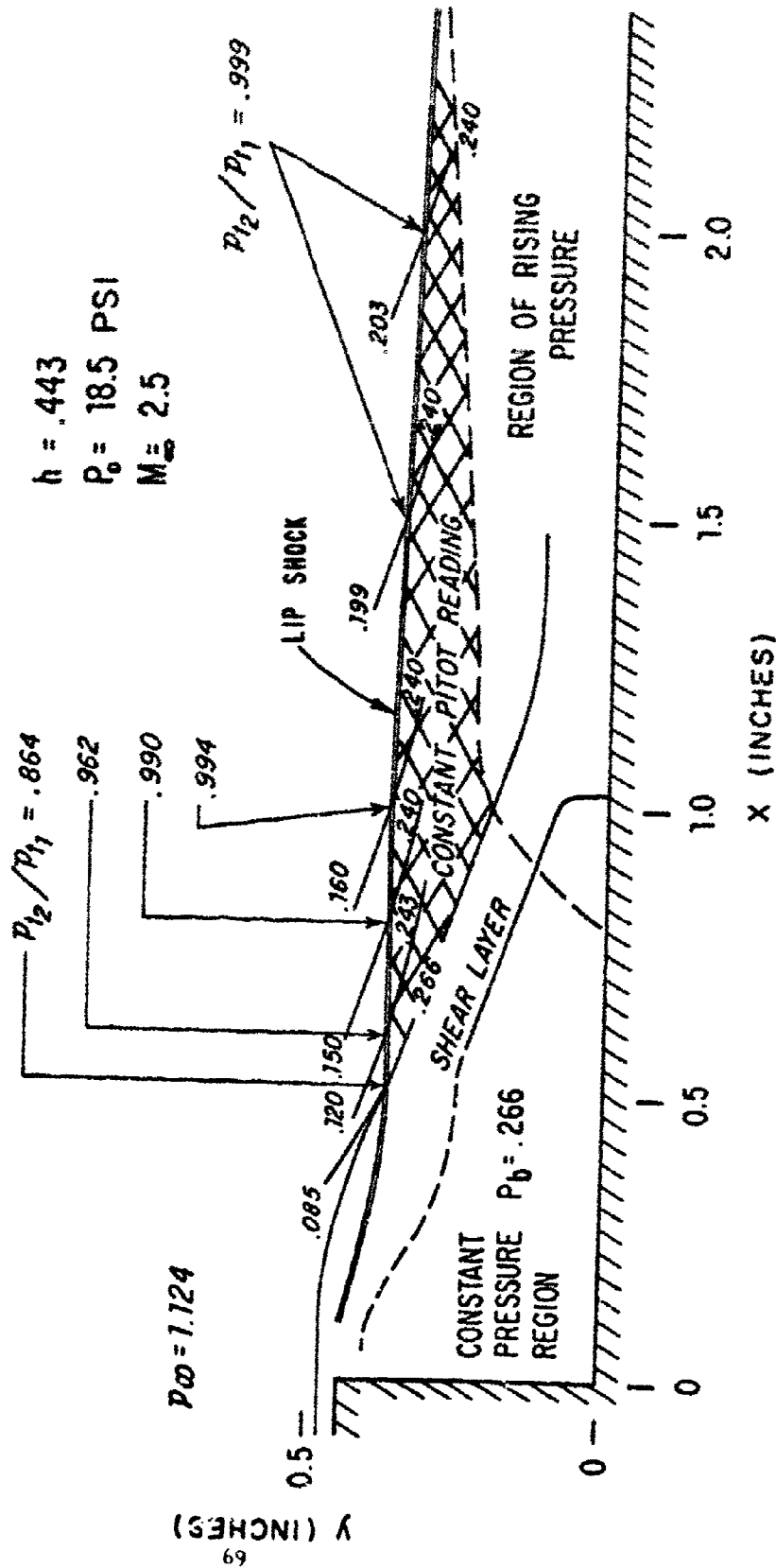


Fig. 20 FLOW FIELD DOWNSTREAM OF STEP
 $h=0.443$ $M_\infty=2.5$ $P_0=18.5 \text{ psia}$

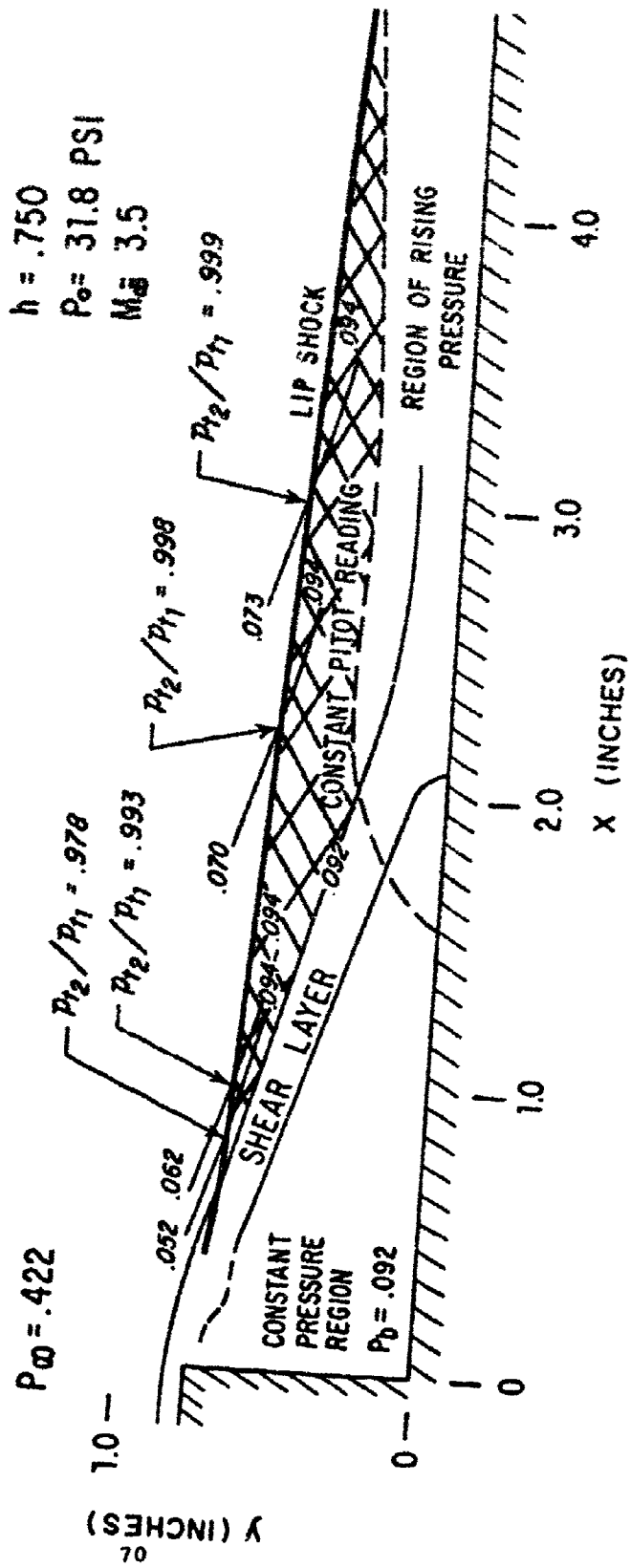


Fig. 21 FLOW FIELD DOWNSTREAM OF STEP

$h = 0.750$ $M_a = 3.5$ $p_0 = 31.8 \text{ psia}$

$h = 0.75$
 $P_o = 54.5$
 $M_\infty = 3.5$

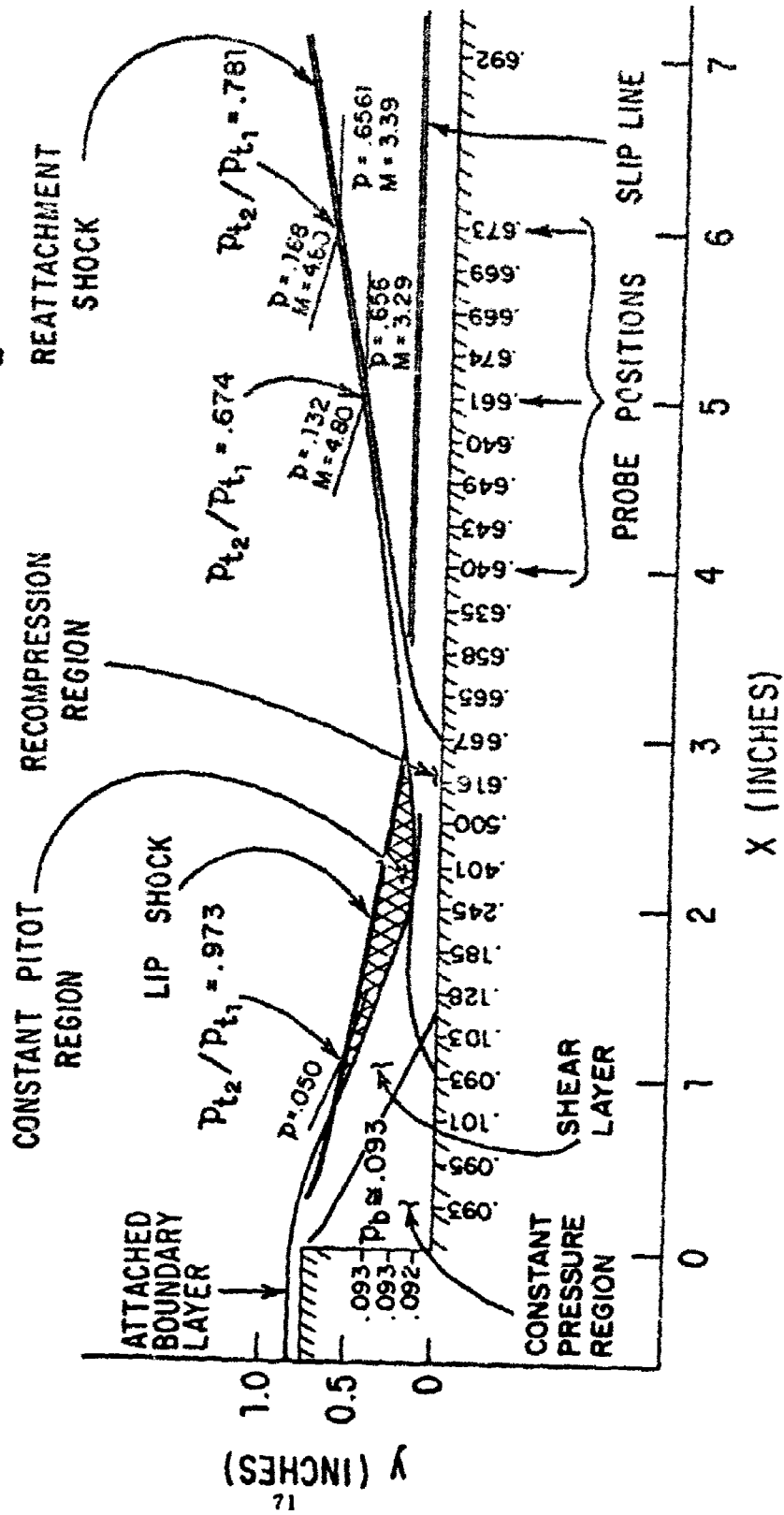


Fig. 22 FLOW FIELD DOWNSTREAM OF STEP
 $h = 0.750$ $M_\infty = 3.5$ $P_o = 54.5$ psia

9 -

$h = .443$

$P_0 = 18.5 \text{ psi}$

$M_\infty = 2.5$

$P_{00} = 1.124$

BOUNDARY LAYER EDGE

Y (INCHES)

72

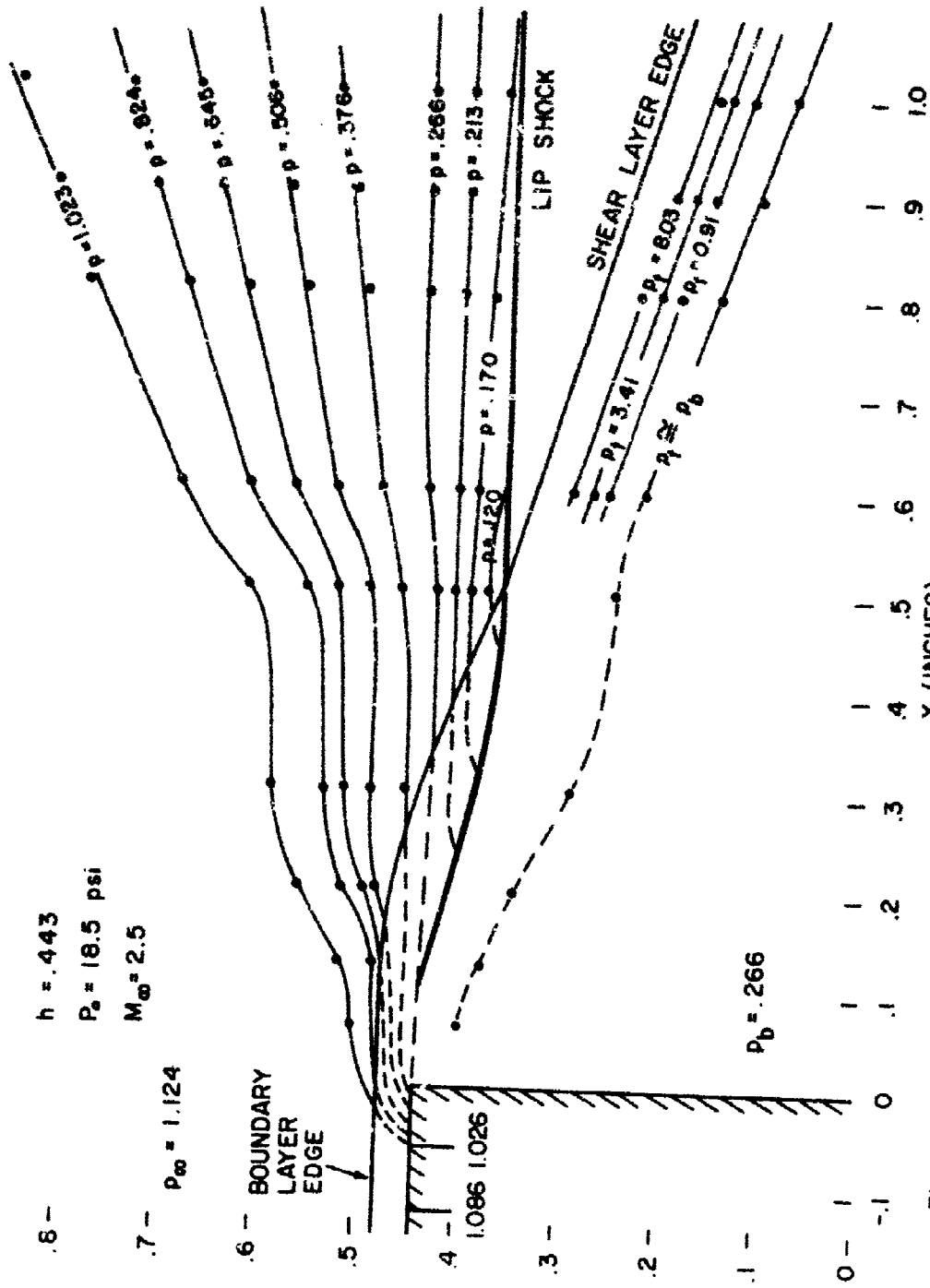


Fig. 23 PRESSURE FIELD IN THE NEIGHBORHOOD OF THE STEP
 $h = 0.443$ $M_\infty = 2.5$ $P_0 = 18.5 \text{ PSIA}$.

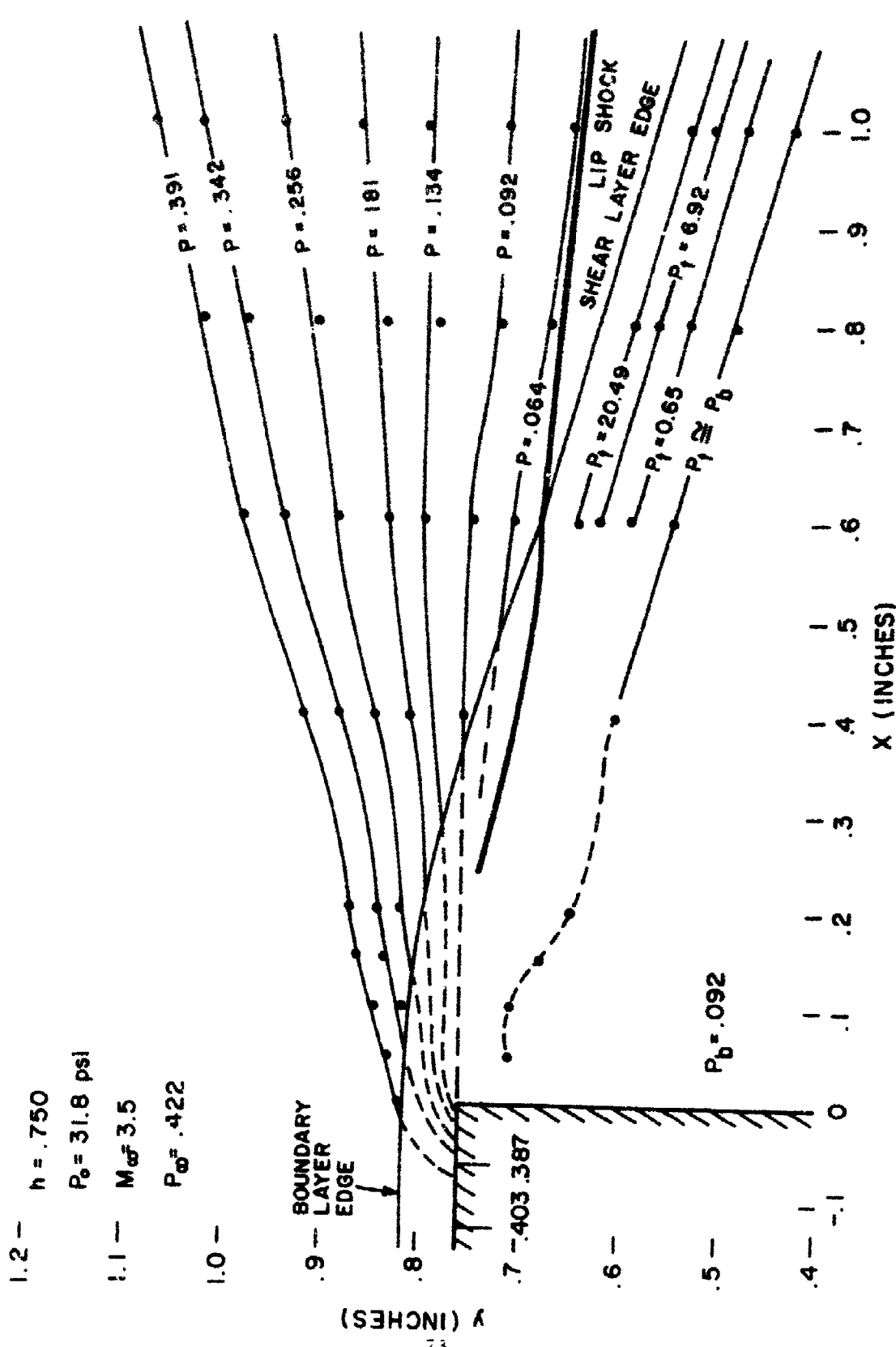


Fig. 24 PRESSURE FIELD IN THE NEIGHBORHOOD OF THE STEP
 $h = 0.75$ $M_\infty = 3.5$ $P_b = 31.8 \text{ PSIA}$.

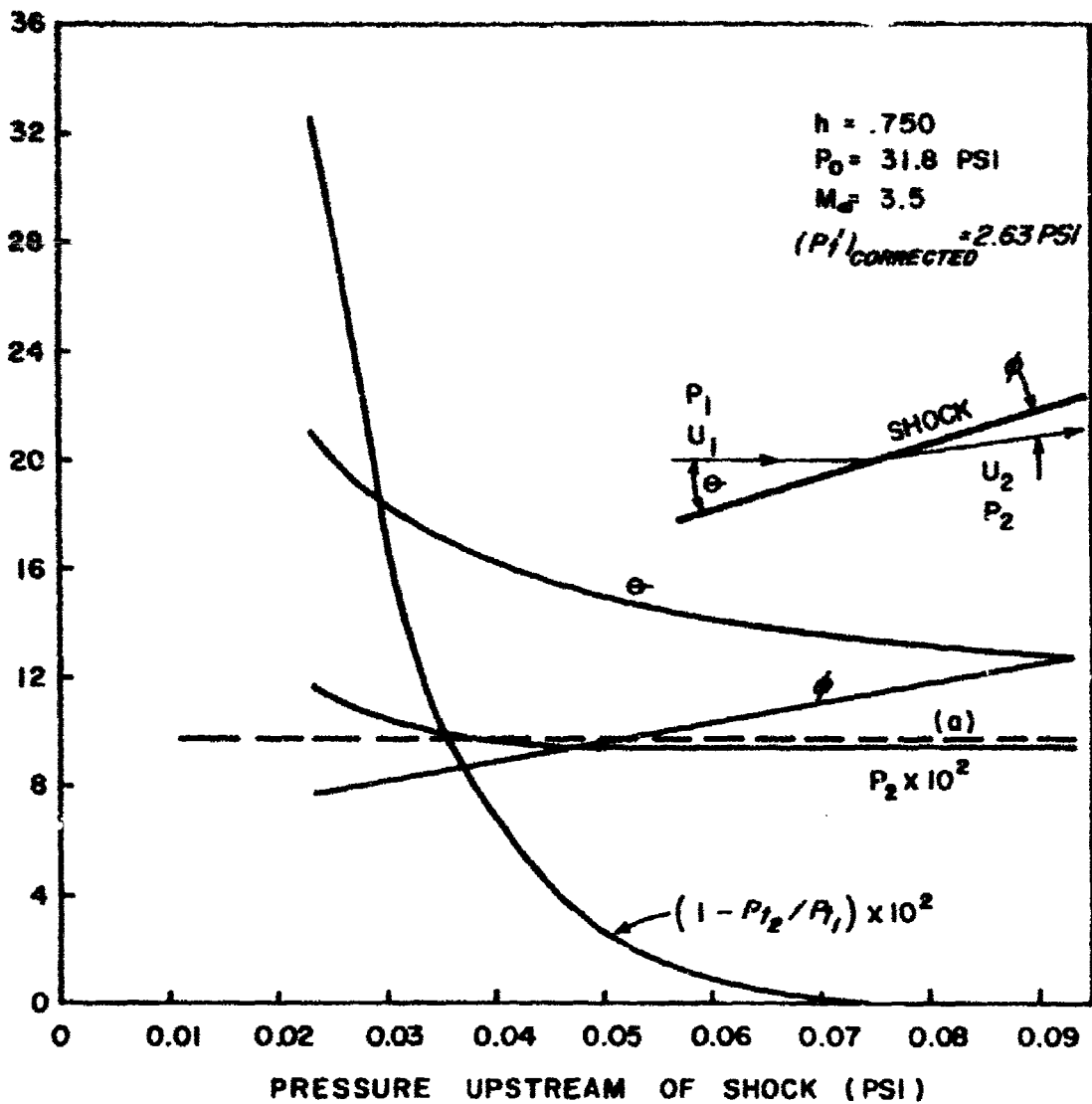


Fig. 25 VARIATION OF PROPERTIES ACROSS AN OBLIQUE SHOCK WITH CONSTANT TOTAL PRESSURE UPSTREAM AND CONSTANT PITOT READING DOWNSTREAM.

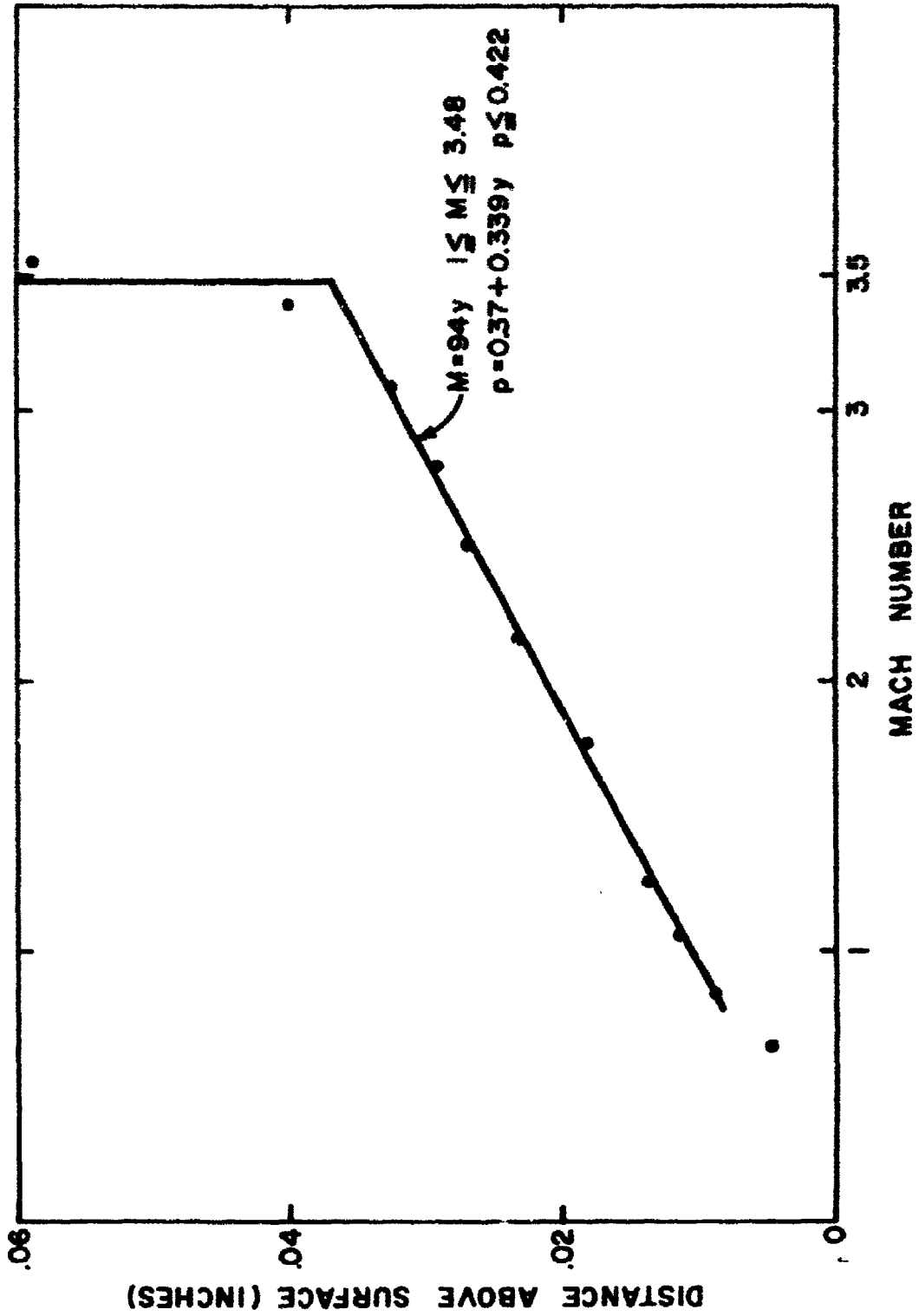


Fig. 26 INITIAL MACH NUMBER PROFILE $h = 0.750$
 $M_\infty = 3.5$ $p_\infty = 31.8$ psia

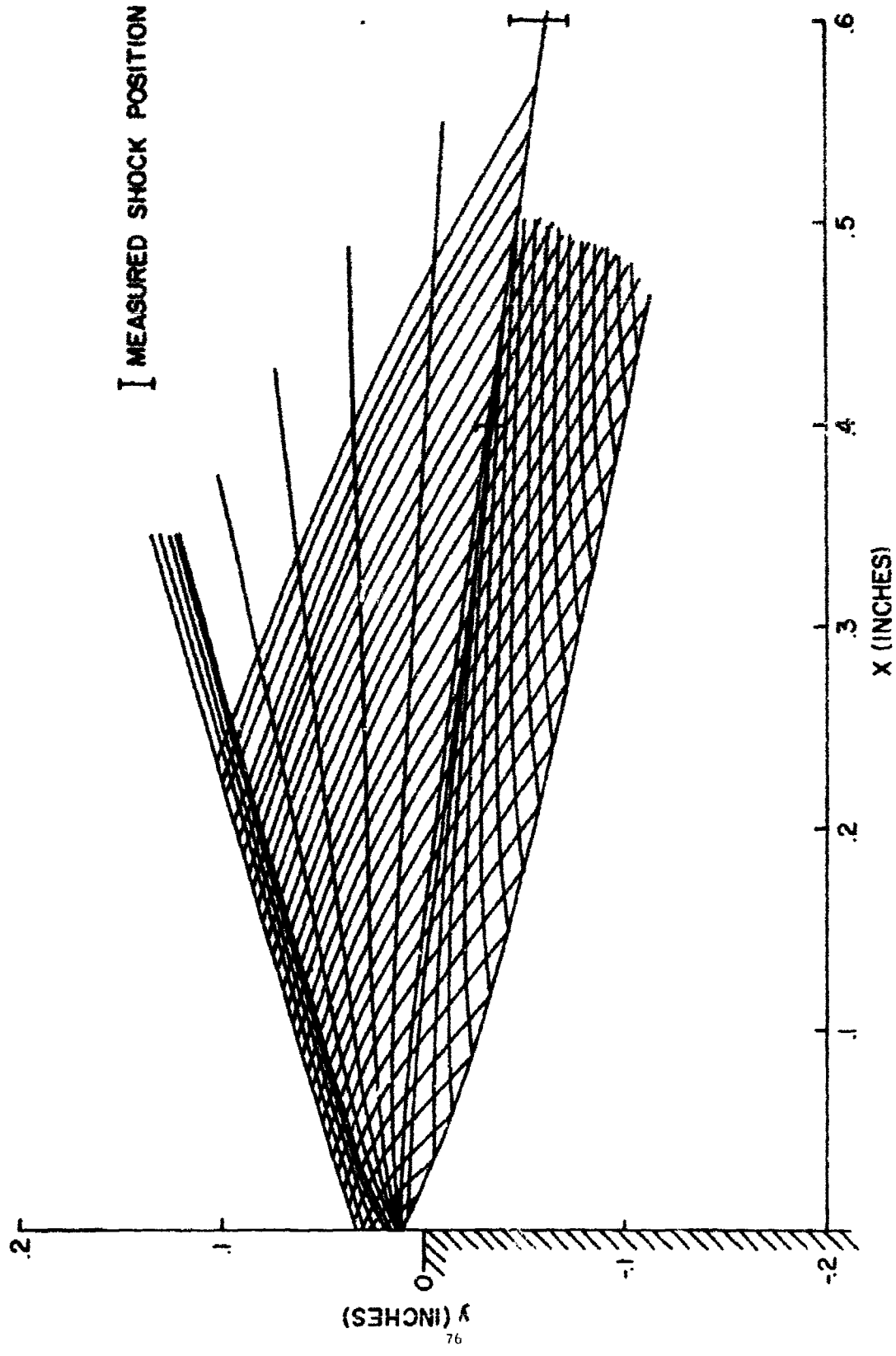


Fig. 27 NETWORK OF CHARACTERISTICS FOR CORNER EXPANSION
 $h=0.750$ $M_\infty=3.5$ $P_0=31.8$ psia

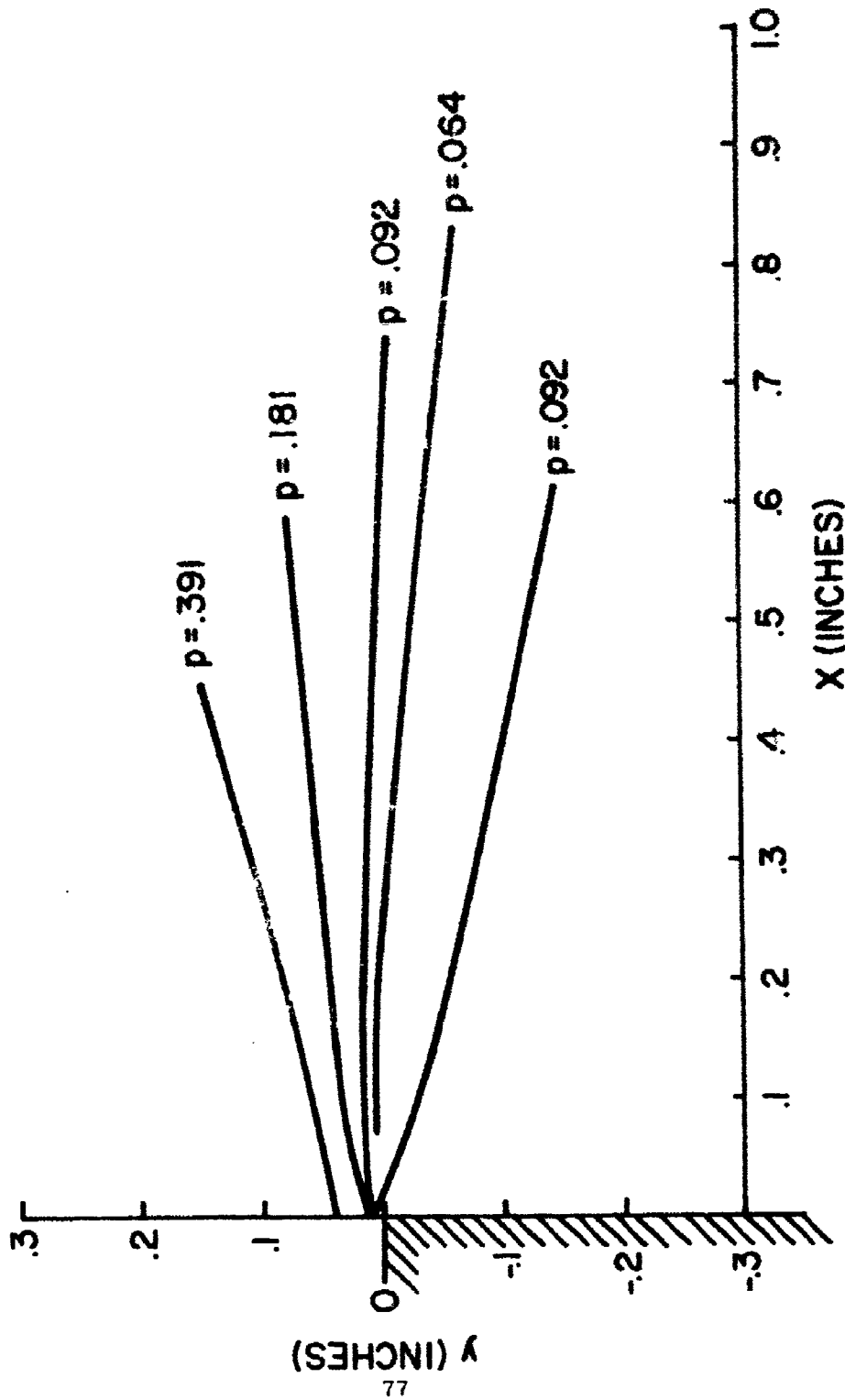


Fig. 28 LINES OF CONSTANT PRESSURE FOR CORNER
 EXPANSION $h=0.750$ $M_\infty=3.5$ $p_\infty=31.8$ psia

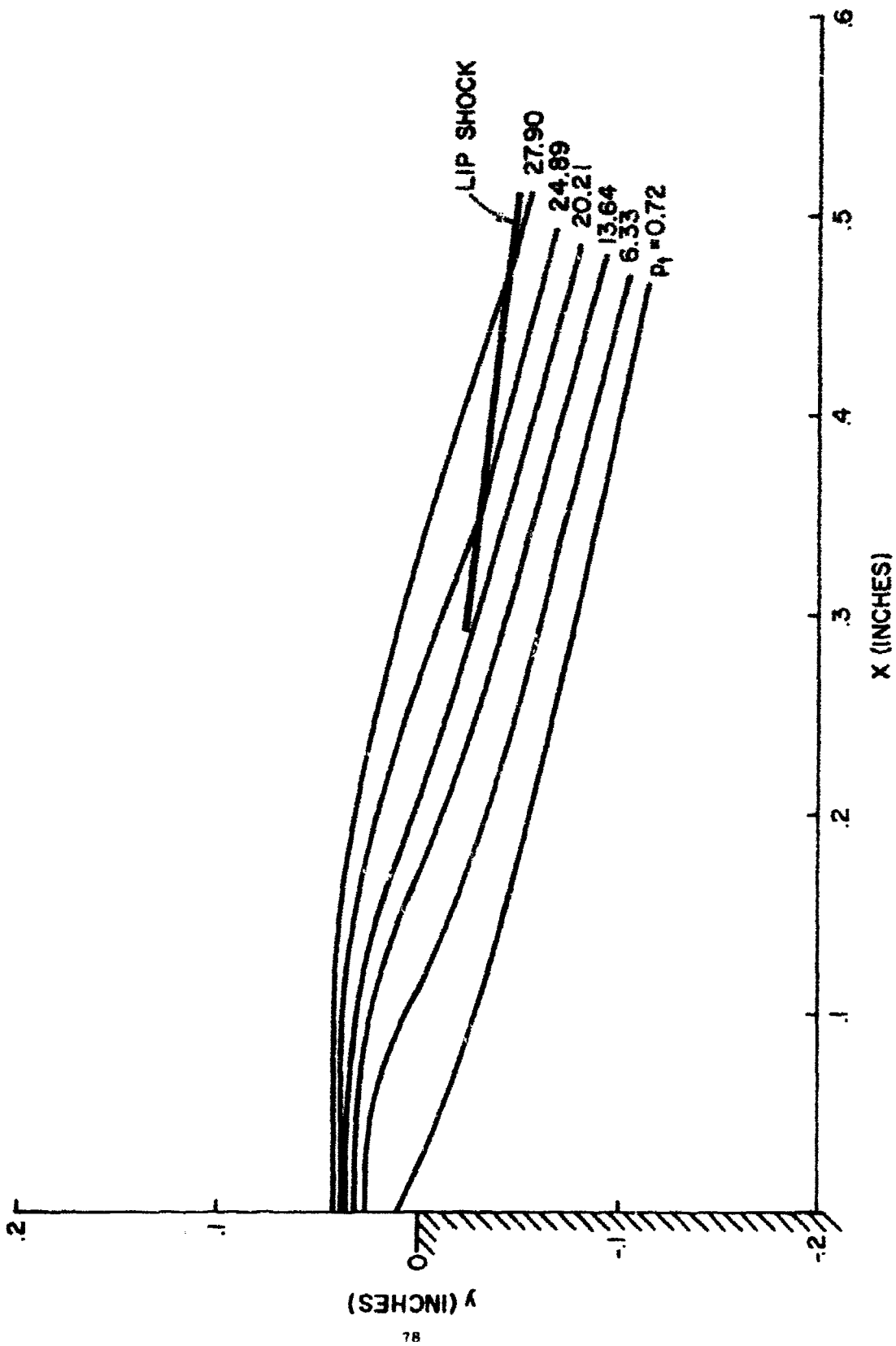


Fig. 29 STREAMLINES PASSING THROUGH CORNER EXPANSION $h=0.750$
 $M_\infty = 3.5$ $p_\infty = 31.8$ psia

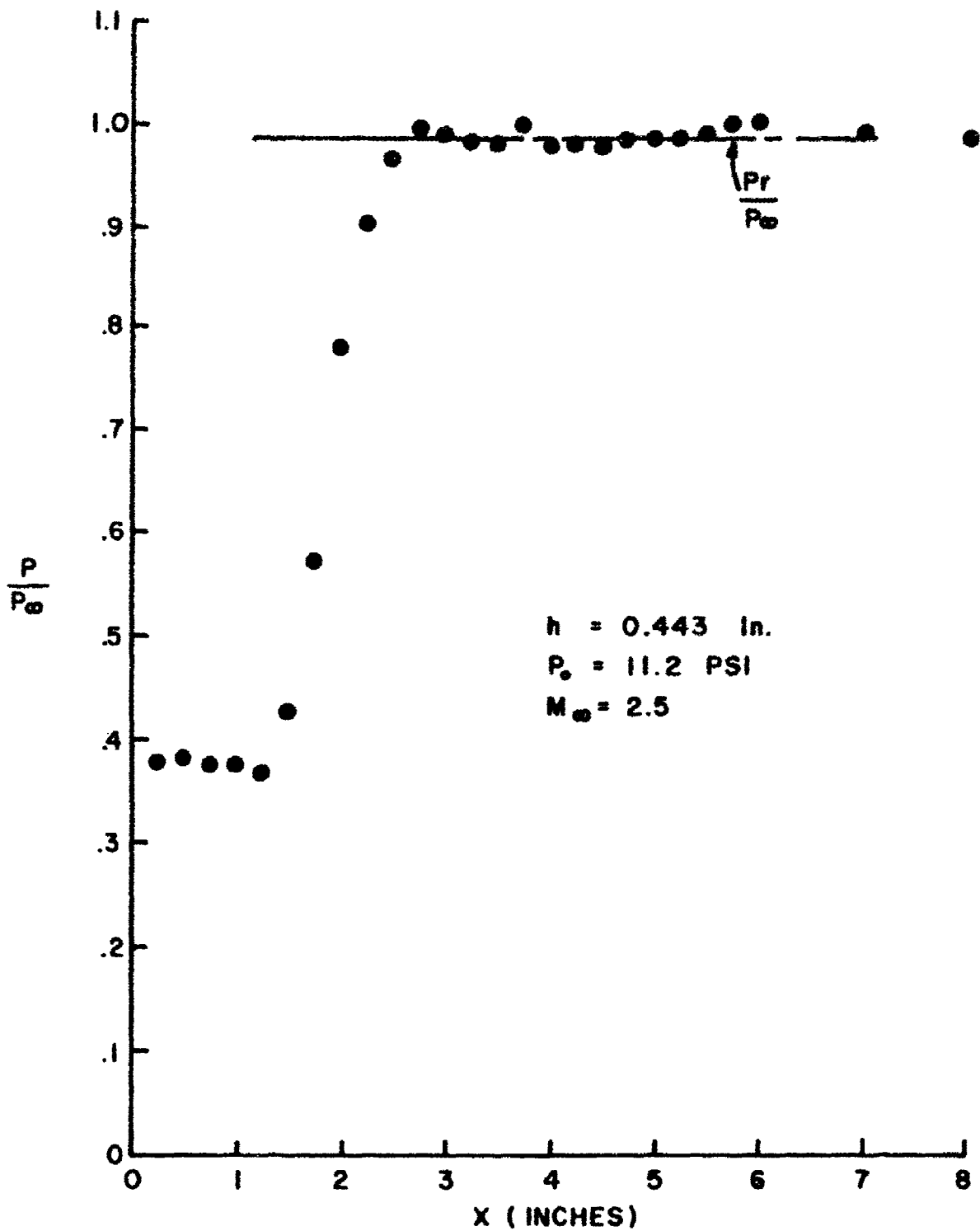


Fig. 30 PRESSURE DISTRIBUTION ON MODEL
 $h = 0.443$ $M_\infty = 2.5$ $P_0 = 11.2 \text{ PSIA.}$

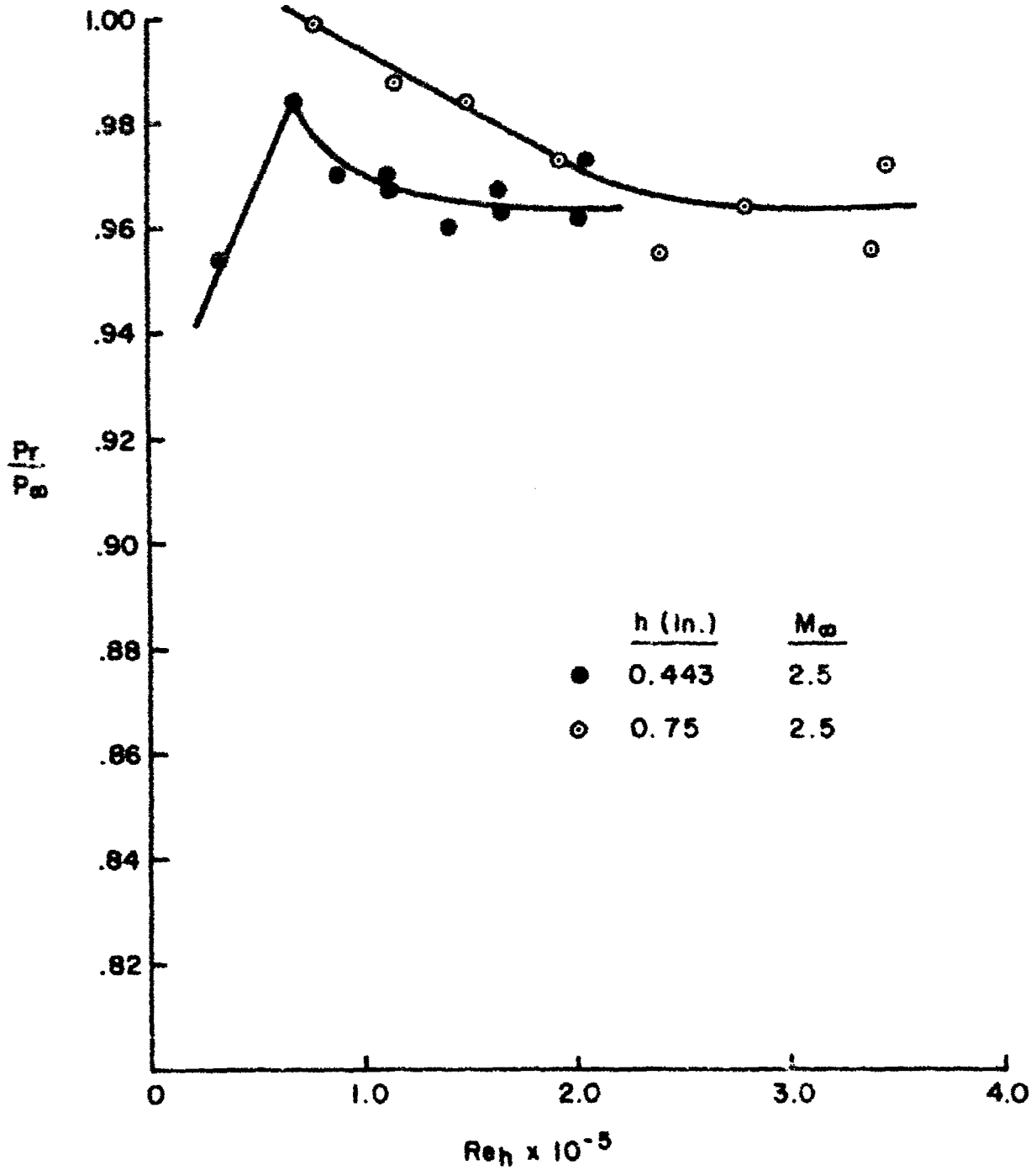


Fig. 31 RECOVERY PRESSURE RATIO VS. Re_h $M_\infty = 2.5$

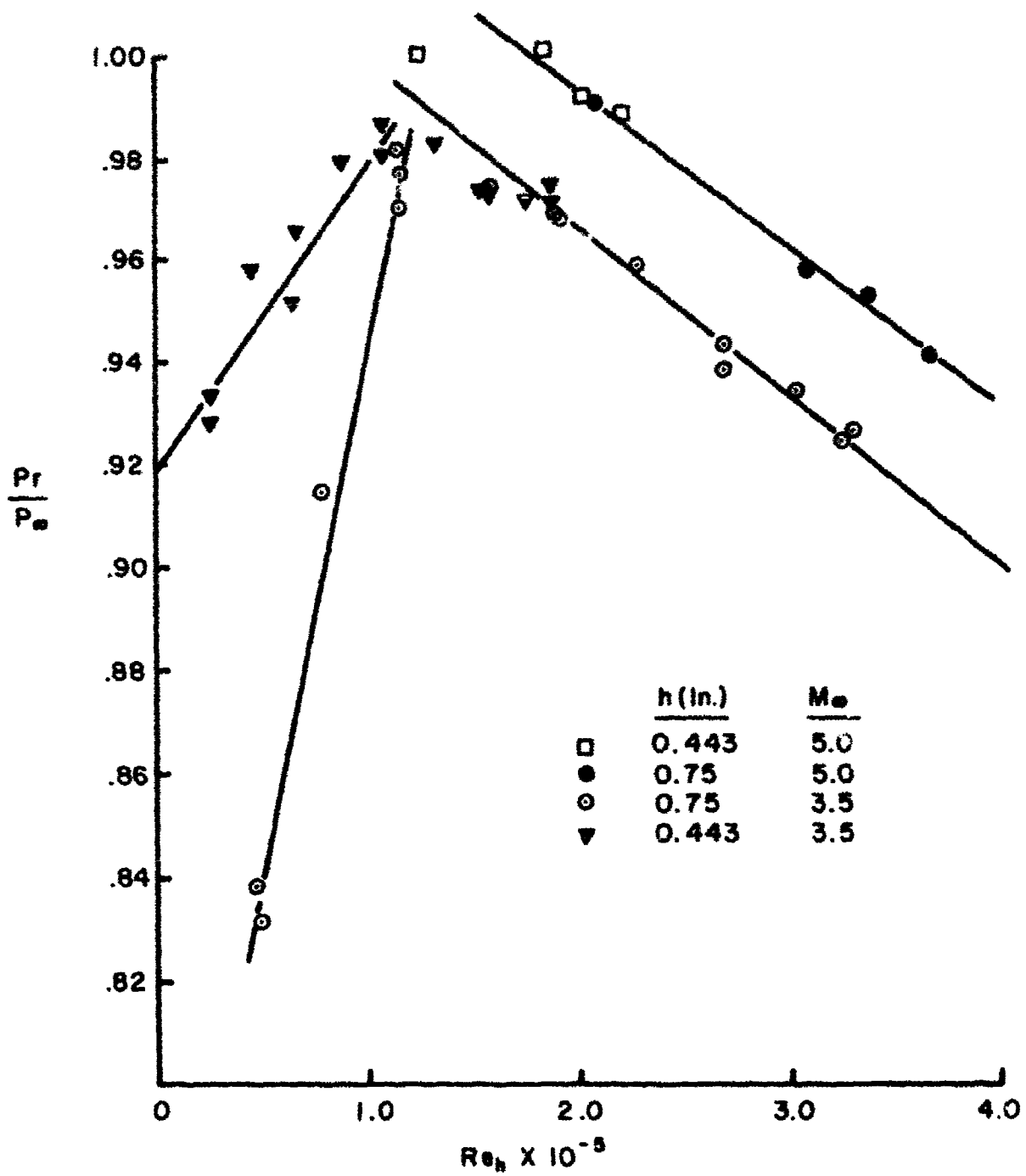


Fig. 32 RECOVERY PRESSURE RATIO VS. Re_h
 $Me = 3.5$ & 5.0
 81

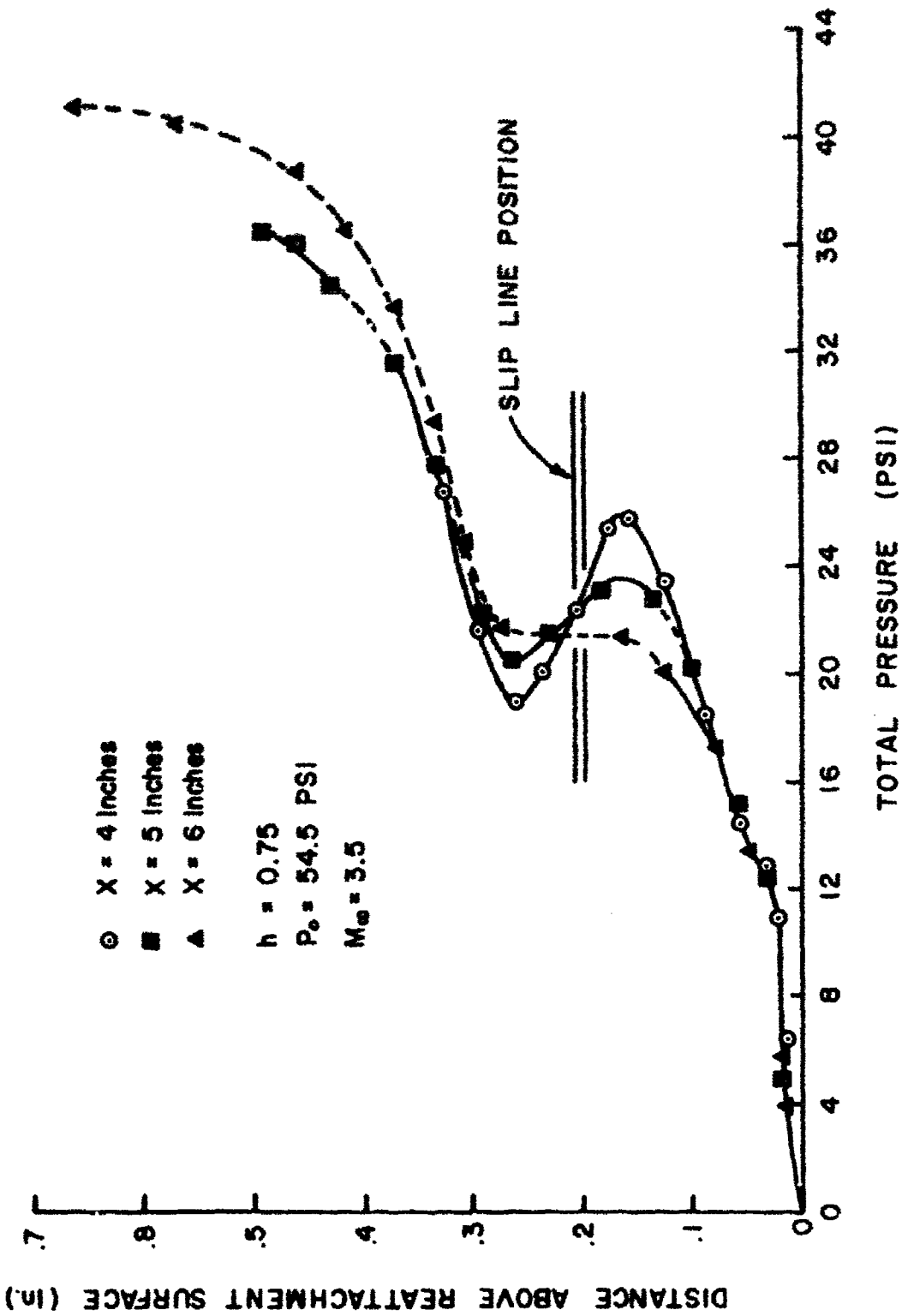


Fig. 33 TOTAL PRESSURE DISTRIBUTION DOWNSTREAM OF REATTACHMENT

Unclassified

Security Classification

DOCUMENT CONTROL DATA - RLD		
<small>(Security classification of title, body of abstract and indexing annotation must be entered when the overall report is classified)</small>		
1. ORIGINATING ACTIVITY (Corporate method) Thermomechanics Research Laboratory (ARN) Aerospace Research Laboratories, OAR		2a. REPORT SECURITY CLASSIFICATION Unclassified 2b. GROUP
3. REPORT TITLE The Flow Field and Heat Transfer Downstream of a Rearward Facing Step in Supersonic Flow		
4. DESCRIPTIVE NOTES (Type of report and inclusive dates) Scientific, Final,		
5. AUTHOR(S) (Last name, first name, initial) SMITH, HOWARD E.		
6. REPORT DATE March 1967	7a. TOTAL NO. OF PAGES 82	7b. NO. OF REFS 26
8a. REPORT NUMBER In-House Research d. PROJECT NO. *7063 - 00 02 e. 61445014 f. 681307		8b. ORIGINATOR'S REPORT NUMBER(S) 8c. OTHER REPORT NO(S) (Any other numbers that may be assigned this report) ARL 67-0056
10. AVAILABILITY/LIMITATION NOTICES Distribution of this document is unlimited		
11. SUPPLEMENTARY NOTES		12. SPONSORING MILITARY ACTIVITY Aerospace Research Laboratories (ARN) Office of Aerospace Research, USAF Wright-Patterson AFB, Ohio
13. ABSTRACT An experimental investigation of the flow field, and the model pressure and steady-state heat transfer distributions for a rearward-facing step in supersonic flow is described. Tests were conducted using a water-cooled model with a step height adjustable to 0.443 and 0.750 inches at free stream Mach numbers of 2.5, 3.5, and 5.0, and at Reynolds numbers based on length of surface ahead of separation of approximately 2.5×10^5 to 1.8×10^6 . It was found that the Reynolds number based on step height (Re_h) is an important parameter and that both the base pressure and the maximum heat transfer at reattachment may be predicted as a function of this parameter. Several representative flow fields are presented along with analyses of the various regions of these fields. It was found that the depressed base pressure is communicated upstream of the step through the subsonic portion of the attached boundary layer resulting in a pressure gradient immediately upstream of the step. It is shown that the rapid corner expansion is not the commonly used Prandtl-Meyer expansion, but rather is accurately described by the method of inviscid rotational characteristics which accounts for both the entropy gradient in the boundary layer and the pressure gradient upstream of the step. This description of the corner expansion also accurately predicts the position of the lip shock associated with the rapid expansion.		

DD FORM 1 JAN 64 1473

UNCLASSIFIED

Security Classification

Unclassified

Security Classification

14. KEY WORDS	LINK A		LINK B		LINK C	
	ROLE	WT	ROLE	WT	ROLE	WT
Supersonic Flow Heat Transfer Separated Flows Base Pressure and Reattachment						

INSTRUCTIONS

1. ORIGINATING ACTIVITY: Enter the name and address of the contractor, subcontractor, grantee, Department of Defense activity or other organization (corporate author) issuing the report.

2a. REPORT SECURITY CLASSIFICATION: Enter the overall security classification of the report. Indicate whether "Restricted Data" is included. Marking is to be in accordance with appropriate security regulations.

2b. GROUP: Automatic downgrading is specified in DoD Directive 5200.10 and Armed Forces Industrial Manual. Enter the group number. Also, when applicable, show that optional markings have been used for Group 3 and Group 4 as authorized.

3. REPORT TITLE: Enter the complete report title in all capital letters. Titles in all cases should be unclassified. If a meaningful title cannot be selected without classification, show title classification in all capitals in parentheses immediately following the title.

4. DESCRIPTIVE NOTES: If appropriate, enter the type of report, e.g., interim, progress, summary, annual, or final. Give the inclusive dates when a specific reporting period is covered.

5. AUTHOR(S): Enter the name(s) of author(s) as shown on or in the report. Enter last name, first name, middle initial. If military, show rank and branch of service. The name of the principal author is an absolute minimum requirement.

6. REPORT DATE: Enter the date of the report as day, month, year, or month, year. If more than one date appears on the report, use date of publication.

7a. TOTAL NUMBER OF PAGES: The total page count should follow normal pagination procedures, i.e., enter the number of pages containing information.

7b. NUMBER OF REFERENCES: Enter the total number of references cited in the report.

8a. CONTRACT OR GRANT NUMBER: If appropriate, enter the applicable number of the contract or grant under which the report was written.

8b, 8c, & 8d. PROJECT NUMBER: Enter the appropriate military department identification, such as project number, subproject number, system numbers, task number, etc.

9a. ORIGINATOR'S REPORT NUMBER(S): Enter the official report number by which the document will be identified and controlled by the originating activity. This number must be unique to this report.

9b. OTHER REPORT NUMBER(S): If the report has been assigned any other report numbers (either by the originator or by the sponsor), also enter this number(s).

10. AVAILABILITY/LIMITATION NOTICES: Enter any limitations on further dissemination of the report, other than those

imposed by security classification, using standard statements such as:

- (1) "Qualified requesters may obtain copies of this report from DDC."
- (2) "Foreign announcement and dissemination of this report by DDC is not authorized."
- (3) "U. S. Government agencies may obtain copies of this report directly from DDC. Other qualified DDC users shall request through _____."
- (4) "U. S. military agencies may obtain copies of this report directly from DDC. Other qualified users shall request through _____."
- (5) "All distribution of this report is controlled. Qualified DDC users shall request through _____."

If the report has been furnished to the Office of Technical Services, Department of Commerce, for sale to the public, indicate this fact and enter the price, if known.

11. SUPPLEMENTARY NOTES: Use for additional explanatory notes.

12. SPONSORING MILITARY ACTIVITY: Enter the name of the departmental project office or laboratory sponsoring (paying for) the research and development. Include address.

13. ABSTRACT: Enter an abstract giving a brief and factual summary of the document indicative of the report, even though it may also appear elsewhere in the body of the technical report. If additional space is required, a continuation sheet shall be attached.

It is highly desirable that the abstract of classified reports be unclassified. Each paragraph of the abstract shall end with an indication of the military security classification of the information in the paragraph, represented as (TS), (S), (C), or (U).

There is no limitation on the length of the abstract. However, the suggested length is from 150 to 225 words.

14. KEY WORDS: Key words are technically meaningful terms or short phrases that characterize a report and may be used as index entries for cataloging the report. Key words must be selected so that no security classification is required. Identifiers, such as equipment model designation, trade name, military project code name, geographic location, may be used as key words but will be followed by an indication of technical context. The assignment of links, roles, and weights is optional.

UNCLASSIFIED

Security Classification

10-655-370

Errata to Document ASD 67-6086

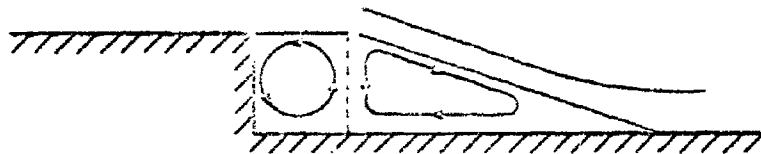
"The Flow Field and Heat Transfer Downstream
of a Rearward Facing Step in Supersonic Flow"

by

Howard E. Smith

Page ii: Replace Foreword with enclosed page.

Page 14: Add sketch:



Page 20: Equation (9) should be written:

$$T_2/T_1 = \xi \left[\frac{(\gamma - 1)\xi + (\gamma + 1)}{(\gamma + 1)\xi + (\gamma - 1)} \right] \quad (9)$$

Page 20: Equation (13) should be written:

$$T_1/T_{O1} = T_1/T_{O2} = \frac{T_2/T_{O2}}{T_2/T_1} \quad (13)$$

FOREWORD

This technical report is taken from a thesis submitted by the author to the Aerospace Engineering Department of the University of Cincinnati in partial fulfillment of the requirements for the degree of Doctor of Philosophy. Dr. Widen Tabakoff, Professor of Aerospace Engineering, is the thesis advisor. The research reported herein was performed by the author while in residence as a Visiting Research Associate at the Thermo-Mechanics Research Laboratory of the Aerospace Research Laboratories, Office of Aerospace Research, USAF.

The author is grateful to Dr. Tabakoff for introducing him to this area of research, and for the guidance and the constant encouragement which he gave throughout the course of this work. The author also wishes to acknowledge Dr. Max G. Scherberg of the Thermo-Mechanics Research Laboratory, ARL, for his advice, contributions, and many fruitful discussions related to this work. Mr. Donald Clemm of the Applied Mathematics Research Laboratory, ARL, is acknowledged for programming the computer solutions of the corner expansion described in this report. The excellent cooperation and helpfulness of Mr. J. C. Donaldson, Project Engineer, together with the staff of the Von Karman Gas Dynamics Facility of the Arnold Engineering and Development Center, Arnold Air Force Station, Tennessee, who conducted the wind tunnel tests reported herein are also acknowledged.